Study of electro-catalytic activity of electrodes materials and polarization phenomena for detection mechanism investigation of a no2 sensor and its optimization.

Ivan Romanytsia

NNT : 2014 EMSE 0760

THÈSE

présentée par

Ivan ROMANYTSIA

pour obtenir le grade de
Docteur de l'École Nationale Supérieure des Mines de Saint-Étienne

Spécialité : Génie de Procédés

ÉTUDE DES PROPRIETES ELECTRO-CATALYTIQUES DES MATERIAUX D'ELECTRODE ET DES PHENOMENES DE POLARISATION POUR LA COMPREHENSION DES MECANISMES DE DETECTION D'UN CAPTEUR D'OXYDES D'AZOTE ET L'OPTIMISATION DE SON FONCTIONNEMENT

à soutenir à Saint-Etienne, le 29 Octobre 2014

Membres du jury

Président :	Claude LUCAT	Directeur de recherche CNRS, CNRS UMR5218, Talence
Rapporteurs :	Armelle RINGUEDE	Chargé de recherche CNRS, ENSCP, Paris
	José Louis VALVERDE	Professeur, University of Castilla la Mancha, Ciudad Real
Examinateurs :	Christophe PIJOLAT	Professeur, ENSM-SE, Saint-Étienne
	Jean MILPIED	Senior Expert FPS, MEAS France, Toulouse
Directeurs de	Jean-Paul VIRICELLE	Directeur de recherche, ENSM-SE, Saint-Étienne
thèse :	Philippe VERNOUX	Directeur de recherche CNRS, IRCELyon, Villeurbanne
Invité:	Alain SEUBE	Manager R&D, MEAS France, Toulouse

Spécialités doctorales	Responsables :	Spécialités doctorales	Responsables
SCIENCES ET GENIE DES MATERIAUX	K. Wolski Directeur de recherche	MATHEMATIQUES APPLIQUEES	O. Roustant, Maître-assistant
MECANIQUE ET INGENIERIE	S. Drapier, professeur	INFORMATIQUE	O. Boissier, Professeur
GENIE DES PROCEDES	F. Gruy, Maître de recherche	IMAGE, VISION, SIGNAL	JC. Pinoli, Professeur
SCIENCES DE LA TERRE	B. Guy, Directeur de recherche	GENIE INDUSTRIEL	A. Dolgui, Professeur
SCIENCES ET GENIE DE L'ENVIRONNEMENT	D. Graillot, Directeur de recherche	MICROELECTRONIQUE	S. Dauzere Peres, Professeur

EMSE : Enseignants-chercheurs et chercheurs autorisés à diriger des thèses de doctorat (titulaires d'un doctorat d'État ou d'une HDR)

ABSI	Nabil	CR		CMP
AVRIL	Stéphane	PR2	Mécanique et ingénierie	CIS
BALBO	Flavien	PR2		FAYOL
BASSEREAU	Jean-François	PR		SMS
BATTON-HUBERT	Mireille	PR2	Sciences et génie de l'environnement	FAYOL
BERGER DOUCE	Sandrine	PR2		FAYOL
BERNACHE-ASSOLLANT	Didier	PR0	Génie des Procédés	CIS
BIGOT	Jean Pierre	MR(DR2)	Génie des Procédés	SPIN
BILAL	Essaid	DR	Sciences de la Terre	SPIN
BOISSIER	Olivier	PR1	Informatique	FAYOL
BORBELY	Andras	MR(DR2)	Sciences et génie des matériaux	SMS
BOUCHER	Xavier	PR2	Génie Industriel	FAYOL
BRODHAG	Christian	DR	Sciences et génie de l'environnement	FAYOL
BRUCHON	Julien	MA(MDC)	Mécanique et ingénierie	SMS
BURLAT	Patrick	PR2	Génie Industriel	FAYOL
COURNIL	Michel	PR0	Génie des Procédés	DIR
DARRIEULAT	Michel	IGM	Sciences et génie des matériaux	SMS
DAUZERE-PERES	Stéphane	PR1	Génie Industriel	CMP
DEBAYLE	Johan	CR	Image Vision Signal	CIS
DELAFOSSE	David	PR1	Sciences et génie des matériaux	SMS
DESRAYAUD	Christophe	PR2	Mécanique et ingénierie	SMS
DOLGUI	Alexandre	PR0	Génie Industriel	FAYOL
DRAPIER	Sylvain	PR1	Mécanique et ingénierie	SMS
FEILLET	Dominique	PR2	Génie Industriel	CMP
FEVOTTE	Gilles	PR1	Génie des Procédés	SPIN
FRACZKIEWICZ	Anna	DR	Sciences et génie des matériaux	SMS
GARCIA	Daniel	MR(DR2)	Génie des Procédés	SPIN
GERINGER	Jean	MA(MDC)	Sciences et génie des matériaux	CIS
GOEURIOT	Dominique	DR	Sciences et génie des matériaux	SMS
GRAILLOT	Didier	DR	Sciences et génie de l'environnement	SPIN
GROSSEAU	Philippe	DR	Génie des Procédés	SPIN
GRUY	Frédéric	PR1	Génie des Procédés	SPIN
GUY	Bernard	DR	Sciences de la Terre	SPIN
HAN	Woo-Suck	CR	Mécanique et ingénierie	SMS
HERRI	Jean Michel	PR1	Génie des Procédés	SPIN
KERMOUCHE	Guillaume	PR2	Mécanique et Ingénierie	SMS
KLOCKER	Helmut	DR	Sciences et génie des matériaux	SMS
LAFOREST	Valérie	MR(DR2)	Sciences et génie de l'environnement	FAYOL
LERICHE	Rodolphe	CR	Mécanique et ingénierie	FAYOL
LI	Jean-Michel	Microélectronique		CMP
MALLIARAS	Georges	PR1	Microélectronique	CMP
MOLIMARD	Jérôme	PR2	Mécanique et ingénierie	CIS
MONTHEILLET	Frank	DR	Sciences et génie des matériaux	SMS
MOUTTE	Jacques	CR	Génie des Procédés	SPIN
NEUBERT	Gilles			FAYOL
NIKOLOVSKI	Jean-Pierre			CMP
NORTIER	Patrice	PR1		SPIN
PIJOLAT	Christophe	PR0	Génie des Procédés	SPIN
PIJOLAT	Michèle	PR1	Génie des Procédés	SPIN
PINOLI	Jean Charles	PR0	Image Vision Signal	CIS
POURCHEZ	Jérémy	CR	Génie des Procédés	CIS
ROBISSON	Bruno			CMP
ROUSSY	Agnès	MA(MDC)		CMP
ROUSTANT	Olivier	MA(MDC)		FAYOL
ROUX	Christian	PR		CIS
STOLARZ	Jacques	CR	Sciences et génie des matériaux	SMS
TRIA	Assia	Ingénieur de recherche	Microélectronique	CMP
VALDIVIESO	François	MA(MDC)	Sciences et génie des matériaux	SMS
VIRICELLE	Jean Paul	MR(DR2)	Génie des Procédés	SPIN
WOLSKI	Krzystof	DR	Sciences et génie des matériaux	SMS
XIE	Xiaolan	PR1	Génie industriel	CIS
YUGMA	Gallian	CR	Génie industriel	CMP

ENISE : Enseignants-chercheurs et chercheurs autorisés à diriger des thèses de doctorat (titulaires d'un doctorat d'État ou d'une HDR)

BERGHEAU	Jean-Michel	PU	Mécanique et Ingénierie	ENISE
BERTRAND	Philippe	MCF	Génie des procédés	ENISE
DUBUJET	Philippe	PU	Mécanique et Ingénierie	ENISE
FEULVARCH	Eric	MCF	Mécanique et Ingénierie	ENISE
FORTUNIER	Roland	PR	Sciences et Génie des matériaux	ENISE
GUSSAROV	Andrey	Enseignant contractuel	Génie des procédés	ENISE
HAMDI	Hédi	MCF	Mécanique et Ingénierie	ENISE
LYONNET	Patrick	PU	Mécanique et Ingénierie	ENISE
RECH	Joël	PU	Mécanique et Ingénierie	ENISE
SMUROV	Igor	PU	Mécanique et Ingénierie	ENISE
TOSCANO	Rosario	PU	Mécanique et Ingénierie	ENISE
ZAHOUANI	Hassan	PU	Mécanique et Ingénierie	ENISE

Outline

Introduction

Continuous decrease of automotive emissions limits obliges the vehicle producers to optimize combustion operation and to implement pollutants aftertreatment in exhausts such as nitrogen oxides (NO_2 and NO). In a parallel way, on-board diagnostic is required to control the aftertreatment efficiency. Therefore, the development of sensors working in this harsh exhaust environment is strongly necessary. The actual demand of the car manufacturers deals with the development of accurate, selective (NO and NO_2), stable and cheap NOx sensors.

The development of chemical sensors with selective detection of NO_2 and NO without any interference to carbon monoxide and hydrocarbons is a logical continuation of the PhD study of J. Gao [Gao 2011 PhD] prepared at the center of Science of Natural and Industrial Process SPIN of Ecole Nationale Supérieure de Mines de Saint Etienne (EMSE). This group has a strong expertise on chemical sensors based on semiconductor, such as SnO_2, and solid electrolyte such as β-Al_2O_3 and Yttria-Stabilized Zirconia (YSZ). This present study was performed, as J. Gao thesis, in close cooperation with Institut de Recherches sur la Catalyse et l'Environnement de Lyon (IRCELYON) and an industrial partner: Measurement Specialties (MEAS).

The PhD study performed by J. Gao in 2007-2011 has evidenced a selective detection of NO_2 in diesel exhaust of a 3-electrodes solid state electrochemical cell based on YSZ electrolyte. A constant polarization current is applied between a gold working electrode and a platinum counter electrode, while the sensor responses (ΔV) are measured between the working electrode and a Pt reference electrode. A significant drop of the ΔV was observed in presence of NO_2 in the range 400 – 500°C. In addition, injections of CO and NO did not produce any variation of the sensor response.

In these operating conditions, 3-electrode Pt(CE)/Pt(RE)/Au(WE) sensors present a high selectivity to NO_2 and could be used as selective sensors for exhaust applications. Despite this advantage of the good NO_2 selectivity, there are still some technological problems to solve such as:

- The problem of the instability with time of the sensor baseline which is the response of the sensor in the base gas containing mainly oxygen. This instability is probably linked with electrochemical reaction of oxygen at the working electrode.

- The mechanism of the electrochemical detection of NO_2 is not clear and has to be understood in order to optimize the sensor performances.

- The problem of the cross-sensitivity with the oxygen concentration in the exhaust feed.

Therefore, the global scientific objective of this PhD is to understand the sensor mechanism especially phenomena occurring at the electrodes, in order to bring solutions to previous mentioned problems in galvanostatic mode..

The present PhD manuscript consists of five parts.

The first chapter describes general sources of NOx pollution and NOx abatement methods. It explains the necessity of electrochemical sensors for monitoring NOx emissions. Finally, this chapter describes major families of chemical sensors for NOx detection in exhausts reported in the literature.

The second chapter presents methods used to prepare and to characterize the solid-state electrochemical sensors. It contains the technological details of exhaust sensors fabrication, and describes their main characteristics and controlled parameters. It also describes the specific sensors made for investigating the position of the electrodes.

Third chapter describes the development and characterizations of alternative composite sensing electrodes. Potentiometric solid-state gas sensors with advanced morphology of Au-based sensing electrode were fabricated by screen-printing and tested for NO_2 detection. Electrochemical impedance spectroscopy was used to measure the polarization resistance in air of various devices with composite Au electrodes. The response time and sensitivity was improved by using composite sensing electrode in comparison with a reference Au|YSZ|Pt sensor.

The fourth chapter is focused on electrochemical sensors working under galvanostatic polarizations. Two and three-electrode sensors were used to study the position of the electrodes as well as the electrochemical properties of both reference and Au-based sensing electrodes. Finally, the sensors responses to pollutants (NO_2, CO and NO) have been recorded at 450°C.

The last chapter deals with the mechanism of the NO_2 detection in galvanostatic mode. The electrochemical properties for the oxygen electrode reaction of both Au and composite electrodes have been carried out at 450°C with systematic measurements of I-V curves for different partial pressures of oxygen. The impact of injections of variations concentrations of NO_2 on the electrochemical properties of the composite sensing electrode was also investigated in order to propose a mechanism of the NO_2 detection.

Chapter 1

State of art:

Automotive pollution and gas sensors for exhaust

Outline

Chapter 1: State of Art

Résumé

Ce chapitre est consacré à la problématique de la pollution atmosphérique issue des émissions aux échappements des véhicules. Le transport routier est responsable de la production de la majeure partie des oxydes d'azote (NOx) émis dans l'atmosphère. Il faut dire, que la majorité de cette pollution est concentrée dans des zones très urbanisées. L'exposition permanente aux gaz d'échappement a des conséquences graves pour la santé humaine, et pour cela les normes d'émission deviennent de plus en plus strictes.

Les technologies présentes dans les voitures ont besoin d'un contrôle continu de l'émission à l'échappement. L'environnement en ligne d'échappement correspond à des conditions d'utilisations très sévères : les fortes variations de température et débits, de composition des gaz, les vibrations et d'autres facteurs (poussières, humidité…) demandent au système de contrôle d'être robuste et précis pendant longtemps.

Aussi, dans ce chapitre, après un rappel d'informations générales sur les émissions polluantes et les normes restrictives associées, un état de l'art sur les systèmes de traitement des NOx, et surtout sur les différents types de capteurs dédiés à l'échappement est présenté.

Summary

Present chapter describes sources and consequences of large exhaust emissions of modern society. Huge demand of mobility in developed and developing countries will increase anthropogenic impact on nature and reminds actuality of exhaust abatement and particularly NOx emission. Modern standards of NOx emissions oblige vehicle manufacturers to integrate cheap, precise and long life system to control and decrease NOx concentration in exhaust.

Such systems require gas sensors to optimize and control their efficiency. Numerous devices based on physical and chemical principles are proposed by scientists but hard working exhausts conditions give an advantage to electrochemical methods. Hence, the second part of this chapter is dedicated to the state of art of electrochemical NOx sensors.

1.1. Air pollution

1.1.1. Sources of emissions: gasoline/diesel engines

In 21-th century high level of urbanization increased anthropologic pollution of atmosphere. Mobility reached by automobile transport with internal combustion engines is responsible for important pollution by exhaust at rural, urban and traffic locations. Among numerous pollutants existing in exhaust, nitrogen dioxides (NO_2) is a high reactive gas that is mainly formed by oxidation of nitrogen monoxide (NO). These two gases are collectively known as NO_X.

According to European Environment Agency, major sources of NOx pollution shows that is issued from road transport (Figure 1.1).

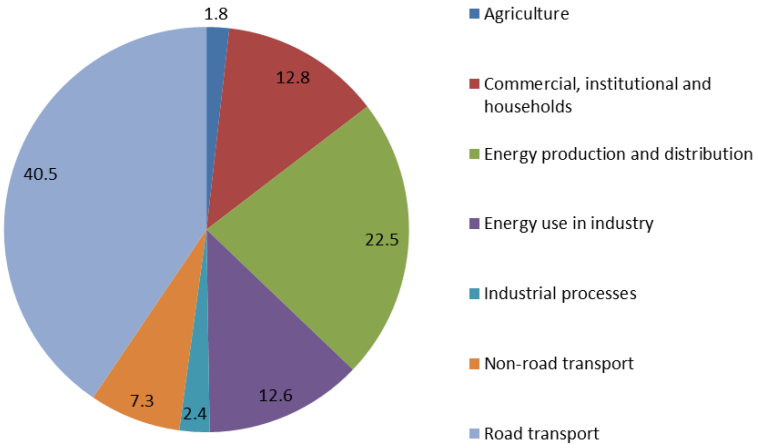

Figure 1.1: Share of NOx pollution in Europe[EEA report]

Presence of NOx in habitable location affects the respiratory system. Short-term exposure to NO_2 can result in adverse health effects such as changes in lung function in sensitive population groups, while long-term exposure can lead to more serious effects such as increased susceptibility to respiratory infection. Table 1.1 shows general chemical composition of exhaust and health effects on human.

Diesel engines has less emission of carbon monoxide (CO), but high quantities of soot, sulphur dioxide (SO_2) and nitrogen oxides (NOx) are present in diesel exhaust. According to CITEPA report in 2010 in France, around 45% of NOx emission comes from diesel vehicles and only around 5% from gasoline cars [CITEPA 2010].

Table 1.1: Composition of gasoline and diesel emission [Sinka 2011]

Pollutant	Gasoline engine	Diesel-engine	Ratio of gasoline/diesel	Health effect
	g emission/dm^3 fuel			
Carbon monoxide	350	20	17.5	non-carcinogenic
Hydrocarbons	50	39	1.28	carcinogenic
Nitrogen oxides	17	23	0.74	carcinogenic
Lead compounds	0.4	0	-	carcinogenic
Soot (particle)	1.5	8	0.2	carcinogenic
Sulphur dioxide	0.2	8	0.03	reduced lung function

Even with higher emission impact on ecology, diesel engine market for light vehicles, heavy trucks, buses and off-highway vehicles has grown continuously during previous years (Figure 1.2). High demand of diesel engines linked with development of human society, will evidently produce increasing NOx emissions. To decrease negative consequences of exhaust emission, especially in urban areas, government of numerous developed countries applied standards of exhaust emissions.

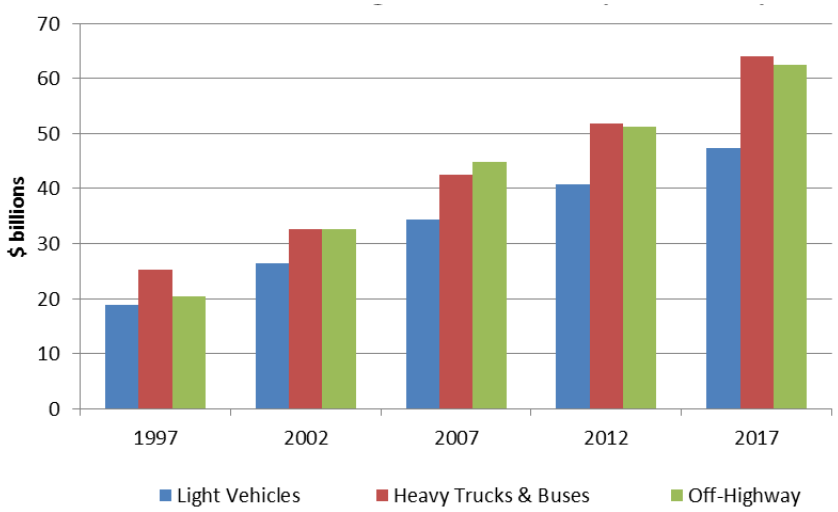

Figure 1.2: Diesel engine demand [The Freedonia Group 2009]

1.1.2. Standards of exhaust emissions

To regulate and decrease negative consequences, a strategy for emissions limits and continuous decrease is applied (Figure 1.3). The emissions of SO_2, nitrogen oxides (NO_X), volatile organic compounds (VOCs) and NH_3 must be strongly reduced to 2020.

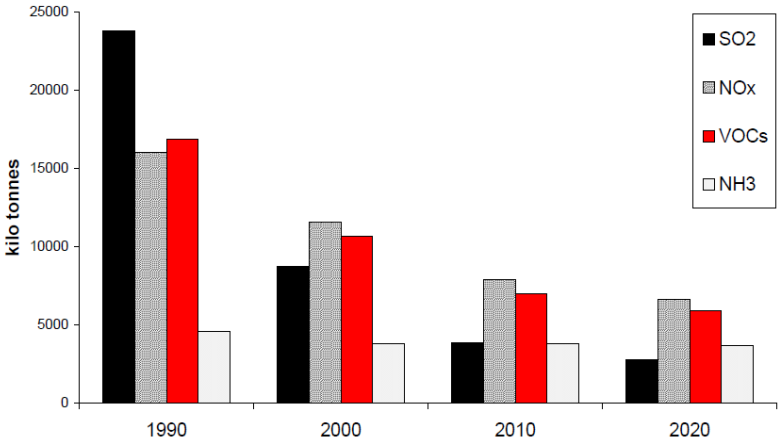

Figure 1.3: Scheduled evolution of emission according to strategy [Thematic Strategy on air pollution 2005]

At same time, as vehicle transport is responsible to air pollution, modern standards for exhaust emissions have been applied since numerous years. As an example, evolution of standards in EU is shown in figure 1.4. The emission of NO_x from diesel engine must be reduced to 6.25 times from 500 to 80 mg/km in 2015.

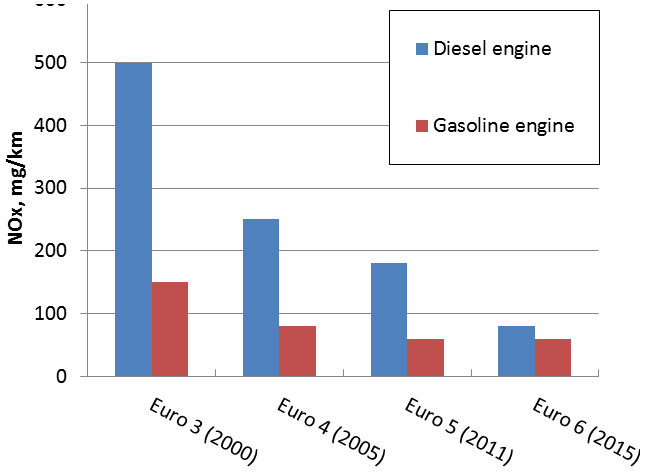

Figure 1.4: Evolution of emission standards in Europe [Regulation of the European Parliament 2007]

To achieve these emission standards, vehicle producers are obliged to modify exhaust treatment system. Nowadays, for NOx abatement, various technologies exist like Selective Catalytic Reduction (SCR), NOx Storage and Reduction (NSR) or NOx trap, Exhaust Gas Recirculation (EGR).

1.2. Exhaust treatment systems for NOx abatement

1.2.1. Selective Catalytic Reduction – Exhaust Gas Recirculation

Selective Catalytic Reduction is based on chemical reduction of NOx (NO_2/NO) with ammonia (NH_3) over suitable catalyst. Numerous catalysts for SCR technology are constituted by oxides V_2O_5-WO_3/TiO_2 type or Cu/Fe exchanged zeolites [DiGiulio 2014] deposited on ceramic support.

As NH_3 source, aqueous solution of ammonia 32.5% is used or Urea. Recently it is called Diesel Exhaust Fluid (DEF). Dosing of DEF is realized according to fuel consumption and engine loop control.

Urea based SCR system requires first step of urea decomposition (equation 1.1); when ammonia solution is used, NH_3 can be injected directly into exhaust stream after diesel oxidation catalyst (DOC) and diesel particle filter (DPF) used usually as aftertreatment device (ATD) for diesel exhaust (Figure 1.5).

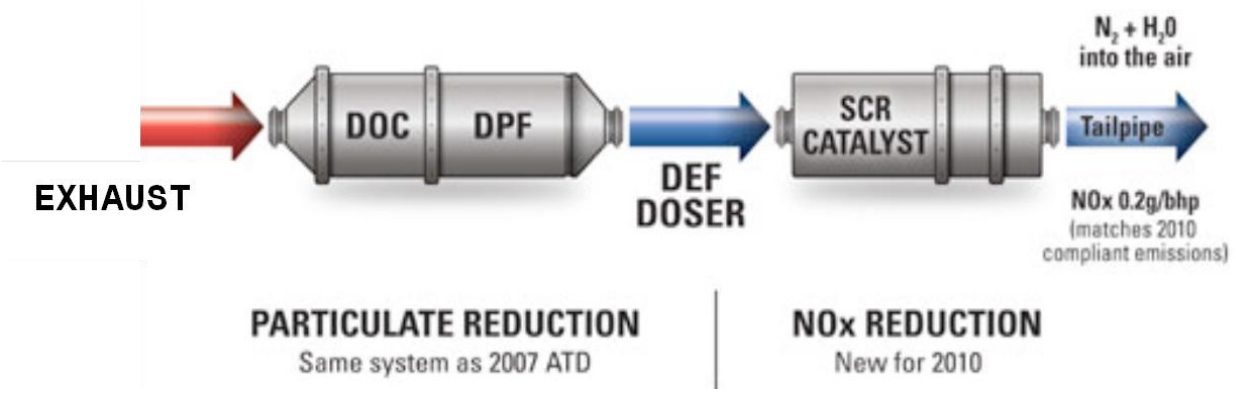

Figure 1.5: Typical EGR-SCR exhaust system [Hill Brothers 2010]

Further steps are SCR reactions on catalyst in exhaust. As we can see from equations 1.2-1.4 complete removal of NOx by SCR depends strongly on composition of exhaust, means O_2 concentration, NO/NO_2 ratio and NH_3 dosing.

$$CO(NH_2)_2 + H_2O \xrightarrow{T} 2NH_3 + CO_2 \quad (1.1)$$

$$4NH_3 + 4NO + O_2 \xrightarrow{SCR\,catalyst,\,T} 4N_2 + 6H_2O \quad (1.2)$$

$$2NH_3 + NO + NO_2 \xrightarrow{SCR\,catalyst,\,T} 2N_2 + 3H_2O \quad (1.3)$$

$$4NH_3 + 3O_2 \xrightarrow{SCR\,catalyst,\,T} 2N_2 + 6H_2O \quad (1.4)$$

Regardless to ammonia or urea, SCR process requires precise control of the ammonia injection rate and outlet NOx concentration. An insufficient injection may result in unacceptably low NOx conversions. An injection rate that is too high results in release of undesirable ammonia to the atmosphere.

Exhaust Gas Recirculation (EGR) system is often coupled with SCR for better performance. The exhaust system returns part of the gases to the engine (Figure 1.6) and decreases the maximum temperature of air-fuel burning mixture to lower the quantity of NOx.

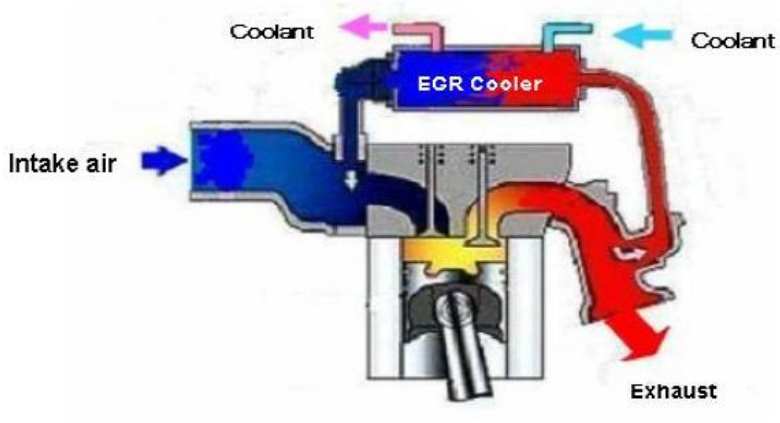

Figure 1.6: Typical EGR exhaust system [Zhang 2010]

1.2.2. NOx trap

NOx trap is based on selective capturing of NOx on Ba-based catalyst and periodical cycles of NOx Storage-Release.

Firstly the NOx are stored during lean engine operation (λ>1, T 150-450 °C, where λ – air/fuel rate), on a porous carrier in the catalytic converter, which is impregnated with metals – Platinum, Rhodium and Barium [Chaugule 2010], [Clayton 2009], [Rico-Pérez 2013], [Hadjar 2011]. In this phase the catalyst converts nitrogen oxide (NO) into nitrogen dioxide (NO_2). The barium carbonate ($BaCO_3$), traps and holds NO_2 as part of an aqueous barium nitrate solution – $Ba(NO_3)_2$ (Figure 1.7)

In the Release Stage (Figure 1.7), reduction of NOx to N_2 at rich burn condition ($\lambda<1$; T 200-500 °C) takes place. The nitrogen oxides are converted into neutral gases (N_2 and CO_2) by hydrocarbon and hydrogen. After this step, NOx Trap, is regenerated and is ready to go on trapping more NOx.

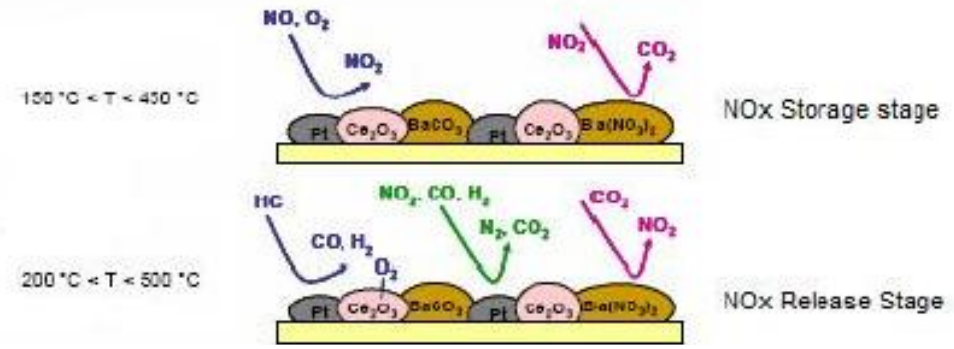

Figure 1.7: NOx trap technology [Schnitzler 2010]

A similar HC-NOx trap technology is presented by Nissan motors. It is based on two layers catalyst combination of hydrocarbon (HC) and NOx catalysts (Figure 1.8) which at lean burn condition can adsorb HC-NOx species. At rich burn a condition, reduction of NOx is realized at same time as HC oxidation; as a result, catalysts can be fully reinitialized.

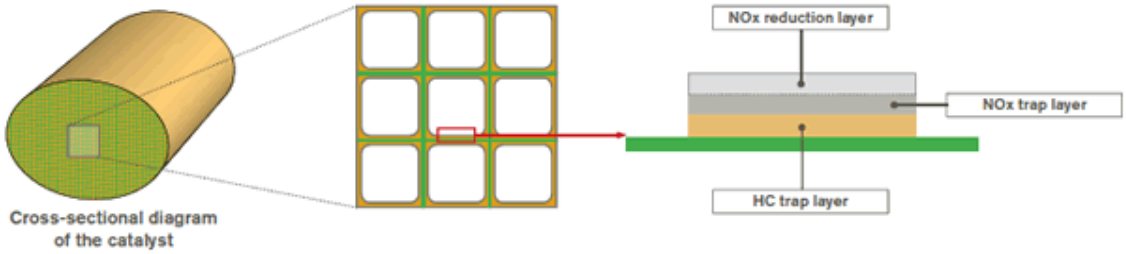

Figure 1.8: HC-NOx trap technology [Nissan Motor Corporation]

As we can see, numerous system are proposed for decreasing of NOx emission from exhaust, but dosing of DEF, control of NH_3, NO/NO_2 ratio and robust control functionalities for the transition between lean and rich engine operation have to be developed and implemented. This permanent and exact control can be realized by using exhaust chemical sensors.

1.3. Gas sensors for exhaust

1.3.1. Chemical sensors - Types of sensors for O_2/NOx/CO/NH_3 detection

Detection of chemical species in combustion environment can be realized by different devices based on optical or solid-state system.

Optical systems are based on detection of emitted or adsorbed electromagnetic waves in infrared (IR) [Ohtani 2004], ultraviolet (UV) or visible (Vis) part of spectra [Di Franco 2009]. Solid state system are based on variation of measured parameter of solid device as, resistivity (Ω) [Sharma 2013], conductivity (σ) [Tuller 2013], capacity (C) [Ishihara 1995], electromotive force (EMF) [Miura 2002], [Chevallier 2008], [Yin 2013], [Gao 2011], current (i) [Kobayashi 2001], etc. Table 1.2 classifies the combustion techniques according to their response time characteristic denote as "Frequency" and working principle and measured parameter.

Table 1.2: Optical and solid state sensors for combustion control. [Docquier 2002]

Optical sensors			
Frequency	Technique[a]	Detector[b]	Parameter
Low	UV–Vis EM	CCD camera WE SPEC	OH^*, CH^*, C_2^*, CO_2^*, $T°$ (soot)
	IR EM	CCD camera	$T°$
High	UV–Vis EM	PMT and filter PD and filter	OH^*, CH^*, C_2^*, CO_2^*
	Vis–IR EM	PD and filter NB SPEC	$T°$
	IR ABS	LD and PD	H_2O, CO_2, $T°$, p
Low	Electrochemical		O_2, CO, HC, NO_x
	Catalytic		CO, NO_x
	Thermocouple, RTD		$T°$
	Viscosimeter		Wobbe index (W_0)
High	Spark plug		Ion current
	Electric, resistive		Pressure (p)

[a] EM-emission, ABS – absorption

[b] NB/WB SPEC – narrow/wide-band spectrometer, PMT – photo multiplier tube, PD – photo diode, LD – laser diode, RTD – resistive temperature detector.

Utilization of optical systems is limited by their size, energy consumption, and necessity of direct access to exhaust or flame and complex algorithm of signal transformation from

electromagnetic waves to electrical signal. Due to this reason, utilization of optical gas sensors is limited in automotive industry.

From numbers of years, electrochemical potentiometric solid-state sensors are used for automobile combustion control because of low power consumption, electrical nature of produced signal, size, high stability and fast response. Most popular and used one is electrochemical potentiometric sensor well known as λ-probe for oxygen (Figure 1.9).

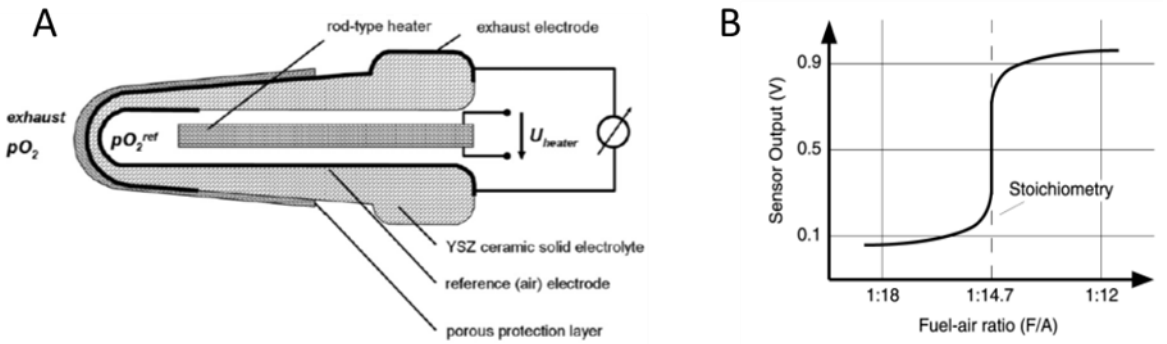

Figure 1.9: Typical λ-probe – A [Fischer 2010] and typical output signal (V) – B [Docquier 2002]

Mechanism of zirconia-based oxygen sensor is well known since Walther Nernst described the physical behavior of galvanic elements known as the Nernst equation (eq.1.5) [Göpel 2000]

$$U = \frac{RT}{4F} \cdot Ln\left(\frac{P_{O_2}(exhaust)}{P_{O_2}(reference)}\right) \tag{1.5}$$

R is universal gas constant (R = 8.314 472 J K^{-1} mol^{-1})
T is absolute temperature (K)
F is Faraday constant (F = 9.648 533×10^4 C mol^{-1})
$P_{O_2}(exhaust)$ is oxygen partial pressure in exhaust,
$P_{O_2}(reference)$ is oxygen partial pressure in reference (air).

Relationship 1.5 is based on thermodynamic equilibrium and fast kinetic reactions at the electrode interface assured by high catalytic activity of platinum electrodes in regards of oxygen reaction

Easily predicted behavior and correct variation of output potential as a function of partial pressure of oxygen in exhaust (Figure 1.10) indicate the fuel/air ratio called lambda (Figure 1.9 B), and allow controlling lean or burning conditions of combustion.

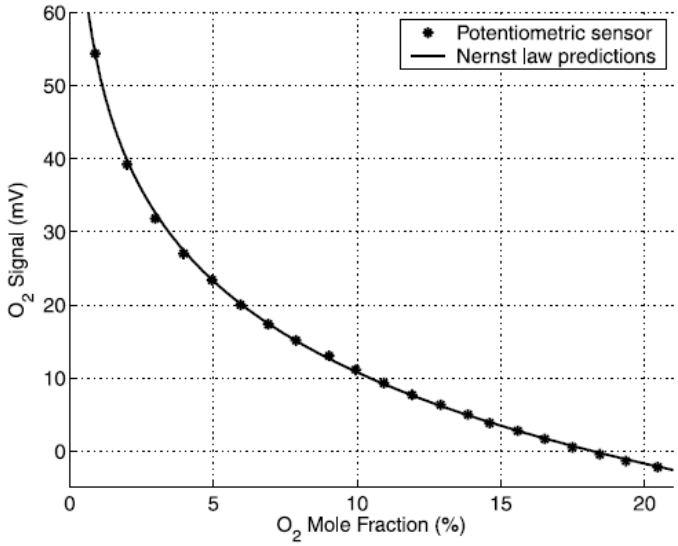

Figure 1.10: Output signal of zirconia based sensor as a function of O_2 fraction in N_2 at 550°C [Docquier 2002]

Another type of potentiometric solid state gas sensors is called mixed-potential or non-Nernstian sensor. When reference electrode (RE) is exposed to same atmosphere as sensing electrode (SE), common EMF could not be calculated from Nernstian equation.

The signal of a two electrodes potentiometric sensor, in a complex gas environment, shows a non-Nernstian behavior due to the establishment of a mixed potential [Gao 2011], [Somov 1996], [Yin 2013] on the sensing electrode. This latter is linked to the superposition of parallel electrode reactions occurring at the triple phase boundaries (TPB) [Yin 2013], [Zosel 2002], [Chevallier 2008], [Miura 2002], such as the oxygen electrode reaction and the electrochemical reduction (oxidation) of NO_2 (NO).

Modification of sensitivity and selectivity can be reached by using different sensing electrode materials or electrochemical methods such as galvanostatic or potentiostatic polarization, or by applying pulsed or alternative current to electrodes. Some recent NO_2, NO, NH_3, CO, CxHy sensors are based on this principle.

1.3.2. Solid Electrolytes for electrochemical sensors

Almost all electrochemical sensors and specially potentiometric and amperometric are composed of a high temperature solid electrolyte such as oxygen conductor O^{2-} –yttria-stabilized zirconia (YSZ) [Gao 2011], [Somov 1996], [Yin 2013], [Zosel 2002], samarium-doped-ceria (SDC) [Pijolat 2009], [Fergus 2011], gadolinium-doped-ceria (GDC) [Brosha 2002] or Na^{+} conductor – β-alumina ($2Na_2O–11Al_2O_3$) [Guillet 2002].

Role of solid electrolyte is to provide ionic contact between electrodes. This contact is possible because of anion or cations vacancies in solid structure of electrolyte. As example, the modification of cubic zirconia by addition of yttrium oxide is shown on figure 1.11.

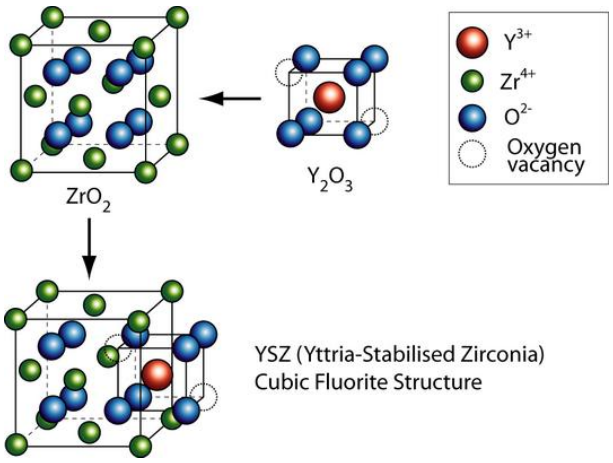

Figure 1.11: Modification of cubic zirconia crystal by addition of yttrium oxide

When cubic zirconia is stabilized by addition of yttrium at high temperature, the dopant cations Y^{3+} substitutes Zr^{4+} sites in the crystal structure and produces oxygen vacancies to maintain the charge neutrality of crystal according to equation 1.6:

$$Y_2O_3 \longrightarrow 2Y_{Zr}^{'} + V_O^{\bullet\bullet} + 3O_O^x \tag{1.6}$$

In equation 1.6, $Y_{Zr}^{'}$ is cation of yttrium replacing zirconium ion, O_O^x - oxygen placed in normal lattice oxygen position and $V_O^{\bullet\bullet}$ - vacancy of oxygen. More than 99% of conductivity is carried by oxygen ions. As we can see, vacancy concentration could reach 4 mol % by addition of 8 mol % of Y_2O_3.

In oxygen containing atmosphere solid adsorbs oxygen at the sample surface. Then, adsorbed oxygen can be incorporated in the solid by diffusion into vacant anion sites, creating the holes, as shown by equilibrium [West, 2014] in equation 1.7:

$$\frac{1}{2}O_2 + V_O^{\bullet\bullet} \longrightarrow O_O^x + 2h^{\bullet} \quad (1.7)$$

Mobility of oxygen ions or other carriers of charge in solid electrolytes depends strongly on temperature and is described by Arrhenius equation 1.8:

$$\sigma = \left(\frac{\sigma_0}{T}\right) e^{\left(\frac{-E_A}{k_b T}\right)} \quad (1.8)$$

σ is ionic conductivity ($S.m^{-1}$),

σ_0 is preexponetial factor ($S.m^{-1}.K$)

T is absolute temperature, K

E_A is activation energy, eV

k_b is Boltzmann constant, $k_b = 8.6173324(78)\times10^{-5}$ eV

Figure 1.12 shows variation of logarithm of ionic conductivity with temperature for different solid electrolytes. As shown the conductivity of solid electrolytes increases exponentially with temperature; for this reason, the temperature during electrochemical measurements must be precisely controlled. The widely used and studied YSZ electrolyte possesses pure ionic conductivity at high temperature range 380-1400°C and oxygen partial pressures from 10^{-25} up to 10^{5} Pa [Zhuiykov 2008].

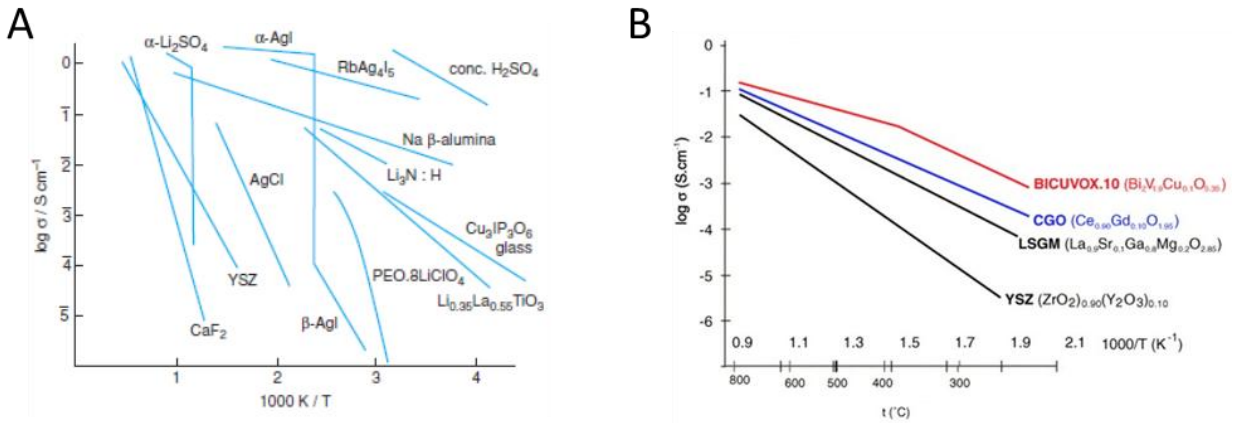

Figure 1.12: The temperature dependence of logarithm of ionic conductivity with temperature of some good solid electrolytes(A)[West 2014] and oxygen conductors (B) [Skinner 2003]

1.3.3. NOx electrochemical sensors: Impedancemetric sensors

Impedancemetric sensors are electrochemical cells with two or more electrodes (Figure 1.13 A). The impedance of a material (Z) describes the electrical response to an alternative applied signal and includes both magnitude (|Z|) and phase angle (θ) information. The relationship 1.9 describes the complex impedance:

$$Z(t) = \mathrm{Re}(Z) + j\,\mathrm{Im}(Z) \tag{1.9}$$

Where Re(Z) is the real component and Im(Z) is the imaginary component:

$$\mathrm{Re}(Z) = |Z|\cos\theta \tag{1.10}$$

$$\mathrm{Im}(Z) = |Z|\sin\theta \tag{1.11}$$

The relationship for phase angle is described by equation 1.12:

$$\theta = \arctan\frac{\mathrm{Im}(Z)}{\mathrm{Re}(Z)} \tag{1.12}$$

and for magnitude |Z| by equation 1.13:

$$|Z| = \sqrt{(\mathrm{Re}(Z))^2 + (\mathrm{Im}(Z))^2} \tag{1.13}$$

Representation of impedance as complex number |Im| and real part |Re| as a function of frequency is named Nyquist plot (Figure 1.13-B). Numbers corresponding to darkened points represent log of frequency in Hz. At 10 Hz, value of $|Z|_1$ in 10.5% O_2 is higher than $|Z|_2$ in 10.5% O_2 +100 ppm NO_2 (or NO). Variation of impedance at low and constant frequency is proportional to target gas concentration and can be used as signal of sensor.

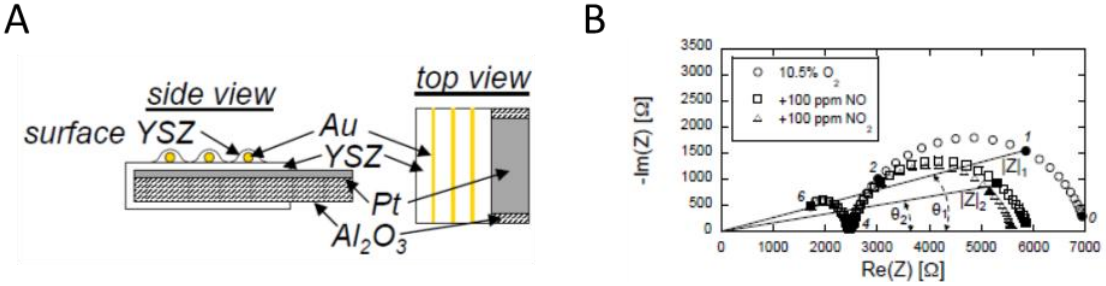

Figure 1.13: Schematic of Pt/YSZ/Au cell – A, and Nyquist plot of Pt/YSZ/Au cell at 650 °C in 10.5% O_2 and in 10.5% O_2 with 100 ppm NO or 100 ppm NO_2 – B [Woo 2007], [Woo 2009]

In the presented impedancemetric devices, low frequency area, around 0.1-10 Hz, reflects the behavior of electrodes, for example Pt and Au, Pt and NiO [Wang 2012], Pt-loaded oxides WO_3, TiO_2, V_2O_5 [Shimizu 2008], which interacts with target gas. High frequency region representing bulk conductivity of electrolyte is not affected by gas.

Despite high number of sensitive materials, utilization of impedancemetric sensor needs high precision measurement system with frequency analyzer. Also, the stability of electrolyte and electrodes with time is strongly required.

1.3.4. NOx electrochemical sensors: Amperometric sensors

In amperometric sensor, measured current is proportional to gas concentration. As example, oxygen amperometric sensor with diffusion barrier is presented on figure 1.14. Constant tension (U) between electrodes produces ionic current I (O^{2-}) in solid electrolyte (YSZ) (Figure 1.14-A). At relative oxygen concentrations below 10%, a linear relation between oxygen partial pressure and limiting current holds to a good approximation of oxygen concentration according to equation:

$$I_{\text{limit}} = -\frac{4FA}{RTL} \cdot D_{O_2} \cdot P_{O_2} \tag{1.14}$$

F is Faraday constant, $F = 9.648\,533 \times 10^4$ C mol^{-1}
A is the cross section of diffusion channel
R is universal gas constant, R = 8.314 472 J K^{-1} mol^{-1}
T is absolute temperature, K
L is the length of diffusion channel
D_{O_2} is the oxygen diffusion coefficient
P_{O_2} is the oxygen partial pressure

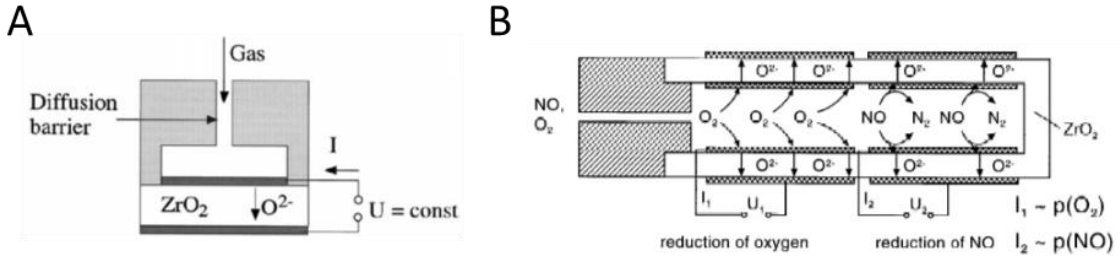

Figure 1.14: Amperometric sensor with diffusion barrier –A and amperometric two electrode cell for the simultaneous detection of oxygen NO – B [Göpel 2000]

M

any

electrochemical reactions can take place on one electrode at constant potential. For improvement of selectivity, amperometric sensors with multielectrodes are used (Figure 1.14-B). Each of electrodes is polarized at different potential to achieve the selectivity to target gas – O_2 and NO by monitoring I_1 (at U_1 - const) and I_2 (at U_2 - const), respectively.

NGK-Siemens commercial NOx sensor is based on same principle (Figure 1.15). Two successive cells are used to separate oxygen and NO_x detection. Oxygen rich exhaust mixture diffuses through first cell. In first cell, oxygen pumping current i_1 is applied and oxygen can be removed from mixture and measured as current i_1. Oxygen concentration in first cell is determined by potentiometric measurement V. Then, gas diffuses in the second cell where NO reduction is possible at low pO_2. Measured current i_2 indicates NO concentration.

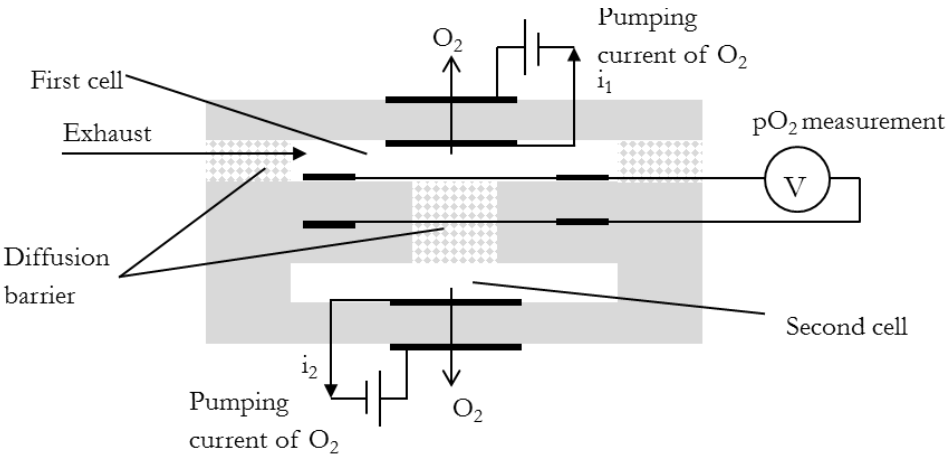

Figure 1.15: NGK-Siemens commercial NOx sensor

Inconvenient of this type of sensor is high complexity, high cost due to the electronics necessary to measure the small sensor signal, and low precision at concentration of NOx below 100 ppm.

1.3.5. NOx electrochemical sensors: Potentiometric sensors

1.3.5.1. Potentiometric sensors without polarization

As was showed in section 1.3.1 potentiometric sensors can be separated in Nernstian and Mixed-potential [Docquier 2002]. For Nernstian sensors, output signal – difference of potential (U) - can be calculated and predicted by Nernst equation 1.5.

The signal of a two electrodes potentiometric sensor (Figure 1.16), in a complex gas environment, shows a non-Nernstian behavior due to the establishment of a mixed potential [Gao 2011], [Somov 1996], [Miura 2002] on the sensing electrode.

Mechanism for mixed potential sensors is more complex, where gases are not in thermodynamic equilibrium at the electrode surface and at the interface with the solid electrolyte. Mixed electrode potential (φ_{MIX}) is obtained from two electrode reactions with different equilibrium potentials (φ_1, φ_2), as for example reactions (1.15) and (1.16).

with φ_1

$$\frac{1}{2}O_2 + V_O^{\bullet\bullet} + 2e^- \longleftrightarrow O_O^x \tag{1.15}$$

with φ_2

$$NO_2 + V_O^{\bullet\bullet} + 2e^- \longleftrightarrow NO + O_o^x \tag{1.16}$$

In general, mixed potential is given by the condition of the net zero current of all involved electrode reactions. This latter is linked to the superposition of parallel electrode reactions, 1.15 and 1.16 for example, occurring at the triple phase boundaries (TPB) of each electrode of potentiometric sensor (Figure 1.16).

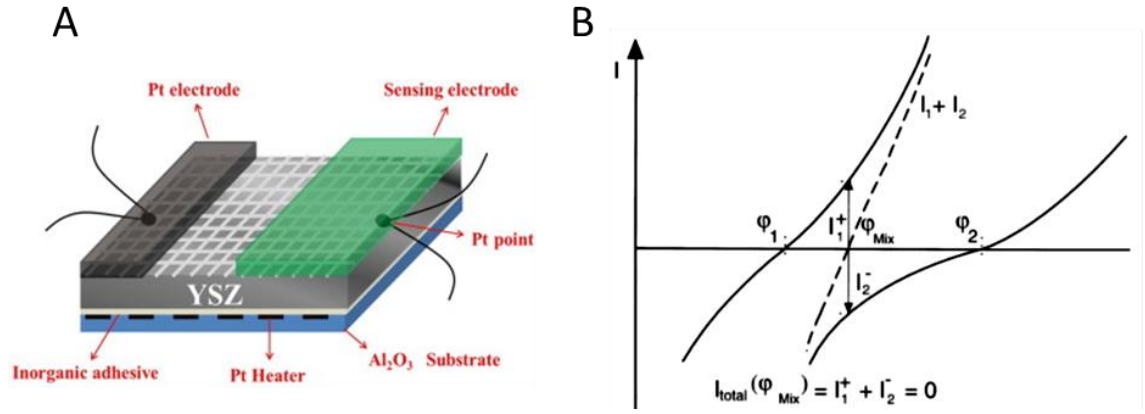

Figure 1.16: Mixed-potential sensor(A) [Yingzhou 2014] and polarization curves for calculation of mixed potential of one electrode (B)

When two electrodes of sensor are exposed to identical atmosphere, a mixed potential φ_{MIX} is realized on each electrode and sensor EMF is the difference of the two φ_{MIX} :

$$EMF = \varphi_{mix}^{RE} - \varphi_{mix}^{SE} \quad (1.17)$$

Where φ_{mix}^{RE} and φ_{mix}^{SE} are respectively the reference and sensing electrode mixed potential.

Sensing characteristics of potentiometric sensor strongly depend on electrode material, temperature and morphology of sensing electrodes. Large numbers of works are concentered to improve sensing characteristics like selectivity and sensitivity of sensors.

Numerous materials have been tested as sensing material in potentiometric sensors at different temperatures In Table 1.3, oxide-based sensing materials are presented for NOx detection.

At the same time, utilization of metals as sensing electrode is possible and widely studied. To produce the EMF, these two electrodes must possess different electrocatalytic activity to detect NOx or other target gases, such as the couples Pt-Au [Gao 2011], [Somov 1996], [Sekhar 2010], Pt-$MnCr_2O_3$ [Yin 2013] or Pt – (Au-oxide) [Zosel 2002].

The morphology of the two electrodes plays a significant role in the number of TPB [Yin 2013], [ChaoYang, 2011], [Zosel 2008] then on the kinetic of the electrode reactions and finally on sensing performances. For instance, a sensor with two Pt based electrodes showing asymmetric morphologies can be effective for NO_2 detection [Yang 2010], [Guillet 2012].

Table 1.3: Materials of sensing electrode for mixed-potential NOx sensors from different authors [Zhuiykov 2007].

Materials of the oxide sensing electrode	Operating temperature (°C)	Measuring concentration (ppm)	Year of publication
WO_3	500–700	5–200	2000
WO_3	450–700	20–1000	2004, 2005
$NiCr_2O_4$	550–650	15–500	2001–2004
$ZnCr_2O_4$	550–650	20–500	2001–2005
$ZnFe_2O_4$	550–700	20–500	2002–2005
ZnO	550–700	50–450	2004, 2005
Cr_2O_3	500–600	100–800	1996, 2003, 2004
Cr_2O_3 + oxidation catalyst	500–600	20–1000	2000–2005
NiO	700–900	50–400	2004, 2005
$LaFeO_3$	450–700	20–1000	2001, 2004
$La_{0.8}Sr_{0.2}FeO_3$	450–700	20–1000	2004
$La_{0.85}Sr_{0.15}CrO_3$/Pt	600–700	20–1500	2005
Tin-doped indium (ITO)	613	100–450	2005
$La_{0.6}Sr_{0.4}Fe_{0.8}Co_{0.2}O_3$	500	100–600	2004
$CuO + CuCr_2O_4$	518–659	10–500	2005

Composite electrodes made of Pt or Au mixed with an oxide is also investigated to improve the sensing performances. Recent studies have reported on Au+YSZ [Striker 2013] composite for

NOx and CO detection at 500°C, Au-NiO, Au-Nb_2O_5 [Zosel 2008] electrodes operated at 650°C, Au-NiO at 600°C [Plashnitsa 2009] and even at 700° or 900°C [Elumalai 2005]. Oxide-based composites often work at high temperature over 550°C allows improving response time and sensitivity, but selectivity of composites does not differ from commonly used materials for potentiometric sensors.

Indeed, the mixed potential solid state sensors are sensitive to numerous gases present in exhaust as NO, NO_2, CO, hydrocarbons, SO_2, NH_3, etc. To solve the problem of cross selectivity, especially to reduce or cancel the response to reducing gases, typically CO and hydrocarbons, a common solution is to use a catalytic filter [Yang, 2008] [Gao 2011], [Yang 2007], [Yang 2010]. Figure 1.17 shows a typical result obtained from J Gao PhD with a Pt/YSZ/Au sensor, at 520°C. Without filter, one can see a positive response to hydrocarbons (C_xH_y), CO and NO, and a negative one with NO_2. With a Pt base filter, the responses to CO and hydrocarbons are removed.

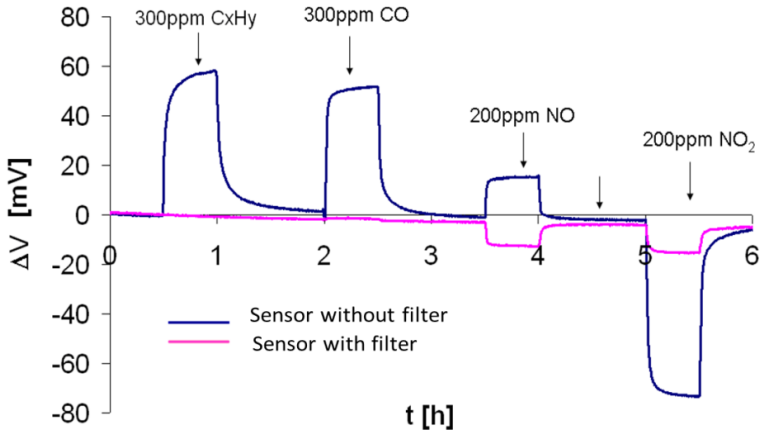

Figure 1.17: Comparison of sensors response with and without catalytic filter at 520°C in 12 % O_2 2 % H_2O, N_2 balance; Flow rate 30 l/h; [Gao 2011]

In the case of NO_x ($NO+NO_2$), another problem is the opposite sensitivity to oxidant (NO_2) and reducing gas (NO). As a result, for a fixed total NOx concentration, the sensor response will vary depending on NO/NO_2 ratio, as shown in figure 1.18 , and even can come close to zero for certain conditions. One can also see that such a sensor has a higher sensitivity to NO_2 than to NO.

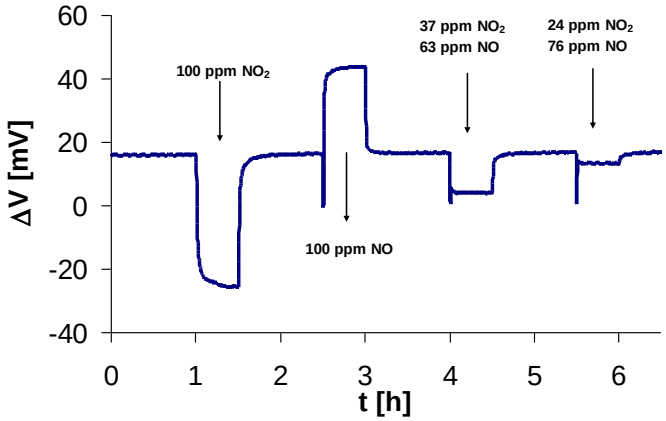

Figure 1.18: Comparison of sensor response without catalytic filter at 520°C in 12 % O_2 2 % H_2O, N2 balance; Flow rate 30 l/h at various proportions of NO_2/NO [Gao 2011]

So, the interest of a catalytic filter is also to set the NO-NO_2 concentrations to a fixed ratio of equilibrium concentrations [NO]/[NO_2] corresponding to the one imposed by thermodynamic equilibrium (eq. 1.18).

$$[NO_2] = [NO] + \frac{1}{2}[O_2] \quad K_{(T,P_{O_2})} = \frac{[NO][O_2]^{\frac{1}{2}}}{[NO_2]} \tag{1.18}$$

Therefore, the [NO]/[NO_2] ratio is only dependent on the temperature, and on partial pressure of oxygen. The decomposition of NO_2 into NO (the white dots) is favored by temperature and at 500 °C for example, only 30% of initial NO_2 concentration is still present (Figure 1.19 B).

A

T (K)	$NO_2 \rightarrow NO + 1/2\ O_2$	
	K_p	α
298	7.23×10^{-7}	1.69×10^{-3}
400	2.53×10^{-4}	3.15×10^{-2}
500	8.00×10^{-3}	1.70×10^{-1}
600	8.09×10^{-2}	4.87×10^{-1}
700	4.22×10^{-1}	8.77×10^{-1}
800	1.47	9.55×10^{-1}

B

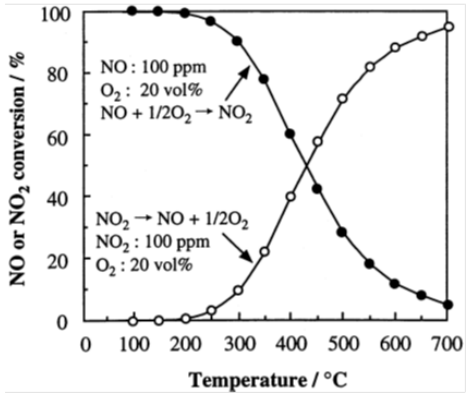

Figure 1.19: Values of the equilibrium constant, Kp, and the dissociation degree, α, corresponding to the thermal decomposition of NO_2 into NO – A [Pârvulescu 1998] and equilibrium conversion of NO and NO_2 at different temperatures – B [Miura 1998]

As a consequence, as seen in figure 1.17, the sensor with a filter presents a similar response to either 200 ppm of NO or NO_2. Indeed, in both cases, the sensor will see the equilibrium concentration, around 140 ppm NO – 60 ppm NO_2 considering NO_2 conversion around 70% at this temperature. As the sensor is more sensitive to NO_2, the resulting response is negative.

To conclude, a only highly NO_2 sensitive to potentiometric sensor equipped with a catalytic filter at a constant temperature and oxygen partial temperature could provide concentrations of NO_2, NO and overall NOx.

1.3.5.2. Potentiometric sensor with polarization

1.3.5.2-a. Potentiometric sensor with constant polarization technic

Another way to obtain selective and sensitive sensors is based on polarized electrochemical cell. Concept of polarized cell for potentiometric measurement of NO or NO_2 in potentiostatic condition of sensing electrode was presented by Miura [Miura 1998], further transformed to amperometric sensor [Miura 1999].

A three-electrode electrochemical cell is showed on Figure 1.20-A. In OCV mode (Open Circuit Voltage, no polarization) sensor produces opposite variation of EMF named E_S, between sensing (SE) and reference (RE) electrodes, to 200 ppm NO and 200 ppm NO_2 (Figure 1.20-B).

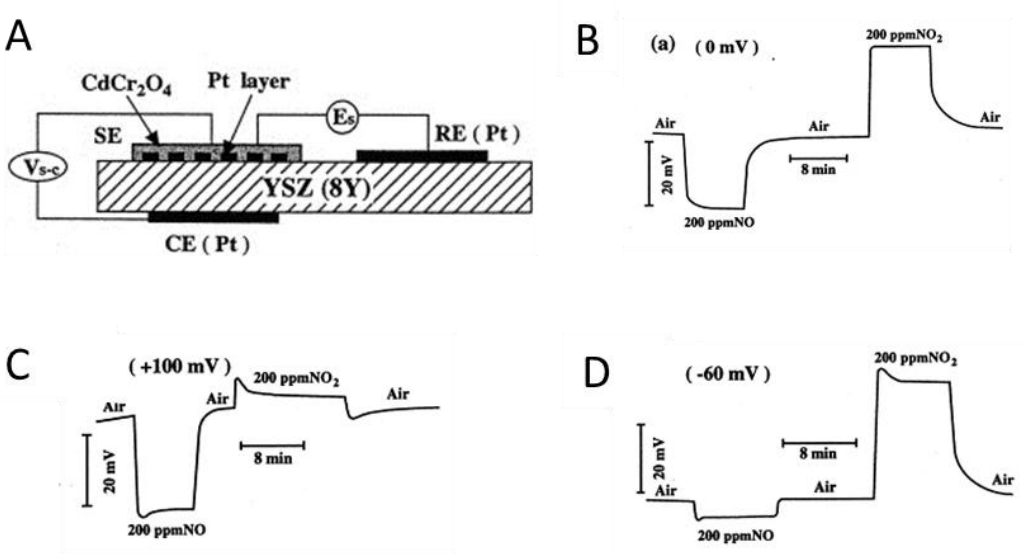

Figure 1.20: Electrochemical cell for NO/NO_2 detection – A and output signal to 200 ppm NO or NO_2 at 500°C without polarization – B, with polarization +100 mV – C, with polarization -60 mV – D [Miura 1998]

When a constant positive polarization V_{C-S} = +100 mV between SE and CE (counter electrode) is applied, in presence of NO, the potential of SE versus RE decrease with identical amplitude than that for V_{C-S}=0. For 200ppm NO_2, the response is 10 times lower (Figure 1.20-C). Opposite behavior of sensor is observed for negative polarization, -60mV (Figure 1.20-D), where response to NO is much lower than for NO_2.

Hence, by applying of voltage to sensing electrode, selectivity to NO over NO_2 or to NO_2 over NO can be controlled electrochemically by using a three-electrode device while keeping sensitivity.

There is also galvanostatic regime, when potential of SE is fixed by constant current. To reach the adjusted current a potential is applied between CE and SE. This method can be applied for two or three electrode cell. In first case, potential is measured between CE and SE, in second – potential of SE is measured versus RE.

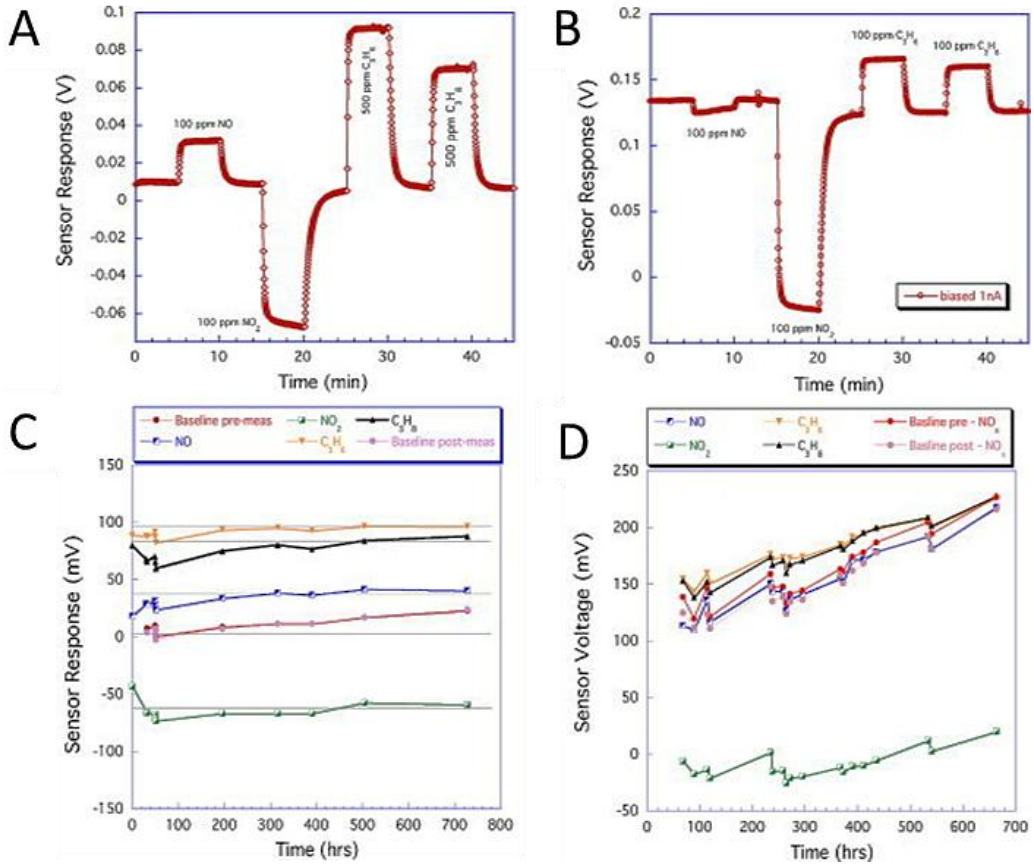

Figure 1.21: Non-biased (A) and biased (B) response of 2-electrode sensor Pt/YSZ/$La_{0.8}Sr_{0.2}CrO_3$, to NO/NO_2 and hydrocarbons; variation of outbut sensor voltage with time non-biased (C) and biased (D) sensor [Sekhar 2010]

Device presented by Praveen K. Sekhar shows increase of sensitivity to 100 ppm NO_2 from -75 mV of non-biased 2 electrodes-sensor to -160 mV for biased by 1 nA (Figure 1.21-A, B). Remarkable is the almost non sensitivity to NO with 1nA bias. At same time, positive response to hydrocarbons C_3H_6 and C_3H_8 is lower than for non-biased device.

Unfortunately, a baseline drift (increase) with time of polarization is observed for biased sensor (Figure 1.21-D. This phenomenon is linked to electrode/electrolyte interface modification under polarization and is observed by numerous authors and for different electrode materials: Au [Raźniak 2011], Pt [Yang 2007], [Mutoro 2008], Pt-YSZ [López-Gándara 2012], Pt-FeOx [Mutoro 2010], Ag [Raźniak 2011], $LaMnO_3$ [Brichzin 2002]. Stability of interface, baseline and sensor signal is very important factors for correct gas detection.

Last PhD work realized by J. Gao in 2007-2011 showed principle possibility of selective and high sensitive detection of NO_2 in exhaust with planar 3-electrode solid state electrochemical cell (Figure 1.22-A).

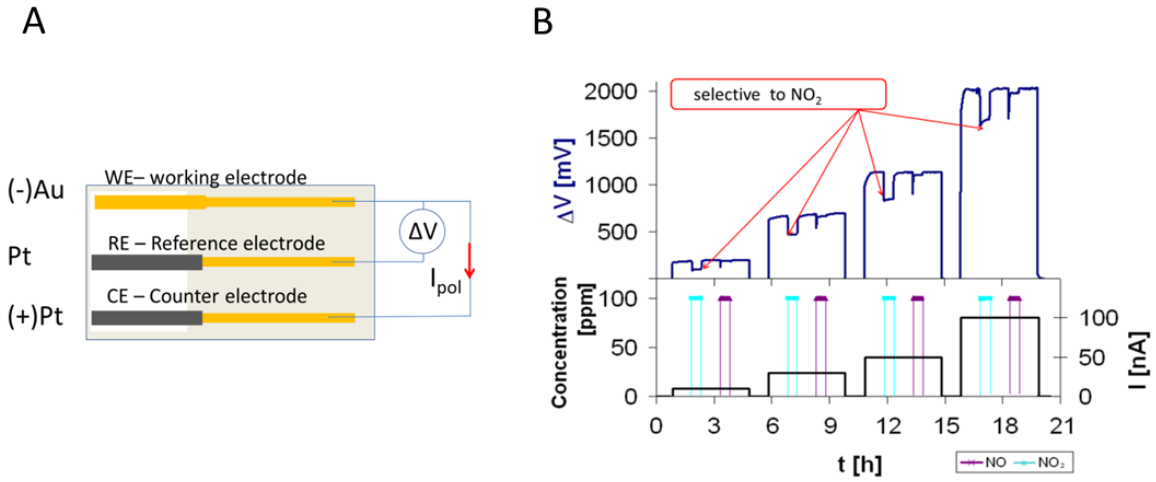

Figure 1.22: Principle design of three electrodes sensor cell (A) and typical response (B) to 100 ppm NO_2 or 100 ppm NO at 450°C in 12% O_2, 1.5% H_2O, N_2 under different polarization current [Gao 2011 PhD].

Electrochemical cell consists in three metallic electrodes on YSZ solid electrolyte deposited on Al_2O_3 substrate with heating element on opposite side. By applying a constant polarization current (I_{pol}) between gold working electrode and platinum counter electrode, measured potential between working and reference electrodes (ΔV) is fixed by polarization current, temperature and oxygen partial pressure. In presence of NO_2 important decrease of measured ΔV is observed and is proportional to NO_2 concentration. Effect of polarization is showed on Figure 1.22 B: by increasing Ipol from 10 nA to 100 nA, decreasing of ΔV grows and it reachs -400 mV for 100 ppm

NO_2 at 100 nA. The selectivity to NO_2 is observed for large region of I_{pol}: 5-100 nA. Moreover, there is no more significant response to NO, but also to any other reducing gases as shown in Figure 1.23. Thus, the polarized sensor is only sensitive to present [NO_2].

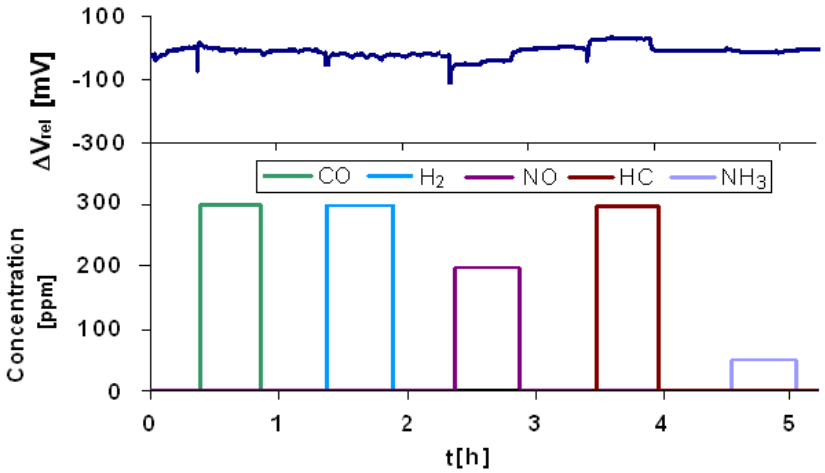

Figure 1.23: The relative response to gases of polarized sensor (Figure 1.22-A) under 100 nA polarization in 12 % O_2; 2 % H_2O; N_2 – balance; Flow rate 30 l/h; Temperature: 450 °C. [Gao 2011 PhD]

As we have previously seen, that the similar sensor without polarization, but with a catalytic filter can give a total NO_x response, an idea was to combine polarization and filter effect. This has been done in Jing Gao PhD and a typical response with polarized sensors, with or without catalytic filter is shown in figure 1.24. The sensor without filter only responds to NO_2. The one with a filter gives a response to NO_2 concentration corresponding to NO/NO_2 equilibrium noted hereafter $[NO_2]_{eq}$.

Knowing the equilibrium constant $K_{(T,P_{O_2})}$ from equation 1.18, this requires temperature but also oxygen concentration knowledge, it is possible to calculate the total NO_x concentration:

$$[NO_X]_{total} = [NO]_{eq} + [NO_2]_{eq} = (1 + K_{(T,P_{O_2})} / [O_2]^{1/2}) \cdot [NO_2]_{eq} \quad (1.19)$$

Finally, combining two sensors and having measurement of [NO_2] with a sensor polarized without filter, one can determine also [NO].

$$[NO] = [NO_X]_{total} - [NO_2] \quad (1.20)$$

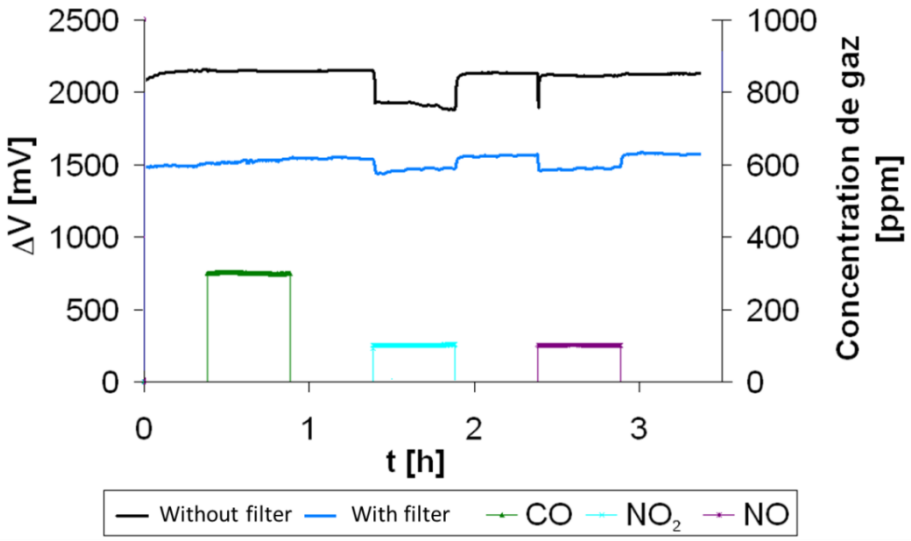

Figure 1.24: The sensor response to CO/NO_2 or NO of polarized sensor equipped or not by catalytic filter (Figure 1.22-A) under 100 nA polarization in 12 % O_2; 2 % H_2O; N_2 – balance; Flow rate 30 l/h; Temperature: 450 °C. [Gao 2011 PhD]

Despite advantages of selectivity, there are still problems to solve:

- Problem of "base line stability" – signal of sensor without NO_2/NO- which is probably linked with electrochemical reaction of oxygen on working electrodes.
- Unknown mechanism of electrochemical detection of NO_2 and origin of "base line"
- Problem of oxygen concentration variation on the sensor response to NOx.

1.3.5.2-b. Potentiometric sensor with pulse polarization technique

The pulsed polarization technique is based on the self-discharge of the electrodes, measured after alternating voltage pulses applied to the electrodes of a conventional lambda sensor [Fischer 2010, Fischer 2012] Figure 1.25 shows electrochemical cell (A) and influence of presence of NO on discharging curves (B): accelerated discharging in NO containing atmosphere compared to that in a base gas at both polarization signs (positive or negative pulse). Presence of NO is calculated as potential of electrode at constant time after polarization pulse.

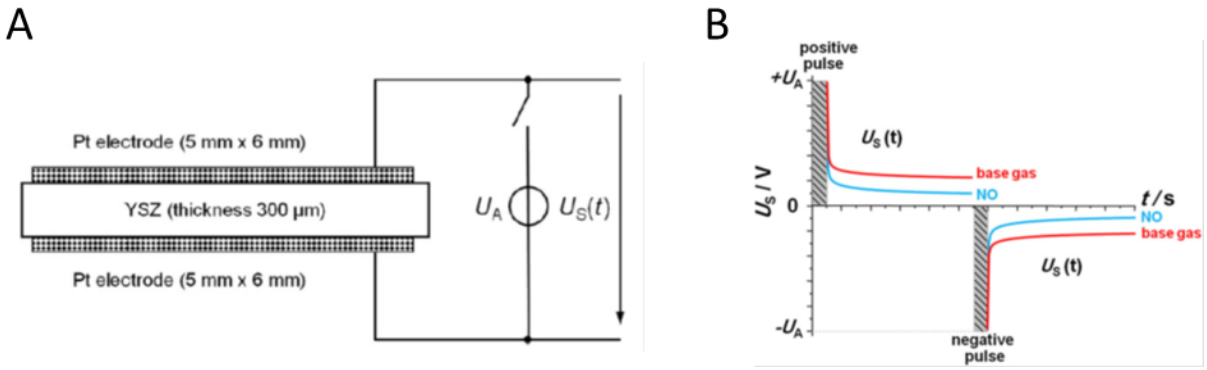

Figure 1.25: Electrochemical cell for NO detection (A) and output signal in presence of NO (B) [Fischer 2012]

This technology is under development. At the moment, it seems that it has low selectivity versus other gases (NH_3, H_2, CxHy) and that there is a high influence of pO_2 on discharging time.

Conclusions

Continuous decrease of automotive emissions limits obliges the vehicle producers to optimize combustion operation and to monitor pollutants in exhaust such as nitrogen oxides – NO_2 and NO. For this application, a sensor working in harsh exhaust environment is needed. In actual demand of industry, it must be precise, stable, cheap and selective to NO_2/NO.

Among numerous possibilities to control NOx in exhaust, electrochemical sensors are widely used and studied. They exist with different technologies with some advantages and inconvenient, as shown previously. Common problem of most of electrochemical sensors is their selectivity to gases, with similar properties to reducing gases like CO, NO, SO_2, NH_3, hydrocarbons etc. Utilization of catalytic filters allows minimizing cross sensitivity by oxidation to inactive CO_2 of CO and hydrocarbons. Transforming by a catalytic filter NO into NO_2 according to thermodynamic equilibrium requires a temperature below 550 °C: at higher temperatures, amount of NO_2 is low, and sensitivity of mixed-potential sensor also decreases because of increasing of catalytic activity of electrodes.

Amperometric sensors can selectively measure concentration of oxygen and NO present in exhaust, but electrochemical reduction of NO to N_2 is unfavorable in oxygen presence. Complex design of amperometric sensors with pumping chambers for O_2 and NO allow separating current from O_2 and NO reduction; meanwhile, current from 10 ppm NO will be around 10^5 times lower than for 10 % O_2. In this condition, precision of amperometric sensor below 100 ppm is low.

Modification of electrode selectivity can be realized by galvanostatic polarization. Potential of electrode fixed by polarization depends on NO_2 concentration. In presence of NO_2, potential of polarized sensing electrode decreases dramatically. This decrease is much higher than for mixed-potential sensors and is absolutely selective to NO_2.

That's why we have decided to continue on the basis of Jing Gao PhD results.

Deeper investigations point out a drift of baseline of sensors with polarization, long term stabilization of baseline and influence of oxygen concentration on it. Published data explain this variation by modification of electrode/electrolyte interface, ageing of solid electrolyte, loss of catalytic activity of electrodes by poisoning. In this context, profound study of role of electrolyte, electrode materials and interface electrode/electrolyte is required.

Utilization of advanced electrode materials like composites allows to increase sensing characteristics of sensor, like response and recovery time, sensitivity, improvement of interface electrode/electrolyte stability, and increases number of triple phase boundaries [Chen 2014 SSE, Chen 2014 S&A], [Zosel 2008], [Striker 2013]. In the objective to optimization of 3-electrodes cell for selective detection of NO_2, this type of electrode material must be developed and studied.

Working in oxygen containing atmosphere, sensing parameters of sensor depend on oxygen concentration. The understanding and interpretation of relationship with sensitivity to NO_2 and O_2 are also a major axis of present work.

The global scientific objective of this PhD is to understand the sensor mechanism under galvanostatic polarization by studying electrochemical parameters of electrolyte and electrodes, role of material and positions of electrodes, then to optimize the sensor design and to define critical parameters of used material: composition, geometry, optimal working conditions.

Bibliography

Brichzin V., Fleig J., Habermeier H.-U., Cristiani G., Maier J., 2002, The geometry dependence of the polarization resistance of Sr-doped LaMnO3 microelectrodes on yttria-stabilized zirconia*, Solid State Ionics,* 152–153, p.499-507.

Brosha E.L., Mukundan R., Brown D.R., Garzon F.H., Visser J.H., 2002, Development of ceramic mixed potential sensors for automotive applications*, Solid State Ionics,* 148, p.61– 69.

ChaoYang X., XuChen L., Yan Y., TiZhuang W., ZhiMin Z., SuPing Y., 2011, Preparation of nano-structured Pt-YSZ composite and its application in oxygen potentiometric sensor*, Applied Surface Science, 257, p.7952-7958*.

Chaugule S.S., Yezerets A., Currier N.W., Ribeiro F.H., Delgass W. N., 2010, Fast NOx storage on Pt/BaO/γ-Al_2O_3 Lean NOx Traps with NO_2+O_2 and NO+O_2: Effects of Pt, Ba loading, *Catalysis Today,* 151(3–4), p.291-303.

Chen Y., Xia F., Xiao J., 2014, Effect of electrode microstructure on the sensitivity and response time of potentiometric NOx sensors based on stabilized-zirconia and La5/3Sr1/3NiO4–YSZ sensing electrode, *Solid-State Electronics, 95, p.23-27*.

Chen Y., Xiao J., 2014, Effects of YSZ addition on the response of La2CuO4 sensing electrode for a potentiometric NOx sensor, *Sensors and Actuators B: Chemical, 192, p.730-736*.

Chevallier L., Di Bartolomeo E., Grilli M. L., Mainas M., White B., Wachsman E. D., Traversa E., 2008, Non-Nernstian planar sensors based on YSZ with a Nb2O5 electrode*, Sensors and Actuators B,* 129 , p.591–598.

Citepa 2010*,* Emission dans l'air en France Métropole - Substances relatives à l'acidification, l'eutrophisation et à la pollution photochimique, *Centre Interprofessionnel Technique d'Etudes de la Pollution Atmosphérique, 2010, (http://www.citepa.org).*

Clayton R.D., Harold M. P., Balakotaiah V., Wan C.Z., 2009, Pt dispersion effects during NOx storage and reduction on Pt/BaO/Al2O3 catalysts, *Applied Catalysis B: Environmental,* 90(3–4), p.662-676.

Di Franco C, Elia A, Spagnolo V, Scamarcio G, Lugarà PM, Ieva E, Cioffi N, Torsi L, Bruno G, Losurdo M, Garcia MA, Wolter SD, Brown A, Ricco M., 2009, Optical and Electronic NO(x) Sensors for Applications in Mechatronics, *Sensors (Basel), 9(5), p.3337-3356*.

DiGiulio C.D., Pihl J. A., Parks II J. E., Amiridis M. D., Toops T. J., 2014, Passive-ammonia selective catalytic reduction (SCR): Understanding NH3 formation over close-coupled three way catalysts (TWC), *Catalysis Today,* 231, p.33–45.

Docquier N., Candel S., *2002,* Combustion control and sensors: a review, *Progress in energy and combustion Science,* 28, p.107-150.

EEA report, 2013, National emissions reported to the Convention on Long-range Transboundary Air Pollution (LRTAP Convention) (http://www.eea.europa.eu).

Elumalai P., Miura N., 2005, Performances of planar NO_2 sensor using stabilized zirconia and NiO sensing electrode at high temperature, *Solid State Ionics,* 176(31–34), p.2517-2522.

Fergus J.W., 2011, Sensing mechanism of non-equilibrium solid-electrolyte-based chemical sensors review, *Journal of Solid State Electrochemistry, 15, p.971–984.*

Fischer S., Pohle R., Farber B., Proch R., Kaniuk J., Fleischer M., Moos R., 2010, Method for detection of NOx in exhaust gases by pulsed discharge measurements using standard zirconia-based lambda sensors, *Sensors and Actuators B: Chemical*, 147(2-3), p.780-785.

Fischer S., Pohle R., Magori E., Schönauer-Kamin D., Fleischer M., Moos R., 2012, Pulsed polarization of platinum electrodes on YSZ*, Solid State Ionics,* 225, p.371–375.

Gao J., Viricelle J-P., Pijolat C., Vernoux P., Boreave A., Giroir-Fendler A., 2011, Improvement of the NOx selectivity for a planar YSZ sensor, *Sensors and Actuators B: Chemical,* 154(2), p.106-110.

Gao, J., 2011 PhD *Etude et mise au point d'un capteur de gaz pour la détection sélective de NOx en pot d'échappement d'automobile*. Thèse de doctorat. École Nationale Supérieure des Mines de Saint-Étienne

Göpel W., Reinhardt G., Rösch M., 2000, Trends in the development of solid state amperometric and potentiometric high temperature sensors*, Solid State Ionics,* 136 –137, p.519 – 531.

Guillet N., Lalauze R., Viricelle J.P., Pijolat C., 2002, The influence of the electrode size on the electrical response of a potentiometric gas sensor to the action of oxygen, *IEEE Sensors Journal*, 2(4), p.349-353.

Hadjar A., Hernández W.Y., Princivalle A., Tardivat C., Guizard C., Vernoux P., 2011, Electrochemical activation of Pt–Ba/YSZ NOxTRAP catalyst under lean-burn conditions, *Electrochemistry Communications,* 13(9), p.924-927.

Hill Brothers, 2010*, Eco-DEF system (http://hillbrothers.com/eco-def).*

Ishihara T., Sato S., Takita Y., 1995*,* Capacitive-type sensors for the selective detection of nitrogen oxides, *Sensors and Actuators B: Chemical, 2*5(1–3), p.392-395.

Kobayashi N., Yamashita A., Naito O., Setoguchi T., Murase T., 2001, Development of Simultaneous NOx/NH3 Sensor in Exhaust Gas, *Mitsubishi Heavy Industries, Ltd. Technical Review, .38(3)*

López-Gándara C., Fernández-Sanjuán J.M., Ramos F.M., Cirera A., 2012, Estimation of the electrodes' three phase boundary sites in electrochemical exhaust gas sensors before and after electric polarization, *Sensors and Actuators B: Chemical,* 175, p.225-233.

Miura N., Lu G., Ono M., Yamazoe N., 1999, Selective detection of NO by using an amperometric sensor based on stabilized zirconia and oxide electrode, *Solid State Ionics,* 117(3–4), p.283-290.

Miura N., Lu G., Yamazoe N., 1998, High-temperature potentiometric/amperometric NOx sensors combining stabilized zirconia with mixed-metal oxide electrode*, Sensors and Actuators B: Chemical,* 52(1–2), p.169-178.

Miura N., Zhuiykov S., Ono T., Hasei M., Yamazoe N., 2002, Mixed potential type sensor using stabilized zirconia and ZnFeO4 sensing electrode for NOx detection at high temperature, *Sensors and. Actuators B,* 83, p.222–229.

Mutoro E., Günther S., Luerßen B., Valov I., Janek J., 2008, Electrode activation and degradation: Morphology changes of platinum electrodes on YSZ during electrochemical polarisation, *Solid State Ionics,* 179(33–34), p.1835-1848.

Mutoro E., Koutsodontis C., Luerssen B., Brosda S., Vayenas C.G., Janek J., 2010, Electrochemical promotion of Pt(1 1 1)/YSZ(1 1 1) and Pt–FeOx/YSZ(1 1 1) thin catalyst films: Electrocatalytic, catalytic and morphological studies, *Applied Catalysis B: Environmental,* 100(1–2), p.328-337.

Nissan Motor Corporation*, HC-NOx trap catalyst (http://www.nissan-global.com)*

Ohtani N., Morita T., Endo M., Nanri K., Fujioka T., and Yamaguchi S., 2004, Development of NOx sensor system by using a mid-IR coherent light source for exhaust emission monitoring" in Conference on Lasers and Electro-Optics, *International Quantum Electronics Conference and Photonic Applications Systems Technologies*, Technical Digest (CD) ,Optical Society of America, 2004), paper CThT18.

Pârvulescu V.I., Grange P., Delmon B., 1998, Catalytic removal of NO, *Catalysis Today,* 46(4), p.233-316.

Pijolat C., Tournier G., Viricelle J.P., 2009, Detection of CO in H_2-rich gases with a samarium doped ceria (SDC) sensor for fuel cell applications, *Sensors and Actuators B,* 141(1) p.7-12.

Plashnitsa V.V., Elumalai P., Fujio Y., Miura N., 2009, Zirconia-based electrochemical gas sensors using nano-structured sensing materials aiming at detection of automotive exhausts, *Electrochimica Acta,* 54(25), p.6099-6106.

Raźniak A., Dudek M., Tomczyk P. 2011, Reduction of oxygen at the interface M|solid oxide electrolyte (M = Pt, Ag and Au, solid oxide electrolyte = YSZ and GDC). Autocatalysis or artifact?, *Catalysis Today,* 176(1), p.41-47.

Regulation No 715/2007 of the European Parliament and of the Council of 20 June 2007. *Official Journal J,* L 171(030), p.284-299.

Rico-Pérez V., M. Ángeles Velasco Beltrán, Qinggang He, Qi Wang, Salinas Martínez de Lecea C., Bueno López A, 2013, Preparation of ceria-supported rhodium oxide sub-nanoparticles with improved catalytic activity for CO oxidation, *Catalysis Communications,* 33, p.47-50.

Riegel J., Neumann H., Wiedenmann H.-M., 2002, Exhaust gas sensors for automotive emission control, *Solid State Ionics,* 152–153, p.783-800.

Schnitzler J., *2010,* Particulate Matter and NOx Exhaust Aftertreatment Systems*, FEV Motorentechnik GmbH (http://www.fev.com)*

Sekhar P.K., Brosha E.L., Mukundan R., Li W., Nelson M. A., Palanisamy P., Garzon F.H., 2010, Application of commercial automotive sensor manufacturing methods for NOx/NH_3 mixed potential sensors for on-board emissions control, *Sensors and Actuators B: Chemical,* 144(1), p.112-119.

Sharma A., Tomar M., Gupta V., 2013, A low temperature operated NO_2 gas sensor based on TeO_2/SnO_2 p–n heterointerface, *Sensors and Actuators B: Chemical,* 176, p.875-883.

Shimizu K, Kashiwagi K., Nishiyama H., Kakimoto S., Sugaya S., Yokoi H., Satsuma A. 2008, Impedancemetric gas sensor based on Pt and WO_3 co-loaded TiO_2 and ZrO_2 as total NOx sensing materials, *Sensors and Actuators B: Chemical,* 130(2), p.707-712.

Sinka Zs., Kovács J., Yuzhakova T., Lako J., 2011,Vehicle exhaust gas emission and its catalytic depollution, *Hungarian journal of industrial chemistry veszprém,* 39(1) p.79-83.

Skinner S.J., Kilner J.A., 2003, Oxygen ion conductors*, Materials Today,* 6(3), p30-37.

Somov S., Reinhardt G., Guth U., Göpel W., 1996, Gas analysis with arrays of solid state electrochemical sensors: implications to monitor HCs and NOx on exhaust, *Sensors and Actuators B,* 35-36, p.409-418

Striker T., Ramaswamy V., Armstrong E. N., Willson P. D., Wachsman E. D., Ruud J. A., 2013, Effect of nanocomposite Au–YSZ electrodes on potentiometric sensor response to NOx and CO, *Sensors and Actuators B,* 181, p.312-318.

The Freedonia Group Study #2470, 2009, World Diesel Engines, Industry Study with Forecasts for 2012 – 2017, 331 pages

Thematic Strategy on air pollution, 2005, *Communication from the commission to the council and the European parliament*, Brussels.

Tuller H.L., 2013, Materials for high temperature electrochemical applications: Automotive sensors, catalysts and traps, *Sensors and Actuators B: Chemical,* 187, p.106-110.

Wang L., Zeng-Chuan Hao, Lei Dai, Yuehua Li, Huizhu Zhou, 2012, A planar, impedancemetric NO2 sensor based on NiO nanoparticles sensing electrode, *Materials Letters,* 87, p.24-27.

West A.R., 2014, Solid State Chemistry and its Applications Second Edition, Department of Materials Science and Engineering, University of Sheffield, K, 2014

Woo L.Y., Glass R.S., Novak R.F., Visser J.H., 2009, Effect of electrode material and design on sensitivity and selectivity for high temperature impedancemetric NOx sensors, *Journal of The Electrochemical Society*, 157, p.81-87.

Woo L.Y., Martin L.P., Glass R.S., and Gorte R.J., 2007, Impedance characterization of a model Au/Yttria-stabilized zirconia/Au electrochemical cell in varying oxygen and Nox concentrations, *Journal of The Electrochemical Society,* 154 (4), p.129-135.

Yang J.-C., Dutta P. K., 2010, High temperature potentiometric NO_2 sensor with asymmetric sensing and reference Pt electrodes, *Sensons and Actuators B: Chemical, 143(2), p.459-463.*

Yang J.-C., Dutta P.K., 2007, High temperature amperometric total NOx sensors with platinum-loaded zeolite Y electrodes, *Sensors and Actuators B: Chemical,* 123(2), p.929-936.

Yang J.-C., John V. Spirig, Dale Karweik, Jules L. Routbort, Dileep Singh, Prabir K. Dutta, 2008, Compact electrochemical bifunctional NOx/O2 sensor with metal/metal oxide internal reference electrode for high temperature applications, *Sensors and Actuators B: Chemical,* 131, p.448–454.

Yin C., Guan Y., Zhu Z., Liang X., Wang B., Diao Q., Zhang H., Ma J., Liu F., Sun Y., Zheng J., Lu G., 2013, Highly sensitive mixed-potential-type NO_2 sensor using porous double-layer YSZ substrate, *Sensors and Actuators B: Chemical,* 183, p.474-477.

Guan Y., Li C., Cheng X., Wang B., Sun R., Liang X., Zhao J., Chen H, Lu G., 2014, Highly sensitive mixed-potential-type NO_2 sensor with YSZ processed using femtosecond laser direct writing technology, *Sensors and Actuators B: Chemical, 1*98, p.110-113.

Zhang J., 2010, *Diesel Emmision Technology – Part II of Automotive After-treatment System, (www.bowmannz.com)*

Zhuiykov S., Miura N., 2007, Development of zirconia-based potentiometric NOx sensors for automotive and energy industries in the early 21st century: What are the prospects for sensors? *Sensors and Actuators B: Chemical,* 121, p.639–651.

Zhuiykov S., 2008. *Electrochemistry of Zirconia Gas Sensors,* CRC Press

Zosel J., Tuchtenhagen D., Ahlborn K., Guth U., 2008, Mixed potential gas sensor with short response time, *Sensors and Actuators B: Chemical,* 130, p.326-329.

Zosel J., Westphal D., Jakobs S., Müller R., Guth U., 2002, Au-oxide composites as HC-sensitive electrode material for mixed potential gas sensors, *Solid State Ionics,* 152-153, p.525-529.

Chapter 2

Materials and methods

Outline

Chapter 2: Materials and methods

Résumé

Ce chapitre est consacré aux techniques d'élaboration et de caractérisation de capteurs potentiométriques.

D'une part, nous présentons la procédure de fabrication d'un capteur à trois électrodes qui peut satisfaire les exigences d'une application industrielle dans le domaine automobile. La technique de sérigraphie permet de réaliser facilement l'élément sensible du capteur, de diminuer le prix et d'avoir une haute reproductibilité en cas de production en série. Ce chapitre définit aussi les paramètres importants étudiés pour les capteurs chimiques : temps de réponse, temps de recouvrement, ligne de base, sensibilité, etc.

D'autre part, le développement et la caractérisation d'un matériau d'électrode avec des méthodes électrochimiques et physiques ont été décrits. Les paramètres importants comme le temps de réponse, la sensibilité, la sélectivité et la stabilité dépendent de la morphologie et de la composition de l'électrode sensible. La spectroscopie d'impédance permet d'étudier les propriétés électriques intrinsèques du matériau. D'autres méthodes ont été utilisées pour l'étude complète des propriétés morphologiques et autres du matériau d'électrode : la microscopie optique, la microscopie électronique, les mesures de la surface spécifique BET, la spectroscopie par fluorescence X, la granulométrie laser, la potentiomètrie, etc….

Summary

Present chapter describes methods used for characterization of materials developed for solid-state electrochemical sensors. It contains the technological details of exhaust sensors fabrication, and describes their main characteristics and controlled parameters.

Screen-printing technology is used for manufacturing of experimental samples and sensors. The advantages of this method are low cost, productivity and acceptable precision of production. But still it needs accurate realization and choice of appropriate materials. The preparation and composition of used ink is also described.

The scanning electron microscopy and electrochemical impedance spectroscopy are major methods for sensor material characterization. The first shows the morphology of electrodes and electrolytes as a function of composition and preparation procedure; the second allows separating different behaviors of material, as electrical resistance of solid state electrolyte and interface resistance of electrode/electrolyte contact.

Also, this chapter describes main parameters of sensor, as response and recovery time, overpotential, ohmic drop, etc.

The used equipment as laboratory handmade potentiostat, test bench with exhaust gas simulated composition and other secondary methods as optic microscopy, fluorescence spectroscopy, measurement of specific surface, laser granulometry, etc., are presented in this chapter.

2.1. Sensor elaboration procedure

2.1.1. Screen printing deposition

Solid state sensors were manufactured by screen-printing. This technology is based on deposition of a smooth ink or paste on substrate through a screen (Figure 2.1). Deposited layer can reach from 10 to 100 µm thickness. For this technology, homemade and commercial pastes were used.

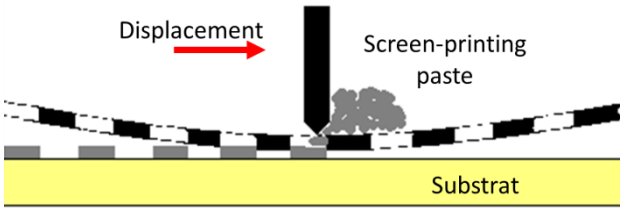

Figure 2.1: Screen-printing deposition

Preparation of sensors was realized in two laboratories, either in ENSM Saint-Etienne or in industrial partner MEAS France in Toulouse. Identical pastes were used in all preparation steps.

Figure 2.2 shows major steps of sensor production. On the alumina substrate with 5 parallel future cell (figure 2.2-A) a functional and porous layer (5x5 mm per cell) (figure 2.2-B) of solid electrolyte (YSZ: $(ZrO_2)_{0.92}(Y_2O_3)_{0.08}$ provided by Superconductive) was deposited by screen-printing (200 mesh mask) from a home-made ink containing 60% of YSZ powder, 25% of organic binder (ESL V400A) and 15% of solvent ESL 404. After deposition, samples were dried for 15 min in air at 120°C (Memmert 100 furnace) and then sintered at 1380 °C in air for 2 hours with a ramp of 5°C/min.

The platinum heating element (Figure 2.2-C) from commercial ink (ESL 5545) with gold contact pads from commercial ink (ESL 8880-H) are deposited on opposite side of substrate, dried for 15 min in air at 120°C (Memmert 100 furnace) and then sintered at 980 °C in air for 1 hour with a ramp of 5°C/min.

The final depositions of electrodes and contacts pads on YSZ were made by using different screens and materials of inks. The detailed descriptions of manufactured cells and the inks composition are presented hereafter.

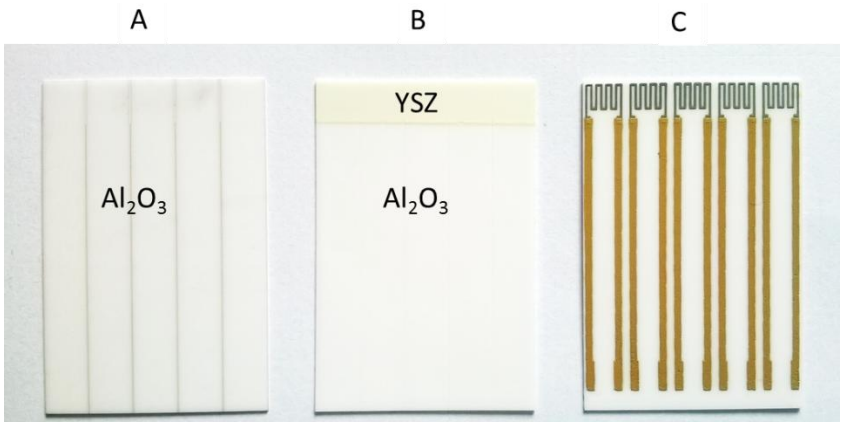

Figure 2.2: Principles steps of screen-printing production of sensors. A – alumina substrate CoorsTek, B – substrate with deposed and fired YSZ electrolyte, C – opposite side with heating element

2.1.2. Commercial and home-made inks compositions

In this work, commercial and homemade inks based on commercial available materials were used. In product data sheet of commercial Au and Pt based inks, detailed composition and impurities contents are not specified. For that reason, we performed ink analysis by ICP (Jobin-Yvon JY138 Ultrace). Results are shown on figure 2.3.

Major impurities in Pt paste are Ti – 2.8 mol %, Zn – 0.9 mol %, Cr – 0.39, Fe – 0.26 mol %, Al – 1600 ppm, Ca – 770 ppm, Cu – 570 ppm, Na – 340 ppm. Gold ink is more pure, major pollution concerns 1500 ppm of Cu, and around 30-20 ppm of Na, Zn, K, Al have been detected in the Au paste.

So we have to keep in mind that the electrodes materials are not pure gold and platinum respectively. This may explain some future results, especially for the behavior of the "gold" electrode.

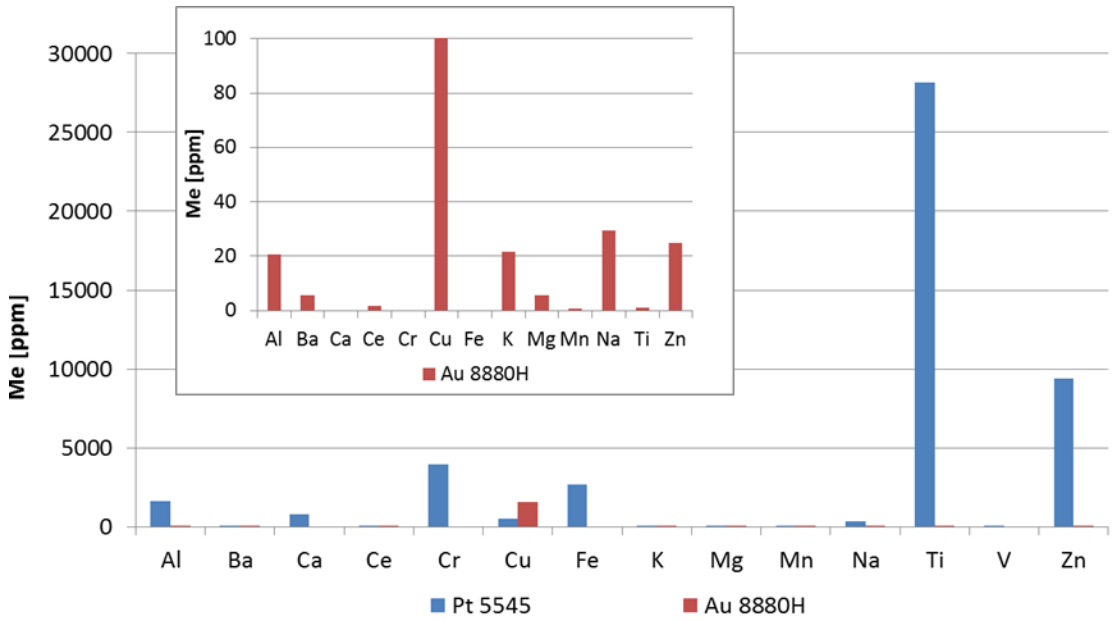

Figure 2.3: ICP analysis of Pt (ESL 5545) and Au (ESL 8880-H) commercial ink

2.1.3. Preparation of electrolyte paste and gold based composite paste

Two composite gold-based pastes for electrodes were prepared by mixing the Au commercial paste (ESL 8880-H) either with 10 wt % homemade YSZ or with 10 wt % homemade ZrO_2 ink. Resulting inks will be denoted respectively AuY and AuZ. Home-made ZrO_2 and YSZ inks have similar composition as mentioned previously for the sensing element (YSZ porous layer), that is 60% of the considered powder (YSZ or ZrO_2 (Merck)), 25% of organic binder (ESL V400A) and 15% of solvent ESL.

For the preparation of homemade inks, the powders (YSZ or ZrO_2) are mixed with ESL V400A and solvent ESL T404 with spatula, in order to obtain an homogeneous paste, and then passed through a 3-roll mill with a constant roll speed and decreasing gap size (always Gap 1>Gap 2) (Figure 2.4 and table 2.2)

For composite Au inks, elaboration is similar: after simple mixing of Au ink with YSZ or ZrO_2 ink with spatula, the result homogeneous paste must be passed through a 3-roll mill with a constant roll speed and decreasing gap size (always Gap 1 > Gap 2). In both cases, the time of mixing is limited to 8-10 minutes to avoid important evaporation of solvent and formation of dense paste particles on ceramic scratcher used for ink extraction.

Final YSZ and ZrO_2 inks are white pastes, without any sand-like particles. Composite gold pastes AuY and AuZ have gold-like color without any white traces.

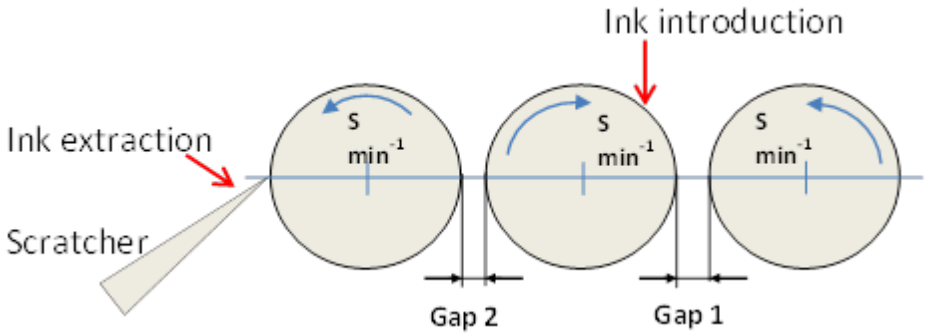

Figure 2.4: Schema of EXACT 3-roll mill.

Table 2.2: Mixing method procedure with 3 roll mill

	First passing	Second passing	Third passing	If necessary
Gap **1**, µm	130 – 80	80 – 30	30 – 10 (5)	10 – 5
Gap **2**, µm	120 – 70	70 – 20	20 – 10 (5)	10 – 5
S, roll speed, min^{-1}	30	30	30	30

The depositions were further dried for 15 minutes at 120°C and then sintered at 850°C for 2 hours in air with a ramp of 5°C/min. After decomposition of all organic compounds estimated to 40% in each pastes Au, YSZ and ZrO_2, final amount of ceramic fraction in composite electrodes reaches around 9.5 wt %.

2.1.4. Preparation of the catalytic filter

Catalytic filter was developed by J.Gao in her PhD work. It consists in an alumina commercial powder with dispersed platinum (5% wt Pt, MERCK) and an aluminum isopropoxide (Aldrich 220418). Alumina powder, before mixing with the isopropoxide, was milled in ethanol by planetary mill (Retsch, model PM400) during 8 hours, 200 min^{-1} rotating rate, 30 min. in each direction, to obtain particle size around 1 µm. Then, it is mixed with the isopropoxide (10wt %) which is an alumina precursor: it's decomposition during thermal treatment allows strengthening the mechanical cohesion of the filter layer and its adhesion on the substrate, that is to say on the sensing element. The mixing method is identical to YSZ paste preparation. Final catalytic filter ink is a black paste, without any sand-like particles.

Deposition of the filter on the electrochemical cell, as shown in figure 2.5-C for example, is the last step of sensor preparation. Deposited layer is further dried for 15 minutes at 120°C and then sintered at 850°C for 2 hours in air with a ramp of 5°C/min.

2.1.5. EMSE sensors

In conventional two-electrode sensor (Figure 2.5-A), platinum electrode placed leftward is used as reference electrode (RE). Gold-based electrode placed rightward is the sensing electrode (SE). In three-electrode cell, reference electrode is placed between counter (CE) and sensing electrodes (Figure 2.5-B). In test with galvanostatic polarization, sensing electrode is also called as Working Electrode (WE). The final sensor is presented on figure 2.5-C: sensing element of sensors is covered by the catalytic filter, the contacts pads and heating element are cowered by a dielectric protective layer (blue color).

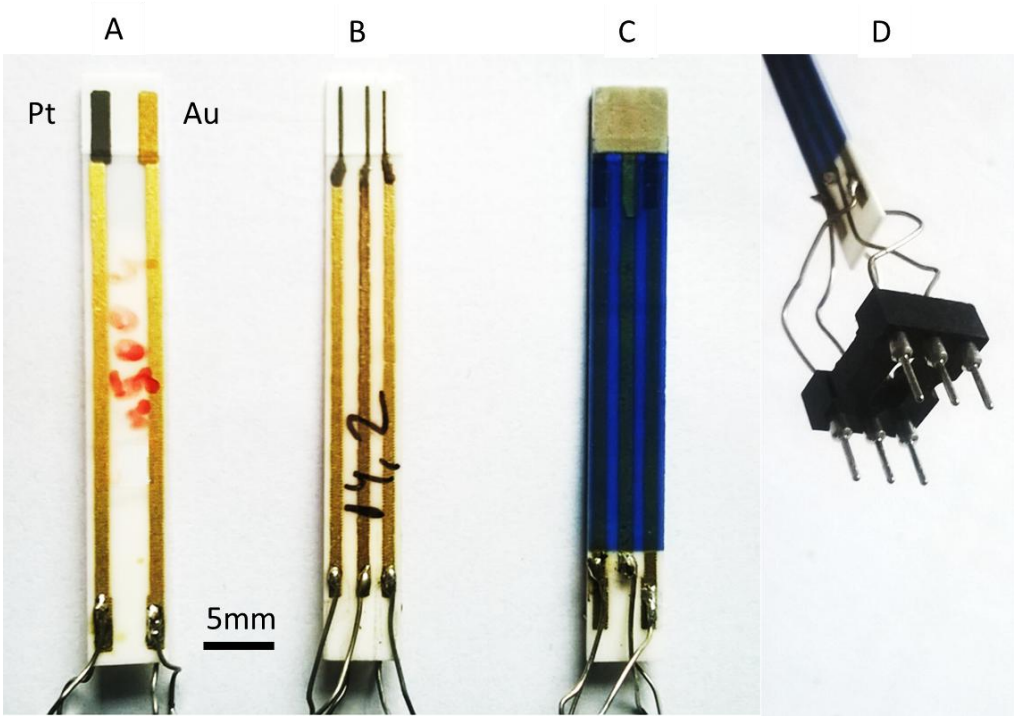

Figure 2.5: Photo of whole sensors: A – two-electrode cell Pt/YSZ/Au, B – three-electrode sensor, C – three-electrodes sensor covered by catalytic filter and dielectric, D – 6-pin connector for EMSE test bench.

In 2-electrodes sensor, platinum and gold electrodes of 0.5-1 mm width and 4 mm length were screen-printed on the surface of the YSZ layer using a commercial paste of Pt (ESL 5545) and Au (ESL 8880-H). Distance between electrodes was around 2 mm. The depositions were further dried for 15 minutes at 120°C and then sintered at 850°C for 2 hours in air with a ramp of 5°C/min.

The three electrodes sensor has much thinner electrodes around 0.2-0.4 mm and identical length of 4 mm. The depositions were further dried for 15 minutes at 120°C and then sintered at 850°C for 2 hours in air with a ramp of 5°C/min.

For electrical contact in test bench, the wires were soldered to gold pads and 6-pin connector (Figure 2.5-D)

2.1.6. MEAS sensors

Sensor prototypes manufactured in Toulouse (Figure 2.6.) were made by screen printing on Al_2O_3 substrate of 52 mm length, 5 mm wide and 0.6 mm thickness. Complete prototype sensing cell is shown in figure 2.6 A-B. It consists of sensing element (Figure 2.6-D) covered with a catalytic filter (Figure 2.6-C) and with a dielectric protector on current collectors (Figure 2.6-B, blue color). On reverse side, the heating element is also protected by the same dielectric (Figure 2.6-A).

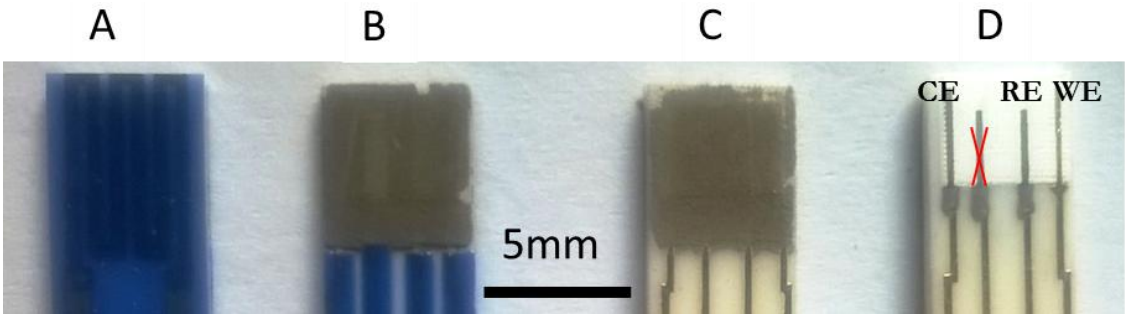

Figure 2.6: Photos of four-electrodes MEAS sensor: A – heating element side, B – top view of cell with catalytic filter on sensing element, C – top view of cell without dielectric on contacts, D – top view of sensing element without any protection

From the four electrodes presented on figure 2.6-D, in working conditions, only three are used: WE, RE and CE. The fourth electrode is not connected in any tests. Prototypes presented on figure 2.6 were used for polarization tests and determination of characteristic of WE materials.

2.1.7. Other EMSE devices for characterizations

Some specific particular cells with two or three-electrode (Figure 2.7) were also fabricated in EMSE for electrochemical characterization of solid electrolyte and electrodes by impedance spectroscopy, polarization and potentiometric measurements.

Indeed, to analyze the behavior of an electrode /electrolyte interface by Electrochemical Impedance Spectroscopy (EIS), a symmetric device with similar nature of the two electrodes is required. Photos of symmetric Au/YSZ/Au (A), Pt/YSZ/Pt (B) are presented on figure 2.7.

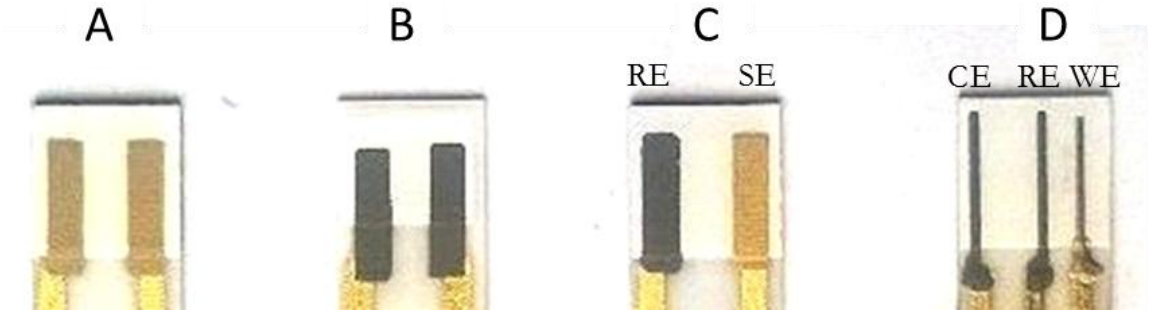

Figure 2.7: Photo of symmetric two electrode cell: A – Au/YSZ/Au, B – Pt/YSZ/Pt, C – typical potentiometric sensor Pt/YSZ/Au and D – three-electrode sensor cell fabricated in EMSE.

Figures 2.7-C depict the sensing element of typical two-electrode EMSE sensor with Pt reference and Au sensing electrodes and the picture 2.7-D a three-electrode sensor with Pt counter and reference electrodes and Au working electrode. The notations of electrodes and measured signals are presented in paragraph 2.3.

In other particular tests, we studied the influence of reference electrode position, between Working and Counter electrodes. To do this, devices with various electrodes spaces were manufactured.

As example, figure 2.8 depicts photos of three-electrode cells with three Pt electrodes. Position of the inner small electrode, used as reference, is varied.

Another set of samples with varying spacing between electrodes, but also length of reference electrode and nature of working electrode (gold instead of platinum) was prepared (Figure 2.9). Distance between electrodes was measured by optic microscope software as shown by red and yellow lines on figure 2.9.

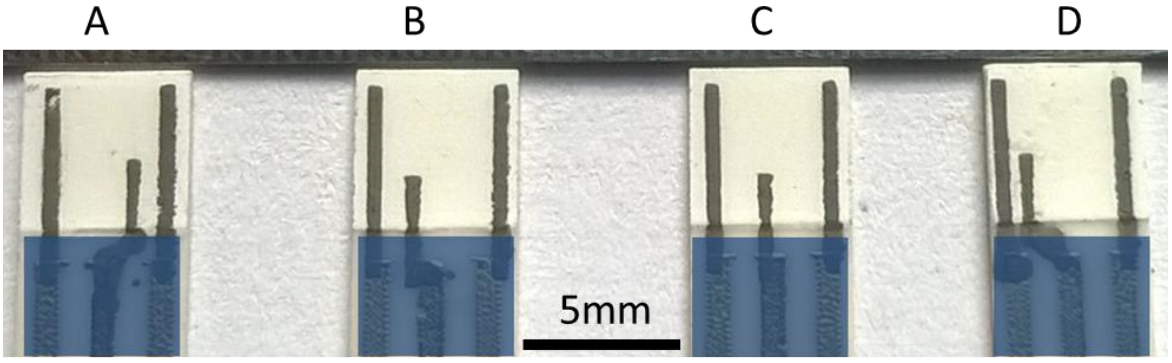

Figure 2.8: Photo of three- electrode cell with different position of reference electrode manufactured in EMSE.

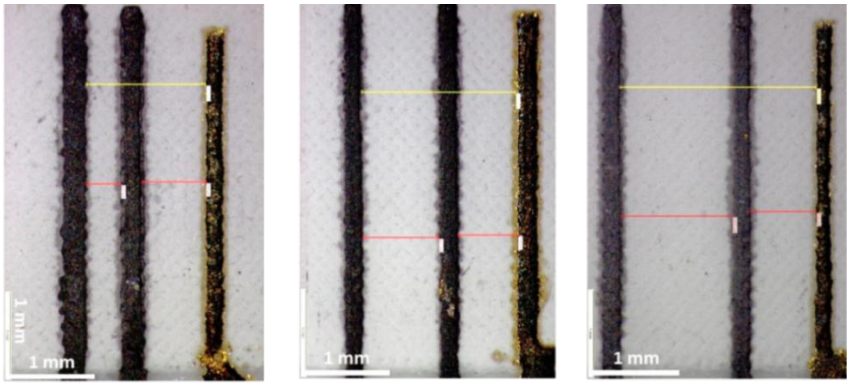

Figure 2.9: Photo of three-electrode sensors with different CE-WE electrode spacing manufactured in EMSE

2.1.8. Repeatability and ageing of sensors before testing

Mass production (millions) of sensors with industrial tools allows reaching good repeatability of sensors characteristics as, thickness of electrolyte and electrodes, resistance of heating element, etc. But in our case, with laboratory equipment, we are limited by low number of instantly produced sensors (tens, hundreds) and initial and continuous control is required.

As we can see on figure 2.10, thickness of electrolyte layer of one cell, measured by a profilometer, oscillates from 25 to 45 µm; such regular oscillations correspond to the mesh of printing screen. Average thickness of YSZ layer for each cell of a 15 cells sheet is reported on figure 2.10 B. It shows thinner YSZ layer on the edges, around 38-40 µm and thicker ones 44-45 in the middle of sheet. This variation may change the heat transfer, resistance of electrolyte, interface electrode/electrolyte. In order to reduce impact of these factors, only samples 3 to 13 of each plate of 15 cells were used in further tests.

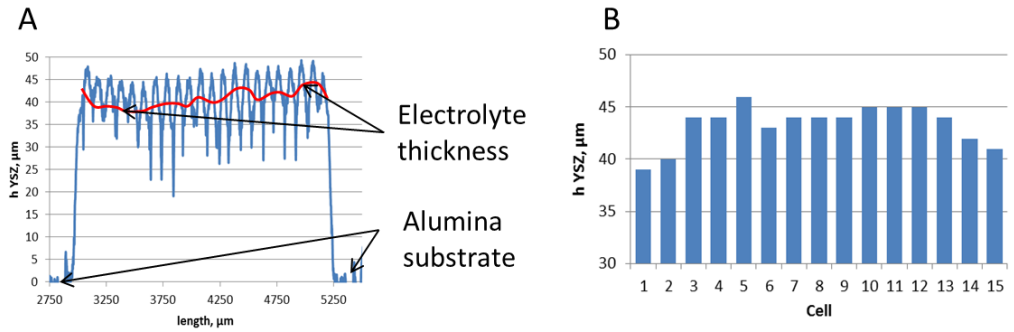

Figure 2.10: Thickness of one MEAS sensor cell – A, and variation of average thickness of YSZ on sheet with 15 cells – B.

As final step of sensors preparation, an ageing procedure was used. Prepared sensors (Figures 2.5 – 2.9) were placed in a furnace. A long-term annealing, 120h at 800°C in furnace, was used as thermal ageing. This step allows maturing of sensors and stabilizing solid electrolyte resistance and electrolyte/electrode interface. As an example, Figure 2.11 depicts variation of open circuit voltage (OCV, measurement described in paragraph 2.2.2) with time of two sensors composed of AuY sensing electrode and Pt reference electrode during first installation and heating in test bench. One of them is a "fresh" as-produced sensor, the other one being "aged" 120h at 800°C.

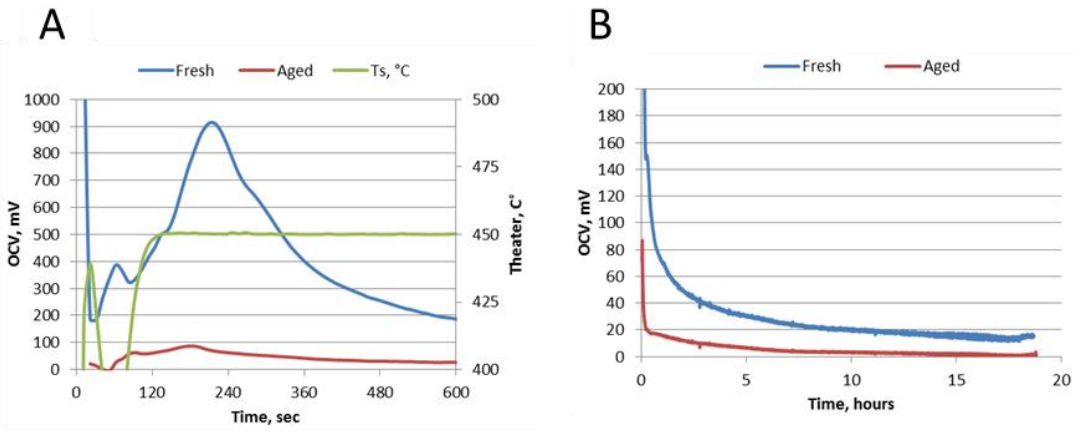

Figure 2.11: Baseline of fresh and aged Pt/YSZ/AuY sensors at 450°C in 12% O_2, 1.5% H_2O, during initial heating 10 minutes (A) and for longer test (B).

After switch on of heating resistance, temperature reaches 450°C in 120 seconds (Figure 2.11-A). OCV of non-aged (fresh) sensor increases continuously from 500 to 900 mV and decreases after, from 900 mV to 200 mV during first 10 minutes. OCV of aged sensors is relatively more stable in the range 20-100mV. For longer tests, a more stable OCV around 20-15 mV is observed after 15 hours, but it decreases continuously (Figure 2.11-B). The aged sensor reaches 25 mV of OCV after 10 min, and after 6.5 hours has a stable value in the range 0-5 mV.

2.2. Test conditions

2.2.1. EMSE exhaust simulation system

The sensing performances of the solid state planar sensors were measured in a synthetic gas bench (Figure 2.12) Test bench allows to prepare gas mixture with various concentrations of tested gases ($CO/NO_2/NO$) under controlled humidity, to control sensor temperature and to measure the sensor signal under polarization. It consists of gas tanks with nitrogen, 1% CO in air, 1% NO_2 in nitrogen and 0.2 % of NO in nitrogen (vol. %). A vaporizer allows performing the tests in

humid atmosphere. The gas composition with 12% of O_2, 1.5 % H_2O and balanced N_2 is denoted as base gas.

The response and recovery times of the sensors were compared taking into account that the dead volume of the sensor cell is around 30 cm^3. Therefore, considering the flow rate in the sensor cell (15 l h^{-1}), around 35 seconds are necessary to deeply change the gas concentration.. Simultaneous tests of 4 sensors can be carried out in two separate cells.

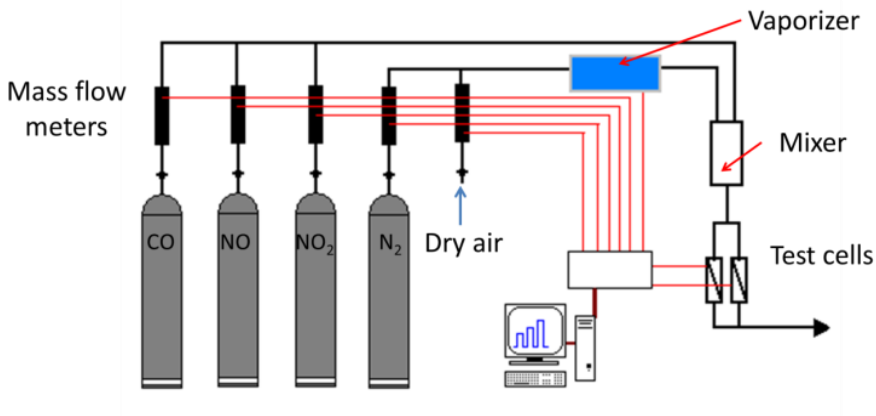

Figure 2.12: Test bench of EMSE

2.2.2. Electrical equipment: potentiostat, laboratory card

Electrical equipment of test bench consists in:

1. electronic cards to control flow meters (Figure 2.12.),
2. measuring and controlling cards to control sensors heating, sensors polarization in galvanostatic mode (Figure 2.13) and to measure resulting sensor signals.

Connectivity of electrical equipment with PC was achieved by LabView interface. In galvanostatic mode, a polarization current from 0 to 100 nA was used. When potentiometric measurements on two-electrode sensors take place, the counter electrode was disconnected. The electrochemical impedance spectroscopy measurements were performed on Galvanostat-Potentiostat VERSASTAT3 – Princeton Applied Research in 2 electrodes setup.

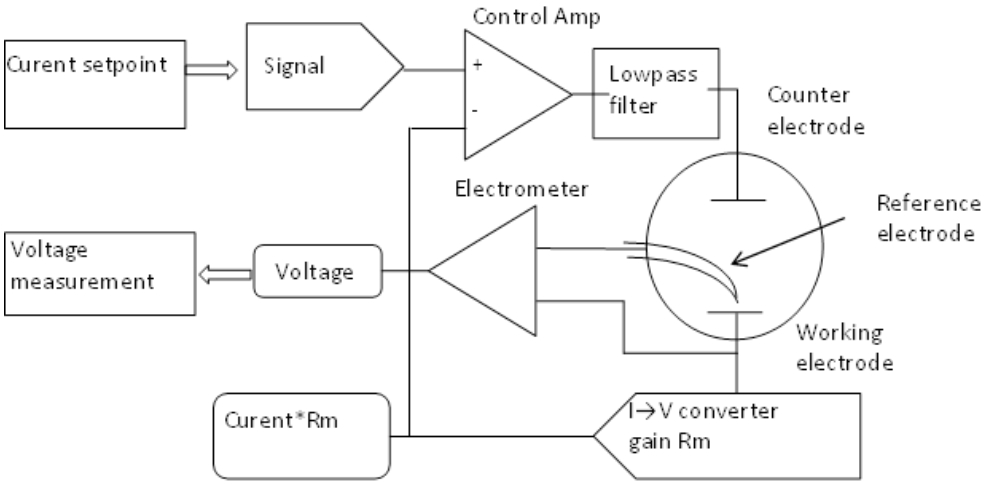

Figure. 2.13: Laboratory testing card in galvanostatic mode of test.

2.3. Measured parameters and notations

2.3.1. Baseline and base gas.

All tests were always performed in a "base gas" stream, composed of 12% O_2 and 1.5 % H_2O, balanced with N_2. In potentiometric mode, the output signal of two-electrode sensor (Figure 2.14-A) at constant temperature is the open circuit voltage (OCV). Values of OCV were arbitrary measured between the RE electrode and the SE one (Figure 2.14-A). The OCV variations with time were considered as the "baseline" of the sensor if measured in the base gas called $\Delta V°$:

$$\Delta V° = V°_{RE} - V°_{SE} \quad (2.1)$$

$V°_{RE}$ – potential of the reference electrode at i_{pol}=0 nA, mV
$V°_{SE}$ – potential of the sensing electrode at i_{pol}=0 nA, mV.

Remark: In Chapter 3 (publication submitted before PhD redaction) the OCV of Pt/YSZ/Au sensor denoted as $OCV=E_{RE}-E_{SE}$ has to be read as $\Delta V°= V°_{RE}-V°_{SE}$.

When electrodes of two-electrode sensor are polarized in galvanostatic mode (Figure 2.14-B) the gold sensing electrode (SE) is used as working electrode (WE) and Pt reference as counter electrode (CE). In this condition, a constant polarization current is passed between electrodes, and the voltage needed to reach this current is called polarization voltage:

$$V_{pol} = V_{CE} - V_{WE} \quad (2.2)$$

V_{CE} – potential of the counter electrode at $i_{pol} \neq 0$ nA, mV
V_{WE} – potential of the working electrode at $i_{pol} \neq 0$nA, mV

V_{pol} consists of $\Delta V° = V°_{RE} - V°_{SE}$, the ohmic drop Ri_{pol}, where R is the resistance of YSZ between CE and WE, and electrodes overpotentials of CE (η_{CE}), and WE (η_{WE}):

Usually, in conventional electrochemical notations, the cathodic current and overpotential are defined as negative value while anodic current and overpotential are positive.

In our system dealing with sensors, a past convention was chosen to define a positive response to reducing gases (CO, Hydrocarbons, NO), and a negative one for oxidant gases (NO_2), which explains the definition of OCV, $V°_{RE} - V°_{SE}$ (equation 2.1).

So, in the present work, where we use mainly cathodic polarization of WE, to be coherent with output signal, the cathodic current and overpotential are determined as positive values (and anodic as negative). Then expression for V_{pol} is given by equation 2.3:

$$V_{pol} = \Delta V° + Ri_{pol} + \eta_{WE} + |\eta_{CE}| \qquad (2.3)$$

In galvanostatic mode for 3-electrodes sensors (Figure 2.14-C), a constant polarization current i_{pol} from 0 to 100 nA is applied between the counter electrode and the sensing electrode. This latter is the working electrode, WE, according to potentiostat connection nomenclature. To reach this current, a polarization voltage between CE and WE is applied in range from 0 to 5 V. This voltage is named also V_{pol} and consisted of $\Delta V° = V°_{RE} - V°_{SE}$, the ohmic drop Ri_{pol}, where R is the resistance of YSZ between CE and WE, and electrodes overpotentials of CE (η_{CE}), and WE (η_{WE}).

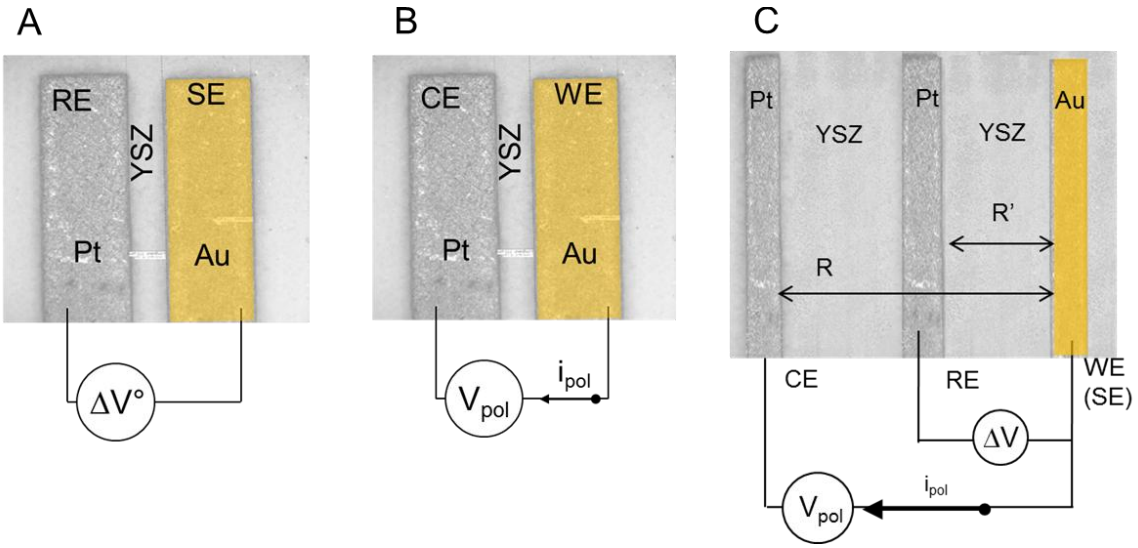

Figure 2.14: Connection setup for two electrodes Au/YSZ/Pt sensor: A – in OCV mode, B – in polarization mode and of three-electrode sensor – C in polarization mode

Measured signal of sensor (response) is the voltage difference between RE and WE

$$\Delta V = V_{RE} - V_{WE} \quad (2.4)$$

or in a more detailed form:

$$\Delta V = \Delta V° + R'i_{pol} + \eta_{WE} + |\eta_{RE}| \quad (2.5)$$

where R' is the resistance between RE and WE (Figure 2.14-C), $\Delta V° = V°_{RE} - V°_{WE}$

By consideration that no current passes by RE in the measurement circuit of ΔV, the overpotential of RE is equal to 0 (or at least negligible compared to η_{WE}), the equation 2.5 transforms to:

$$\Delta V = \Delta V° + R'i_{pol} + \eta_{WE} \quad (2.6)$$

This sensor response in galvanostatic mode was considered as the baseline when measured in base gas. The OCV value of ΔV° is measured when sensor is not polarized ($R'i_{pol}=0$ and $\eta_{WE}=0$), then $\Delta V = \Delta V°$.

2.3.2. Gas sensor responses

In the following, we will distinguish the sensor response to a pollutant gas (CO, NO, NO_2), named gas response, from the previously defined baseline (response sensor in the "base gas"). For two-electrode potentiometric sensors, opposite responses to CO (or NO) and NO_2 are observed.

A typical OCV response to 100 ppm NO_2 at 500 °C is shown on Figure 2.15. In potentiometric mode, OCV is the sensor signal. The sensor response to NO_2 corresponds to the variation of OCV values in presence of NO_2, defined as $\Delta V°_{NO_2}$.

So, this potentiometric sensor response will be noticed as: $\Delta V°_{gas}$.

$$\Delta V°_{gas} = \Delta V°_{\text{without gas}} - \Delta V°_{\text{with gas}} \quad (2.7)$$

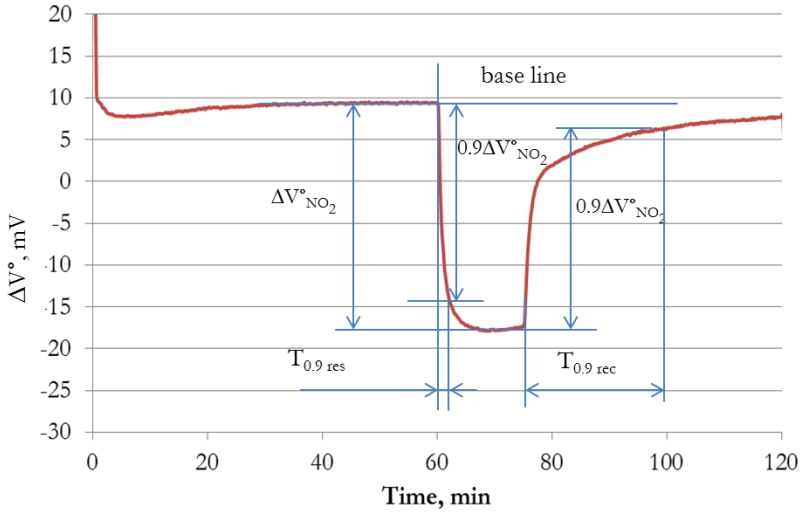

Figure 2.15: Typical OCV response to 100 ppm NO_2 of Pt/YSZ/Au sensor at 500°C in potentiometric mode

The response ($T_{0.9\ res}$) and recovery ($T_{0.9\ rec}$) times, (Figure 2.15) are measured and correspond to the time to reach (or to re-cover) 90% of the maximum sensor response ΔV_{gas}.

For 3-electrodes cell in galvanostatic mode, mostly identical parameter is used (Figure 2.16):

$$\Delta V_{gas} = \Delta V_{without\ gas} - \Delta V_{with\ gas} \quad (2.8)$$

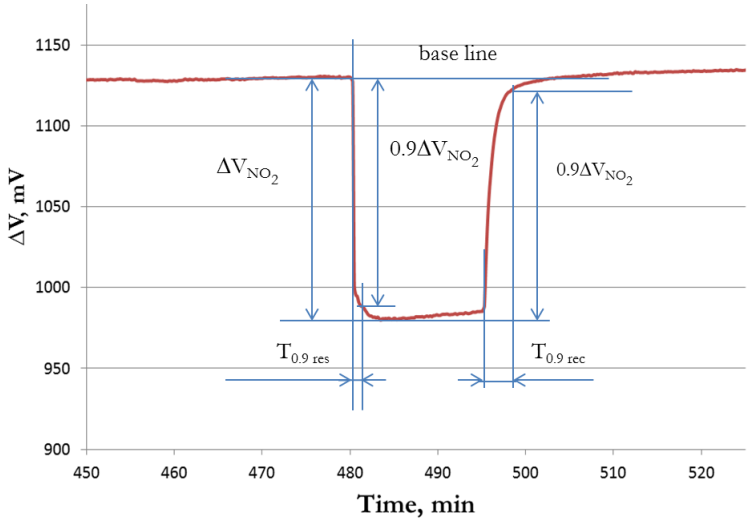

Figure 2.16: Typical response of polarized potentiometric three-electrode cell to 100 ppm NO_2 at 500°C.

2.3.3. Potentiometric measurements. Galvanostatic polarization.

As was described in paragraph 2.3.1, when electrodes of two-electrode sensor are polarized in galvanostatic mode (Figure 2.14-B) the constant polarization current is passed between electrodes, the voltage needed to reach this current is called polarization voltage (Equation 2.3):

$$V_{pol}=\Delta V°+Ri_{pol}+\eta_{WE}+|\eta_{CE}|$$

The separation of cathodic and anodic overpotential is not possible, but the calculation of overall overpotential (η_{total}) of the cell can be realized simply from 2.3 :

$$\eta_{total}=V_{pol}-\Delta V°-Ri_{pol} \quad (2.9)$$

where $\eta_{total}=+\eta_{WE}+|\eta_{CE}|$

In the case of three electrodes sensor, in a similar manner, one can use Equation. 2.6:

$$\Delta V=\Delta V°+R'i_{pol}+\eta_{WE}$$

From equation 2.6 the overpotential of WE can be determined as:

$$\eta_{WE}=\Delta V-\Delta V°-R'i_{pol}$$

where R' is the resistance between RE and WE (Figure 2.14-C), i_{pol} – polarization current, $\Delta V°=V°_{RE}-V°_{WE}$.

2.3.4. Temperature regulation

Screen printing method allows to produce heating element (Figure 2.2 C) with average electrical resistance around 10-15 Ohm at room temperature. Sensors with resistance over than 15 Ohm were not used in test.

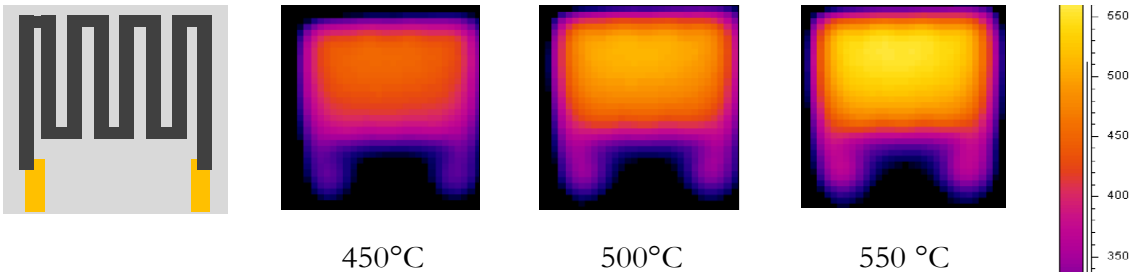

Figure 2.17: Simulation of distribution of temperature on sensing element [Gao 2011]

Due to Joule effect, electrical current passed in heating element produce increase of temperature and resistance of Pt. Temperature of cell was controlled in range from 25 to 550 °C (Figure 2.17). Continuous measurement of resistance of heating element allows controlling temperature with 0.1°C precision. Tests realized in PhD work of Jing Gao show good homogeneity of cell heating. Platinum resistance keeps electrical properties during long lifetime.

2.4. Characterizations techniques

2.4.1 Electrochemical impedance spectroscopy measurements

Electrochemical impedance spectroscopy (EIS) is a method to study electrochemical systems based on application of an alternative potential (E+dE) to an electrochemical cell and measuring the current (I+dI) passed through this cell (Figure 2.18 A)

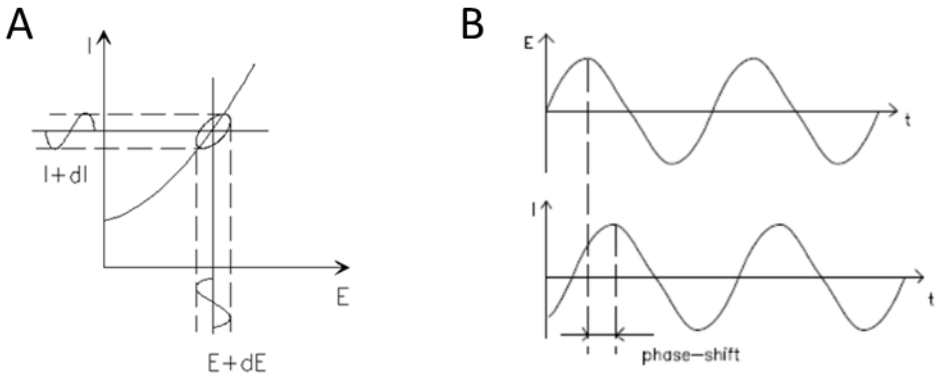

Figure 2.18: Principle of EIS measurement (A) and excitation and response signals as function of time (B)

Applied potential is described as sinusoidal function:

$$E(t) = E_o \sin(\omega t) \tag{2.10}$$

Resulted response of current with phase shift – θ is written:

$$I(t) = I_o \sin(\omega t - \theta) \tag{2.11}$$

Impedance as function of time, Z is described in equation 2.12:

$$Z = \frac{E_o \sin(\omega t)}{I_o \sin(\omega t - \theta)} = |Z| \frac{\sin(\omega t)}{\sin(\omega t - \theta)} \tag{2.12}$$

By using Euler's relationship $\exp(j\theta) = \cos\theta + j\sin\theta$, expression 2.12 can be transformed to 2.13:

$$Z(\omega) = \frac{E_o \exp(j\omega t)}{I_o \exp(j\omega t - j\theta)} = |Z|(\cos\theta + j\sin\theta) \quad (2.13)$$

The impedance is then represented as a complex number:

$$Z(\omega) = \mathrm{Re}(Z) + j\,\mathrm{Im}(Z) \quad (2.14)$$

The expression 2.14 for Z is composed of a real Re(Z) and an imaginary part –Im(Z). Presentation when the real part is plotted on the X axis and the imaginary part on the Y axis of a chart, is named a "Nyquist plot". Typical Nyquist Plot is presented on Figure 2.20-A

$$|Z| = \sqrt{(\mathrm{Re}(Z))^2 + (\mathrm{Im}(Z))^2} \quad (2.15)$$

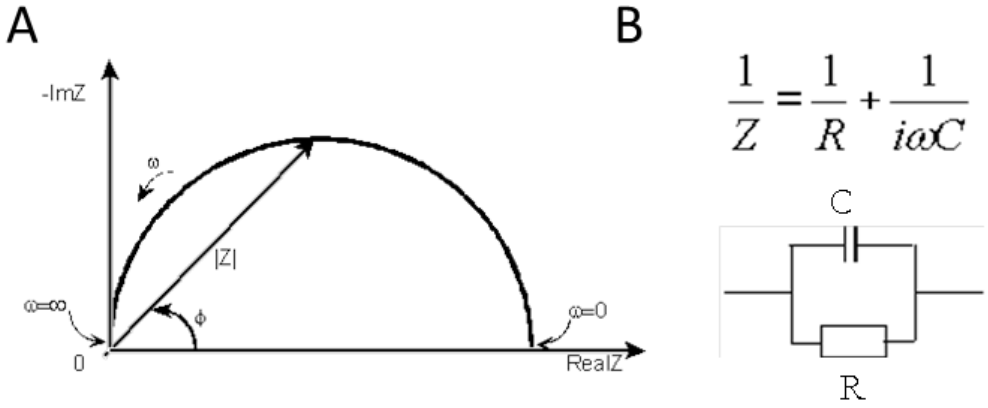

Figure 2.20: Typical Nyquist Plot (A) and electrical equivalent circuit (B).

Nyquist plot can be also described by an equivalent electrical circuit (Figure 2.20-B), here, for ideal semicircle, parallel Resistance (R) – Capacity (C) circuit is shown.

In this work, EIS measurements were performed in a tubular furnace (Figure 2.21). in the base gas flow 15 l h^{-1}. During measurements, gold wires were connected to electrodes by identical gold paste ESL 8880-H.

Electrochemical Impedance Spectroscopy was used to investigate the electrochemical properties of the symmetric cells (Figure 2.7-A) Au/YSZ/Au, AuY/YSZ/AuY and AuZ/YSZ/AuZ. Experiments below 550°C were not possible to be carried out due to the extremely high resistivity of the solid electrolytes, of the order of 10 MΩ. This high value is due to the high porosity of the electrolyte layer.

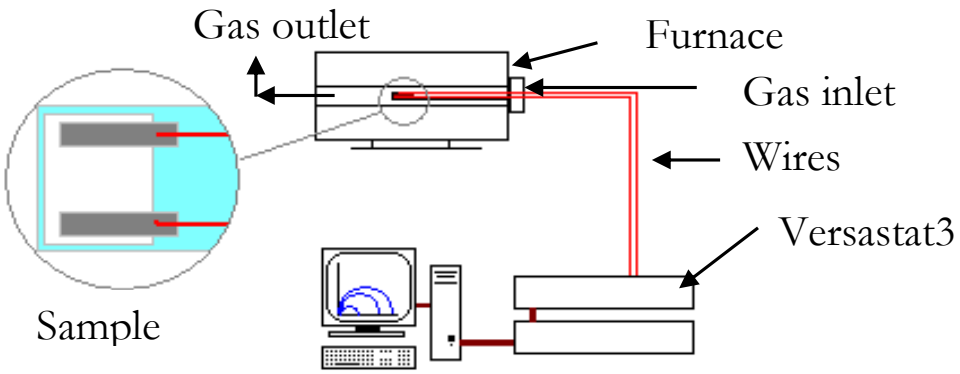

Figure 2.21: EIS measurement test bench.

Figures 2.21 shows a typical Nyquist plot of the Au-Au sample at 551°C in air. Impedance spectrum exhibits two well-defined semicircles that can be separated and resolved. The first semicircle, in the high frequency domain 10^4-10^2 Hz, represents the resistivity around $1.8x10^6$ Ohm of the YSZ solid electrolyte layer (R_{YSZ}) which is mainly due to the blocking of the conduction by the pores. The second contribution equal to $5x10^5$ Ohm, in the low frequency range (from 10^2 to 10^{-3} Hz), corresponds to the overall polarization resistance (R_{POL}) at the two symmetrical electrodes linked with the kinetic of the electrode reactions. Influence of different electrodes composition and morphology on R_{POL} is discussed in Chapter 3.

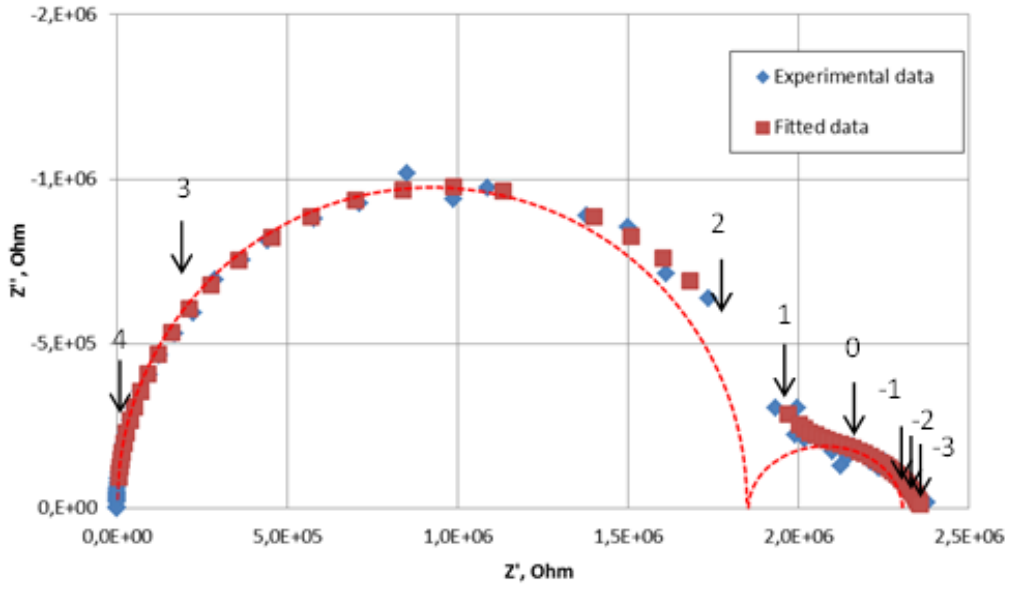

Figure 2.22: Experimental and fitted Nyquist plot of Au-Au sample at 551°C in air. The numbers indicates the decimal log of signal frequencies

2.4.2. Scanning electron microscopy

Scanning microscopy was used for study of morphology of solid electrolyte layers and electrodes, their porosity, thickness and surface. Field Emission Scanning Electron Microscope JEOL 6400 was used in this work for SEM characterization of samples.

For measurement of electrolyte thickness, prepared sensors were placed in epoxy-resin form and polished (Figure 2.23).

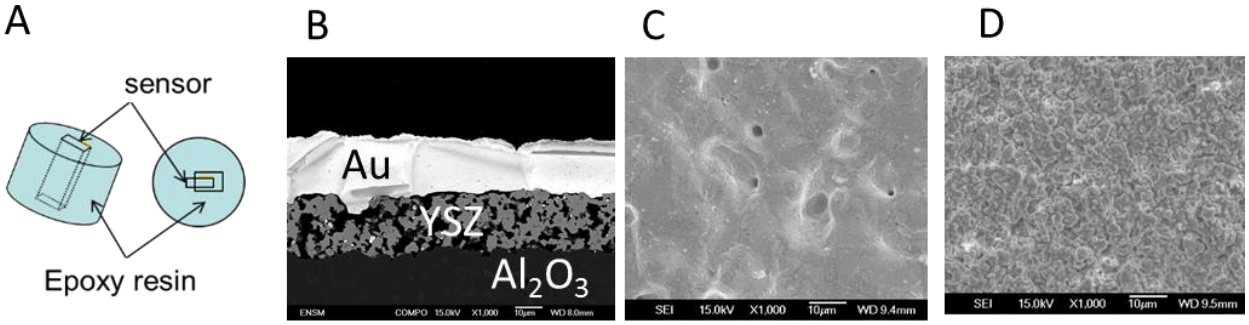

Figure 2.23: Placement of sensor cell for cross section – A, SEM investigation and micrographs of Au/YSZ/Al_2O_3 layers – B, surface view x1000 of Au electrode – C and YSZ electrolyte – D.

For surface investigation, samples were placed on metallic sample holder. For better conduction and evacuation of charge from sample, they were covered by conductive carbon layer (Quorum Q150R ES)

2.4.3. Laser granulometry

Laser granulometry is a method to study particle size distribution, based on light diffusion and diffraction on solids. The sample is dispersed in liquid media, water or ethanol. The laser passes through the dispersion media and is diffracted by the particles (Figure 2.24)

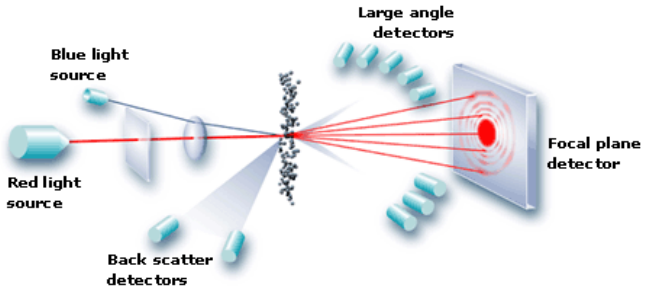

Figure 2.24: Laser granulometry method.

MASTERSIZER 2000 from MALVERN was used in this work. Water was used as liquid media for particle dispersion.

2.4.4. Analysis of specific surface area in nitrogen (BET)

Method of specific area measurement is based on physical gas adsorption of an inert gas, often nitrogen, on the surface of a solid material. This occurs in the pores if material is porous or in surface in case of non-porous material.

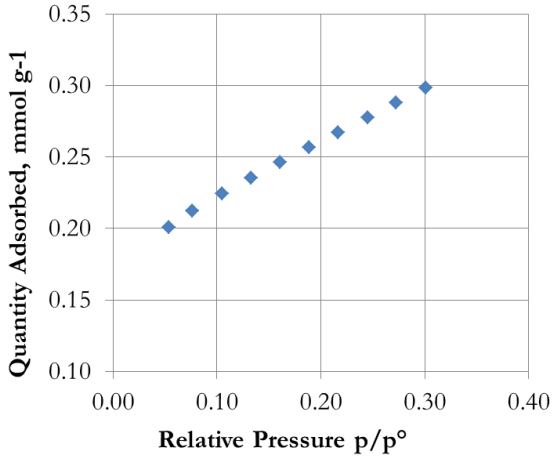

Figure 2.25: BET isotherm for ZrO_2 sample

Most widely known is the determination of the BET surface area by gas adsorption. Adsorption of nitrogen at a temperature of 77 K leads to a so-called BET isotherm (figure 2.25), from which the specific area (in m^2/g) can be calculated. This method was used for the characterization of the used powders, YSZ and ZrO_2.

Chapter 3

Application of advanced morphology Au-X (X = YSZ, ZrO_2) composites as sensing electrode

Outline

Chapter 3 : Advanced morphology composites

Resumé

Ce chapitre a fait l'objet d'une publication soumise et en cours de review à Sensors and Actuators B : "*Application of advanced morphology Au-X (X = YSZ, ZrO_2) composites as sensing electrode for solid state mixed-potential exhaust NOx sensor"* Il est présenté sous la forme de cette publication.

Parmi les différents types de capteurs NOx développés, le capteur potentiométrique à base de zircone stabilisée (YSZ) avec une architecture planaire simple Au/YSZ/Pt possède des performances intéressantes. Des électrodes composites à base d'or ont été étudiées pour améliorer les performances de détection. Ces capteurs potentiométriques de gaz ont été fabriqués par sérigraphie et testés pour la détection de NO_2 dans des conditions proches de celle d'un pot d'échappement. L'étude par spectroscopie d'impédance électrochimique a montré que l'addition d'YSZ dans l'électrode en or diminue la résistance de polarisation sous l'air. En plus, le capteur (Au+10% mass YSZ)/YSZ/Pt a un temps de réponse plus court et une plus grande sensibilité à NO_2 (gamme de 20 à 100 ppm) de 450 à 550 °C en comparaison avec un capteur référence Au/YSZ/Pt. D'autre part, l'ajout de ZrO_2 non-conducteur ne modifie pas significativement les propriétés électrochimiques, mais endommage fortement les réponses des capteurs à NO_2.

Summary

This Chapter constitutes a publication "*Application of advanced morphology Au-X (X = YSZ, ZrO_2) composites as sensing electrode for solid state mixed-potential exhaust NOx sensor*" submitted to *Sensors and Actuators B* journal.

Application of advanced morphology Au-X (X = YSZ, ZrO_2) composites as sensing electrode for solid state mixed-potential exhaust NOx sensor.

Ivan ROMANYTSIA[a,b], Jean-Paul VIRICELLE[a*], Philippe VERNOUX[c] , Christophe PIJOLAT[a]

[a] Ecole Nationale Supérieure des Mines, CNRS:UMR5307, LGF, 158 cours Fauriel, 42023 Saint-Etienne, France ;
[b] Measurement Specialties France, Impasse Jeanne Benozzi, CS 83 163, 31027 Toulouse ;
[c] Institut de Recherches sur la Catalyse et l'Environnement de Lyon, Université LYON 1, 2 avenue Albert Einstein 69626 Villeurbanne ;
* Corresponding author : viricelle@emse.fr

Abstract

Among various NOx sensors developments, mixed potential sensor based on Yttria Stabilized Zirconia (YSZ) with a simple planar architecture Au/YSZ/Pt is of practical interest. Au composites electrodes were investigated to improve sensing performances . Such potentiometric solid-state gas sensors were fabricated by screen-printing and tested for NO_2 detection. Electrochemical impedance spectroscopy has shown that the addition of YSZ in the Au electrode decreased the polarization resistance in air. In addition, the (Au+10 wt% YSZ)/YSZ/Pt sensor has a shorter response time and higher sensitivity to NO_2 (range 20-100 ppm) at 450-550 °C in comparison with a reference Au/YSZ/Pt sensor. On the other hand, the addition of non-conductive ZrO_2 doesn't significantly modify the electrochemical property but strongly damages the sensor responses toward NO_2.

1. Introduction

Continuous stringent legislations in automotive exhausts oblige the vehicles manufacturers to optimize combustion operations and to monitor pollutants such as nitrogen oxides [1, 2]. From 2014, Euro 6 standards require the utilization of a NOx (NO and NO_2) catalytic after-treatment device for Diesel engines. Selective catalytic reduction (SCR) of nitrogen oxides by ammonia or

urea [2, 3] is the most advanced technology used in heavy diesel engine trucks but also in Diesel passenger cars. Conversion of NOx depends on oxygen partial pressure as well as on NH_3/NO and NO/NO_2 ratios, and could reach above 99% at 573 K [3].In this context, fast and accurate on-board diagnostics of NOx concentration in the exhaust are strongly required.

Due to this strong demand, there are numerous studies dealing with the development of NOx sensors for on-board detection in light and heavy duty vehicles. In this paper, we will focus only on potentiometric gas sensor designed with two electrodes and working in the same atmosphere, according to the mixed potential principle. A recent development of such a sensor is reported in [4] . Most of these sensors are composed of a solid electrolyte based on yttria-stabilized zirconia (YSZ) [4-10], but other electrolyte may be used: β-alumina ($2Na_2O–11Al_2O_3$) [11] or samaria-doped-ceria (SDC) [12]. Two electrodes, a reference one and a sensing one are associated with the electrolyte. These two electrodes must present different electrocatalytic activity to detect NO_x such as the couples Pt-Au [5, 11], Pt-$MnCr_2O_3$ [8], Pt – (Au-oxide) [9, 13], or Pt with other oxide [4]. The signal of a two electrode potentiometric sensor, in a complex gas environment, shows a non-Nernstian behavior due to the establishment of a mixed potential [4, 5, 6, 8] on the sensing electrode. This latter is linked to the superposition of parallel electrode reactions occurring at the triple phase boundaries (TPB) [8, 9, 10, 14], such as the oxygen electrode reaction and the electrochemical reduction (oxidation) of NO_2 (NO). The sensitivity of NO_2 is always higher than that of NO. In addition, by using the Au/Pt couple of electrodes interfaced on YSZ, NO_2 and NO exhibit opposite responses, positive for NO and negative for NO_2 [5].

The morphology of the two electrodes plays a significant role in the number of TPB [8, 14], then on the kinetic of the electrode reactions and finally on sensing performances. For instance, a sensor with two Pt based electrodes showing asymmetric morphologies can be effective for NO_2 detection [15, 16]. Composite electrodes made of Pt or Au mixed with an oxide [7, 13, 17-19] are also strongly investigated to improve the sensing performances. Recent studies have reported the sensing performances of Au+YSZ [19] and Au-NiO [13, 20] composite electrodes.

Cross sensitivity to exhaust gases as CO and hydrocarbons can be eliminated by using a catalytic filter [5, 21] deposited on the top of the electrodes. This catalytic layer can fully oxidize these molecules into CO_2 which is not detected by the sensor. It can also catalyze the NO oxidation into NO_2 to reach the thermodynamic equilibrium. Therefore, the NO/NO_2 ratio is only dependent on the temperature for a fixed partial pressure of oxygen. Our aim is to develop a potentiometric sensor highly sensitive to NO_2 equipped with a catalytic filter. Then, at a constant temperature and oxygen partial temperature, this system could provide concentrations of NO_2, NO and overall NO_x.

This paper describes the sensing performances for NO_2 detection of YSZ-based solid state planar sensors using Pt as a reference electrode and Au-composites as sensing electrodes. The objective was to increase the porosity and then the number of TPBs of the sensing electrodes. These latter were composed of Au mixed either with YSZ or ZrO_2. The addition of YSZ into the Au electrode could provide a mixed electronic and ionic conductivity into the sensing electrode in

order to delocalize the TPBs in the overall volume, while the incorporation of ZrO_2 should only act on the porosity. Electrochemical performances for the oxygen electrode reaction were investigated by impedance spectroscopy and compared with those of pure Au sensing electrode. Finally, the sensing performances for NO_2 were evaluated between 450 and 550°C.

2. Experimental

Solid state planar sensors (Figure 1) were fabricated by screen-printing (Aurel C890) on alumina substrates (CoorsTek). A functional and porous layer 5x5 mm of solid electrolyte (YSZ: $(ZrO_2)_{0.92}(Y_2O_3)_{0.08}$ provided by Superconductive) was deposited by screen-printing (200 mesh) from a home-made ink containing 4 g of YSZ powder, 1.7 g of organic binder (ESL V400A) and 1 g of solvent (ESL 404) mixed 10 minutes in a three-roll mill (Exakt 80E). Then, the samples were dried for 15 min in air at 120°C and sintered at 1380 °C in air for 2 hours with a ramp of 5°C/min. Platinum and gold electrodes, of 1 mm width and 4 mm length, were screen-printed on the surface of the YSZ layer using a commercial paste of Pt (ESL 5545) and Au (ESL 8880-H). The distance between the electrodes was 2 mm. The deposited electrodes were further dried for 15 minutes at 120°C and then sintered at 850°C for 2 hours in air with a ramp of 5°C/min. The gold and platinum electrodes were denoted as the sensing (SE) and the reference (RE) electrode, respectively.

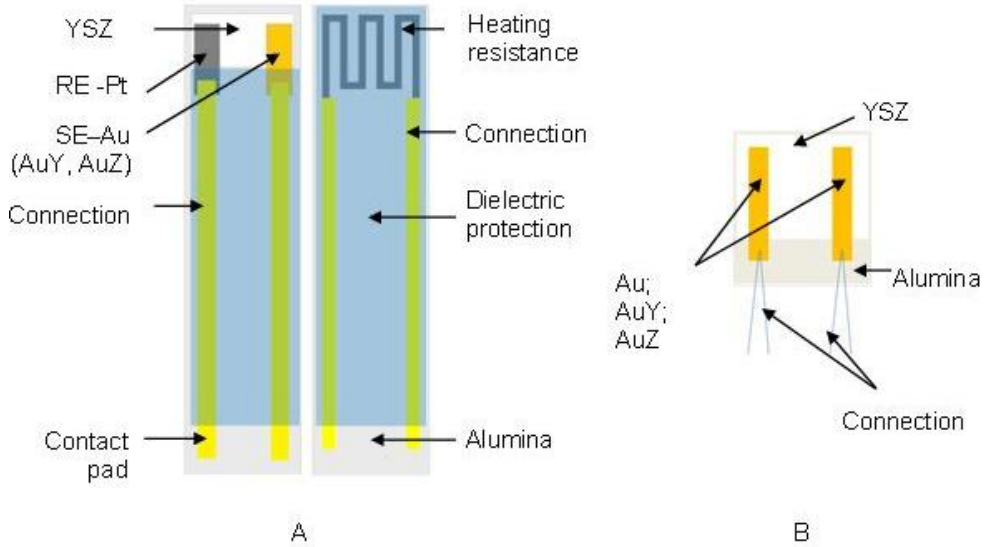

Figure 1: A) Schematic drawing of solid state gas sensors and B) symmetric samples for EIS measurements

Gold based composite electrodes were prepared by mixing the Au commercial paste (ESL 8880-H) with 10 wt% YSZ (denoted as AuY) or with ZrO_2 (denoted as AuZ) homemade inks. YSZ ink is the same as for electrolyte. ZrO_2 ink was composed of 4 g of ZrO_2 powder (Merck), 1.7 g of organic binder (ESL V400A) and 1 g of solvent ESL (59 wt % of ZrO_2). This ZrO_2 ink (10 wt%) was mixed in a three roll mill with the Au commercial paste. The depositions were further dried for 15 minutes at 120°C and then sintered at 850°C for 2 hours in air with a ramp of 5°C/min. Final amount of ceramic fraction in composite electrodes is 9.5 %wt.

The powders (YSZ and ZrO_2) were characterized by using laser granulometry (MASTERSIZER 2000 MALVERN) and BET measurements with nitrogen (ASAP 2020). Specific area of YSZ powder after calcination at 850 °C in air was found to be 15 m^2/g while that of ZrO_2 was 3.8 m^2/g. Mean particle size of agglomerates was 1.6 μm and 0.288 μm, for YSZ and ZrO_2, respectively.

Number and nature of impurities in the commercial ink of Pt (ESL 5545) and Au (ESL 8880-H) were controlled by ICP (Jobin-Yvon JY138 Ultrace). The presence of 1500 ppm of Cu and around 30 ppm of Al, Na, and Zn have been detected in the Au paste whereas significant loadings of Ti (29000 ppm), Zn (9000 ppm), Fe (2500-3500 ppm), Cr (1500 ppm) and Al (1500 ppm) have been analyzed in the Pt ink sample.

Scanning electron microscopy (JEOL JSM 6500F) was used to investigate the morphology of the electrodes and of the YSZ layer. Samples were placed in epoxy resin and polished to obtain cross section. Surface of samples was covered with a conductive carbon layer (Quorum Q150R ES).

The control of the sensor heating was performed with a Pt-resistance element (ESL 5545) placed on opposite side of the alumina support (Figure 1A). Before testing, all sensors were aged at 800°C for 120 hours in air. Symmetric sensors were also made to investigate the electrochemical performances of the Au based electrodes (Figure 1B). Three series of symmetric sensors were prepared by screen-printing with the same procedure than used for the electrolyte layer and the electrodes: Au/Au as a reference sample, AuY/AuY and AuZ/AuZ.

Resistivity of the YSZ porous layers and electrochemical properties of the Au composite electrodes were measured by using electrochemical impedance spectroscopy (EIS, VersaSTAT 3 - Princeton Applied Research). Each symmetric sensor was placed in a tubular furnace (CARBOLITE) in ambient air. AC signal amplitudes of 150 mV were applied between the two electrodes in the frequency range 10^5 Hz – 10^{-3} Hz. EIS measurements were performed between 550°C and 700°C with a step of 25°C both during heating and cooling down. Impedance diagrams were recorded during a temperature plateau of 3 h. EIS measurements were not possible below

550°C, due to the extremely high resistivity (higher than 10 MΩ) of the YSZ porous layer. Fitting of the Nyquist plots was realized in ZView interface.

The sensing performances for NO_2 of the solid state planar sensors (Figure 1A) were measured in a synthetic gas bench (Figure 2) with a "base gas" containing 12 vol% O_2, 1.5 vol% H_2O, balanced with N_2. Amounts of 20, 50 and 100 ppm of NO_2 for 15 min were added in the base gas. The total flow rate was 15 L h^{-1} per cell, simultaneously four sensors were tested. For heating control and signal processing, an electronic card coupled with a LabView interface was used. Response and recovery times of the sensor responses were compared taking into account that the dead volume in the sensor cell is around 30 cm^3. Therefore, considering the flow rate in the sensor cell (15 l h^{-1}), around 35 seconds are necessary to deeply change the NO_2 concentration. Response (and recovery) times were measured and correspond to the time to reach (or to recover) 90% of the maximum sensor response.

Sensors have been tested between 450 and 550 °C. The open-circuit voltage (OCV) was measured as follow:

$$OCV = E_{RE} - E_{SE} \quad (1)$$

where E_{RE} was the potential of the reference electrode (Pt) and E_{SE} was the potential of the sensing electrode (Au, AuY or AuZ). The responses of the sensors toward NO_2, ΔV, were calculated according to the following relationship:

$$\Delta V = OCV_{NO_2} - OCV \quad (2)$$

when OCV_{NO2} was the stabilized sensor signal measured during NO_2 injection.

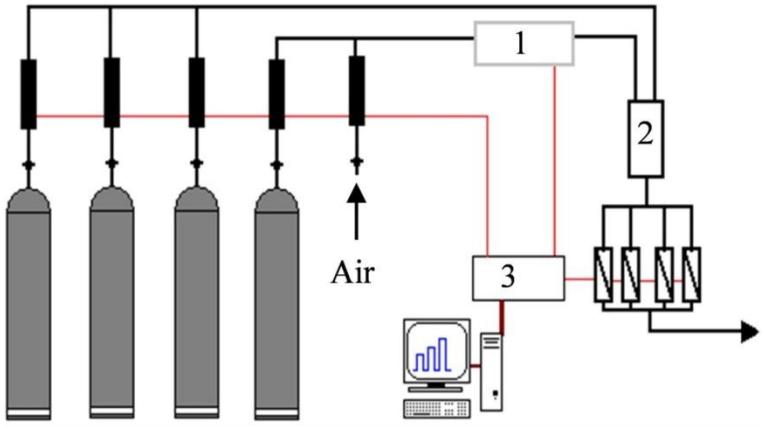

Figure 2: Test bench1 – Humidifier, 2 – Mixing chamber, 3 –Control card/potentiostat

3. Results and discussion.

3.1. SEM characterizations

Figures 3 and 4 display that the YSZ layer is extremely porous, probably due to the presence of evaporated binder (30 wt%) and solvent in the initial paste. However, the surface of this layer evidences percolation between micrometric YSZ grains ensuring bulk ionic conductivity.

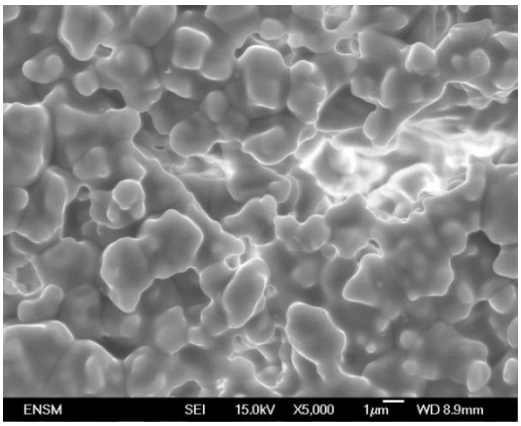

Figure 3: Surface SEM images of the screen-printing YSZ layer

Figure 4A shows that the Au sensing electrode is dense and totally covers the surface of the electrolyte. The interactions between the gold film and the porous YSZ layer are poor. In this case, TPB electrode/electrolyte/gas is limited by the perimeter of the Au dense film. Addition to the gold paste of 10 wt% of ZrO_2 or YSZ ink, produces strong modifications of the electrodes morphology (Figures 4B, 4C). The Au-Z composite electrode presents open pores in which the gas can diffuse from the electrode surface to the electrolyte layer. The diameter of these pores varies from 0.5 to 5 μm. Metallic phase contain a wide size distribution of Au grains from 1 to 20 μm. Agglomerates of ZrO_2 larger than 2 μm can be observed inside the composite electrode Au-Z. Au particles in the Au-Y composite layer present a similar size from 1 to 20 μm. YSZ particles, between 1 and 5 μm, are dispersed in the vicinity of the electrode layer. High porosity with continuous electric contact between Au and YSZ electrolyte grains forms an electrode with a higher number of TPBs. Contrary to the Au electrode, the platinum reference electrode (Figure 4D) is highly porous. This Pt electrode contains micrometric Pt particles (1 - 5 μm) smaller than the Au grains observed in the Au-composite electrodes.

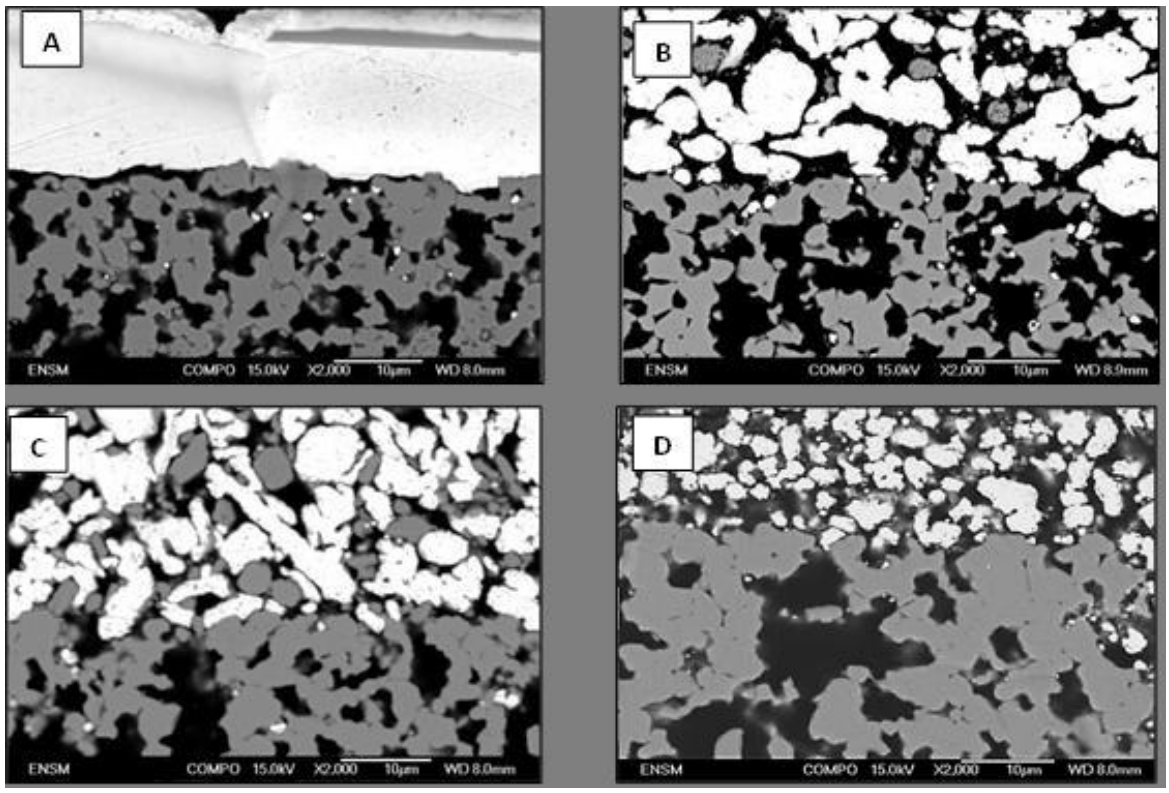

Figure 4: SEM images of electrode/YSZ interface (Au :white, YSZ or ZrO_2 grey): A – Au; B – AuZ; C – AuY; D – Pt.

3.2. Electrochemical characterizations

Electrochemical Impedance Spectroscopy was used to investigate the electrochemical properties of the symmetric sensors Au/Au, AuY/AuY and AuZ/AuZ. Experiments below 550°C were not possible to carry out due to the extremely high resistivity of the sensors, of the order of 10 MΩ. This is due to the high porosity of the electrolyte layer. Indeed, literature data reports high increase of the YSZ electrolyte resistance with the porosity [22, 23].

Figure 5 shows a typical Nyquist plot of the Au-Au sample at 551°C in air. Impedance spectra exhibit two well-defined semicircles that could be separated and resolved. The first semicircle, in the high frequency (HF) domain, represents the resistivity of the YSZ solid electrolyte layer (R_{SE}) which is mainly due to the blocking of the conduction by the pores [22]. The second contribution, in the low frequency (LF) range (from 10^2 to 10^{-3} Hz), corresponds to the overall polarization

resistance (Rpol) at the two symmetrical electrodes linked with the kinetic of the electrode reactions [7, 17, 23, 24].

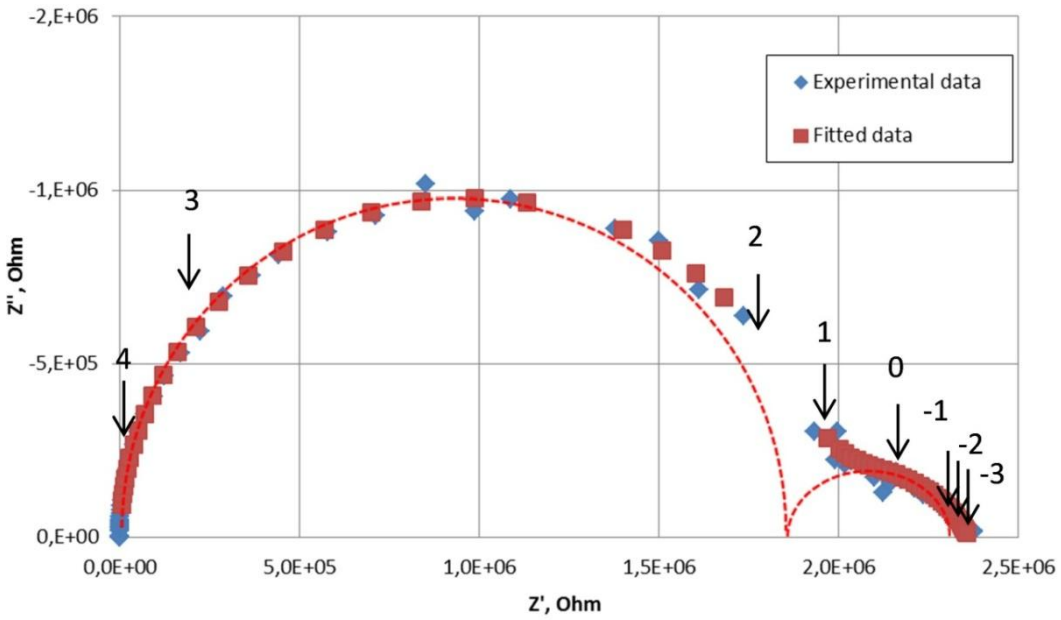

Figure 5: Experimental and fitted Nyquist plot of Au-Au sample at 550°C in air (numbers with arrow indicate the $\log_{10}$ of the measuring frequency)

The SE semi-circle can be reasonably fitted with a parallel $R_{SE}C_{SE}$ element [7, 24] with R_{CE} and C_{SE}, the resistance and the capacitance of the YSZ layer (Figure 5). The resistance of the YSZ layer is extremely high, around $2*10^6$ Ω at 550°C and is almost similar for the three sensors (Figure 6). This underlines the good repeatability of the preparation method. This value is higher than the ones reported in previous studies [22, 23]. This could be related to the high porosity of the screen printed YSZ layer. The activation energy is similar for the three symmetrical sensors, at around 1.13 eV. This value is in good agreement with that reported for porous YSZ membranes impregnated with 1 wt% Pt [23]. On the other hand, Kleitz et al [22] have found similar activation energies, at around 1.04 eV for both bulk and pores conductivity.

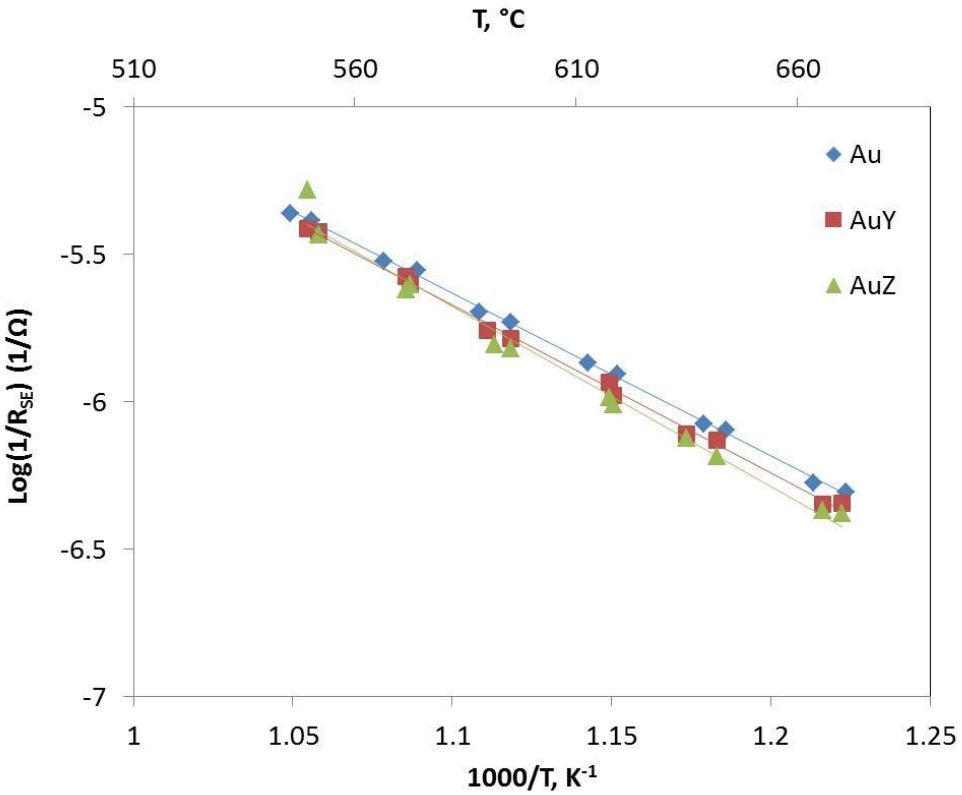

Figure 6: Arrhenius diagrams of the solid electrolyte resistance (R_{SE})

Modeling of LF part of impedance spectra can be performed with a RC element [7, 18], but better fits were obtained by using a parallel combination of a resistance (Rpol) with a constant phase element (CPEpol) [24-27]. Figure 7 depicts the Arrhenius diagram of the polarization resistance in air between 550 and 700 °C. From a general point of view, polarization resistances of the two symmetrical electrodes are one order of magnitude lower than resistances of the YSZ layer. The two samples Au/Au and AuZ/AuZ show similar values of polarization resistances as well as of the apparent activation energy (1.54 ± 0.03 eV). Therefore, the enhancement of the electrode porosity with the addition of an insulating material such as zirconia seems to not significantly modify the oxygen electrode kinetic. Opposite results were reported in the literature data for Pt composites electrodes containing Ga_2O_3 [7] deposited on a dense YSZ sheet. The presence of the oxide phase was found to inhibit the cathodic electrode reaction.

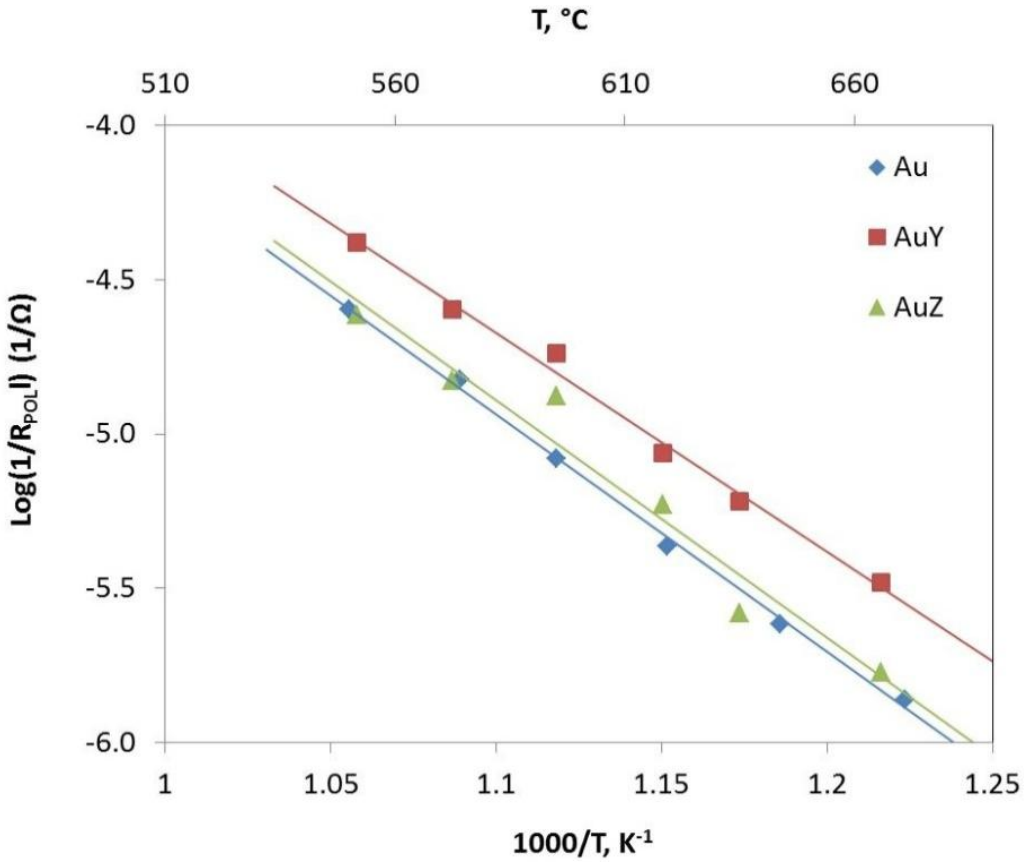

Figure 7: Arrhenius diagrams of the polarization resistance (R_{POL}) of the three symmetric sensors Au/Au, AuZ/AuZ and AuY/AuY.

The electrode composite of Au with YSZ shows the highest electrochemical performances (Figure 7) and the lowest apparent activation energy (1.43 ± 0.3 eV). For instance, at 550°C, the value of R_{POL} decreases from 5 10^5 Ω for Au and AuZ down to 3 10^5 Ω for AuY. The apparent activation energy values at the Au/YSZ interface in oxygen, reported in the literature data, are in the order of 0.9 - 1 eV [25, 28]. For instance, Woo et al. [25] have recently performed experiments on a symmetrical Au/YSZ/Au sensor using thin Au plates contacted on a porous spray-coated YSZ layer. In the temperature range 600-700°C, they found an activation energy value of 1.02 eV under oxygen.

Our experimental data evidence high Ea values. Blocking process of the charge transfer may occur at the Au/YSZ interface which could be linked with the extremely high YSZ layer porosity as well as with the presence of impurities (Cu ~1500 ppm, Al, Na, Zn ~30ppm) in the Au paste.

3.3. Sensor performances

3.3.1. OCV measurements in the base gas.

The evolution of OCV in the base gas (12% O_2, 1.5% H_2O) was monitored as a function of time (Figure 8) at 450°C. These responses correspond to potential differences between the Pt electrode and the Au-based one (Figure 1a). Initial signal abrupt variations are due to the temperature regulation. Regarding the Au sensor, OCV values significantly increase with time during the first two hours and then gradually raise but never reach a steady-state. After 18 hours on stream, the OCV value of the Pt/Au sensor is + 57 mV. The OCV, in oxygen atmosphere, between Au and Pt electrodes is generally attributed to a difference in the O_2 electrode kinetic rate linked with different oxygen activity [29]. A positive value indicates that the oxygen activity is higher on Pt than on Au, in good agreement with the morphology of the two electrodes (Figure 4). The two Au composites present similar behaviors with an initial increase followed with a gradual decay of the OCV with time. Responses of AuZ and AuY sensors reach a steady-state value of +10 mV and +2 mV after 6.5 and 13 hours on stream, respectively. These results underline that the electrode porosity increases the surface specific area and the number of TPB, active for the oxygen adsorption. Therefore, the electrochemical properties of AuY for the oxygen electrode reaction become closest to those of the Pt electrode, in good agreement with EIS data (Figure 7).

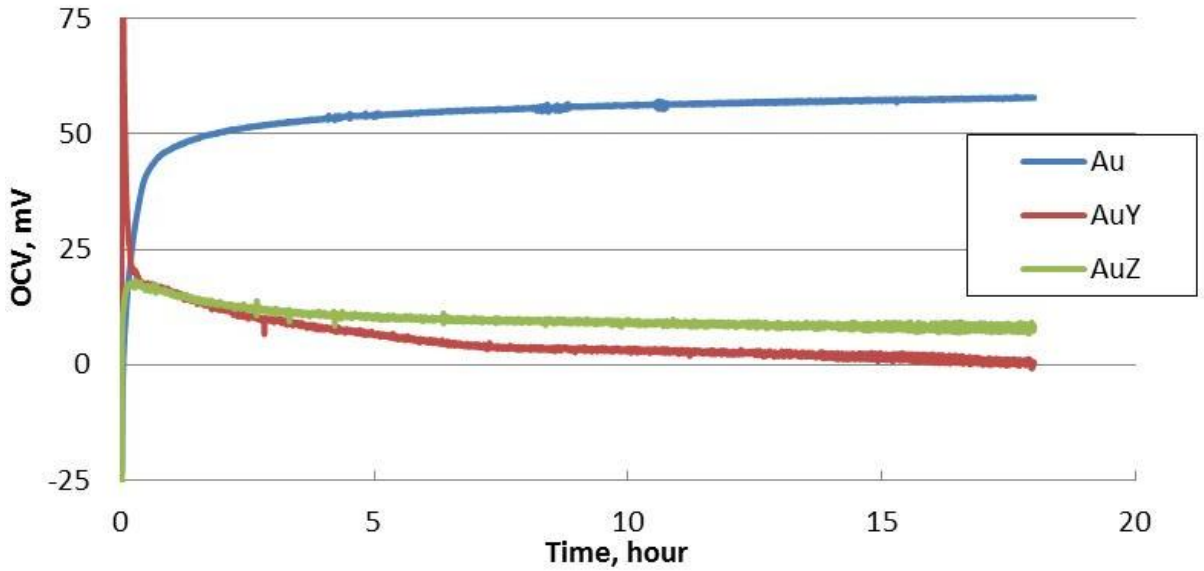

Figure 8: Sensor Pt/YSZ/SE baseline at 450°C in 12% O_2, 1.5% H_2O

3.3.2. NO_2 sensing performances

NO_2 sensing performances such as the response time and the signal stability were monitored as a function of the morphology and the composition of the sensing electrodes. In oxygen-rich atmosphere, in presence of NO_2, a mixed potential is established between the oxygen electrode reaction and the electrochemical reduction of NO_2 [3, 30].

As already reported in the literature [5, 19], whatever the temperature and the nature of the electrodes, the responses to NO_2 and NO are opposite. As expected, the sensors responses to NO_2 are negative (Figure 9). At 450°C, the AuZ sensor presents a strange and non-usable behavior, suggesting extremely slow and complex interactions of NO_2 with the porous electrode. On the opposite, the AuY sensor shows stable and reversible responses. In addition, this electrode exhibits the highest sensing performances with sensitivity to NO_2 of around -52 mV/decade. The recovery time of pure Au electrode is extremely high, most probably because a slow diffusion of NO_2 into the dense Au layer.

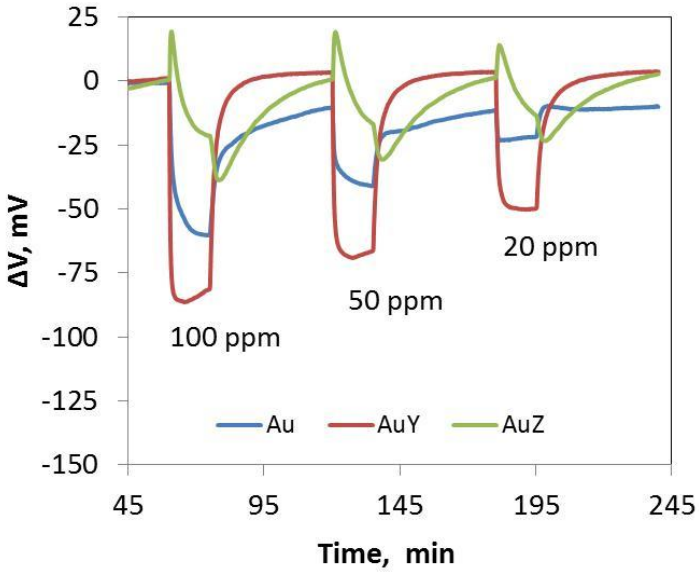

Figure 9: Sensor responses (ΔV) Au, AuZ and AuY sensors to different concentrations of NO_2 in presence of 12% O_2 and 1.5% H_2O at 450°C

By increasing temperature to 500°C and 550 °C, the sensitivity decreases for all sensors. For instance on AuY, the response drops from 42 mV/decade at 500°C down to 28 at 550°C. In parallel, response and recovery times are strongly decreased (Figure 10). Responses of both Au and AuZ electrodes become reversible. However, the response time of AuZ remains much longer. Whatever the temperature, AuY exhibits the highest sensitivity and the lowest response time.

Sensitivity of AuY sensor is two times higher than that of Au at 500°C and 550°C. Nevertheless, the AuY response tends to decrease with time during the NO_2 injections.

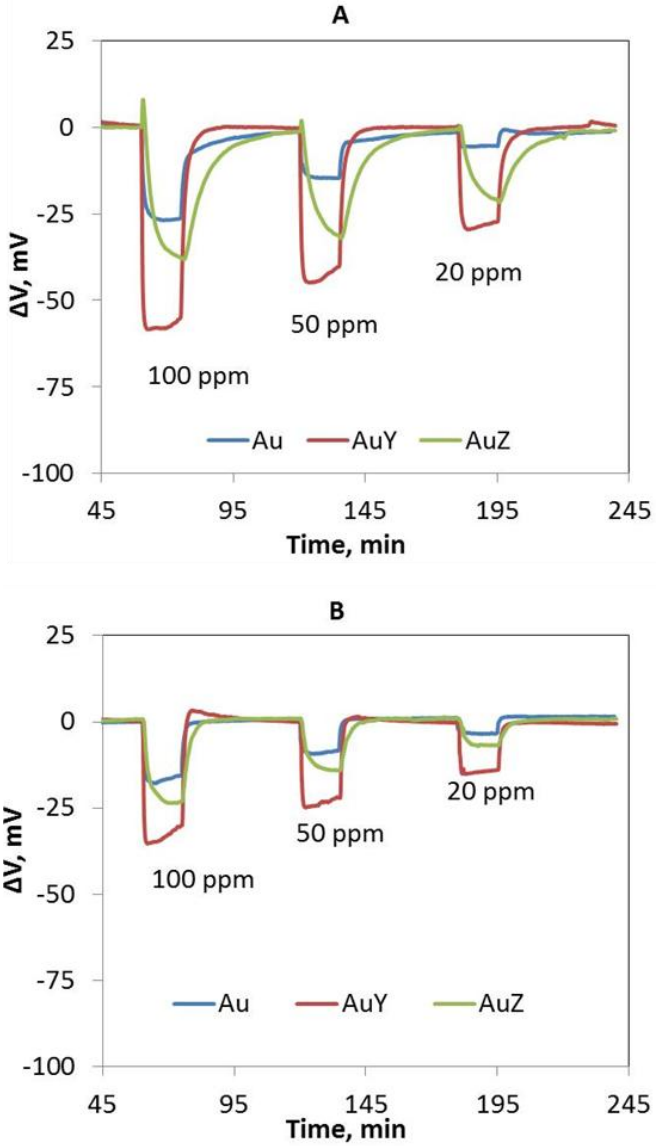

Figure 10: Sensor responses (ΔV) of Au, AuZ and AuY sensors to different concentrations of NO_2 in presence of 12% O_2 and 1.5% H_2O at A) 500°C and B) 550°C

For example, Figure 11 allows to compare responses and recovery times of the three sensors during addition of 100 ppm NO_2 at 500°C. Response time for AuY is the shortest one, at approximately 50 s. The Au sensor shows a longer response time around 120 s. The AuZ sensor is extremely slow: even after 15 min, the signal is not stable. Whatever the electrode, several minutes are necessary to recover the initial response after the end of the NO_2 exposure at 500°C. The

utilization of Au-Y composite can strongly reduce this recovery time which is 8 min instead of 45 min for both Au and AuZ. These long recovery times are probably linked with a strong adsorption of NO_2 onto the electrodes. At higher temperature (550°C) and for a lower concentration of NO_2 (20 ppm), the recovery times become reasonable (considering the dead volume of the cell) on AuY (130 s) and Au (70 s).

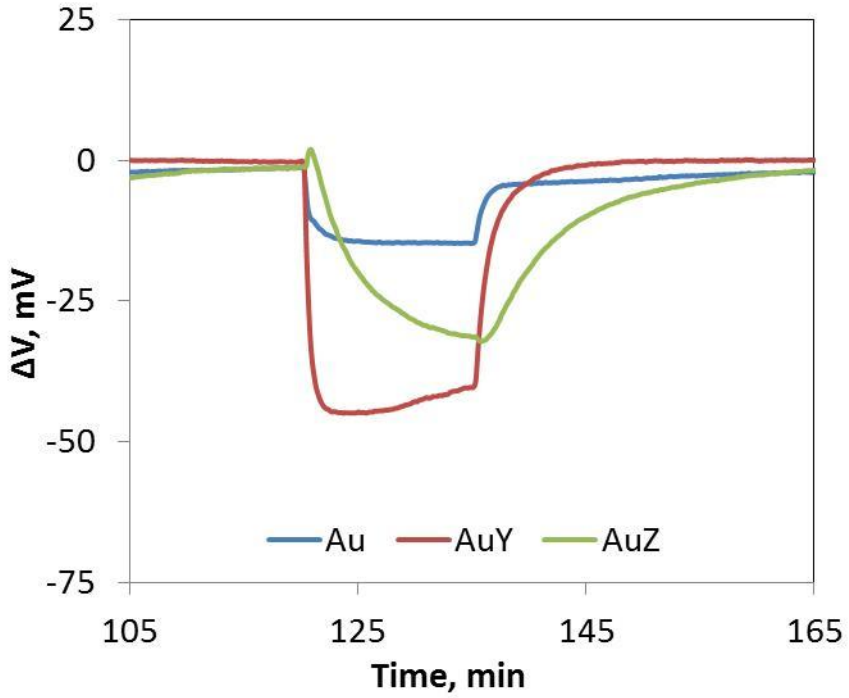

Figure 11: Sensor responses (ΔV) of Au, AuZ and AuY sensors to 100 ppm of NO_2 in presence of 12% O_2 and 1.5% H_2O at 500°C

Conclusions

The objective of this study was to study the influence of gold composite electrodes on the performances of a mixed potential Au/YSZ/Pt sensor. The effect of YSZ and ZrO_2 additions to the gold electrode on the response toward NO_2 was investigated between 450°C and 550°C. The initial gold electrode was quite dense. SEM characterizations evidenced that the porosity and then the number of triple phase boundaries were increased when ZrO_2 and YSZ were incorporated into the Au electrode. However, with ZrO_2 addition, polarization resistance was not modified compared to reference Au/YSZ/Pt sensor. In this case, the presence of porosity in the electrode damages the sensor performances both in terms of NO_2 sensitivity and of signal stability. On the contrary, as shown by electrochemical impedance measurements, the polarization resistance was

significantly reduced in the case of Au-YSZ electrode. Such a result indicates that the electrochemical properties for the oxygen electrode reaction were only improved for the Au-YSZ composite electrode because the ionic conductivity of YSZ can delocalize the electrode reaction in the overall electrode volume. Furthermore, the addition of YSZ improved the sensitivity toward NO_2 as well as the response time of Au-based electrodes. As a conclusion, porous Au-YSZ composite electrodes in a YSZ-based sensor have a beneficial effect compared to pure gold electrode.

References

1. Regulation No 715/2007 of the European Parliament and of the Council of 20 June 2007. Official Journal J L 171, 29.6.2007, 030, 284-299.

2. N. Docquier, S. Candel, Combustion control and sensors: a review Progress in energy and Combustion science, 28, (2002) 107-150.

3. V.I. Pârvulescu, P. Grange, B. Delmon, Catalytic removal of NO, Catalysis Today, 46, (1998) 233-316.

4. D. Wang, D. Racine,H. Husted and S. Yao, Sensing Exhaust NO2 Emissions Using the Mixed Potential Principle, SAE Technical Paper 2014-01-1487, 2014, doi:10.4271/2014-01-1487.

5. J. Gao, J.-P. Viricelle, C. Pijolat, P. Breuil, P. Vernoux, A. Boreave, A. Giroir-Fendler, Improvement of the NOx selectivity for a planar YSZ sensor, Sensors and Actuators B, 154, (2011) 106–110

6. S. Somov, G. Reinhardt, U. Guth, W. Göpel, Gas analysis with arrays of solid state electrochemical sensors: implications to monitor HCs and NOx on exhaust, Sensors and Actuators B, 35-36, (1996) 409-418

7. W.-F. Zhang, P. Schmidt-Zhang, U. Guth, Electrochemical studies on cell M/YSZ/Pt (M=Pt, Pt-Ga2O3) in NO, O2, N2 mixtures, Solid state Ionics, 169 (2004) 121-128

8. C. Yin, Y. Guan, Z. Zhu, X. Liang, B. Wang, Q. Diao, H. Zhang, J. Ma, F. Liu, Y. Sun, J. Zheng, G. Lu, Highly sensitive mixed-potential-type NO2 sensor using porous double layer YSZ substrate, Sensors and Actuators B, 183 (2013) 474-477.

9. J. Zosel, D. Westphal, S. Jakobs, R. Müller, U. Guth, Au-oxide composites as HC-sensitive electrode material for mixed potential gas sensors, Solid State Ionics, 152-153 (2002) 525-529

10. N. Miura, S. Zhuiykov, T. Ono, M. Hasei, N. Yamazoe, Mixed potential type sensor using stabilized zirconia and ZnFeO4 sensing electrode for NOx detection at high temperature, Sensors and. Actuators B, 83 (2002), 222–229

11. N Guillet, R Lalauze, J.-P Viricelle, C Pijolat, L Montanaro, Development of a gas sensor by thick film technology for automotive applications: choice of materials—realization of a prototype, Materials Science and Engineering: C 21 (2002), 97–103

12. C. Pijolat, G. Tournier, J.P. Viricelle, Detection of CO in H2-rich gases with a samarium doped ceria (SDC) sensor for fuel cell applications, Sensors and Actuators B, 141, 1(2009), 7-12

13. J. Zosel, D. Tuchtenhagen, K. Ahlborn, U. Guth, Mixed potential gas sensor with short response time, Sensors and Actuators B, 130 (2008), 326-329

14. C. Yin, Y. Guan, Z. Zhu, X. Liang, B. Wang, Q. Diao, H. Zhang, J. Ma, F. Liu, Y. Sun, J. Zheng, G. Lu, Highly sensitive mixed-potential-type NO2 sensor using porous double-layer YSZ substrate, Sensors and Actuators B, 183 (2013), 474-477

15. J.-C. Yang, P. K. Dutta, High temperature potentiometric NO2 sensor with asymmetric sensing and reference Pt electrodes, Sensons and Actuators B, 143, 2 (2010) 459-463

16. N. Guillet, R. Lalauze, J.P. Viricelle, C. Pijolat, The influence of the electrode size on the electrical response of a potentiometric gas sensor to the action of oxygen, IEEE Sensors Journal, Vol.2 n°4 (2002) 349-353

17. X. ChaoYang, L. XuChen, Y. Yan, W. TiZhuang, Z. ZhiMin, Y. SuPing, Preparation of nano-structured Pt-YSZ composite and its application in oxygen potentiometric sensor, Applied Surface Science, 257, (2011) 7952-7958

18. H.-S. Song, J. Moon, H. Jin Hwang, Electrochemical decomposition of NO over composite electrodes on YSZ electrolyte, Journal of the European Ceramic Society, 26 (2006), 981-986

19. T. Striker, V. Ramaswamy, E. N. Armstrong, P. D. Willson, E. D. Wachsman, J. A. Ruud, Effect of nanocomposite Au–YSZ electrodes on potentiometric sensor response to NOx and CO, Sensors and Actuators B, 181 (2013), 312-318

20. V. V. Plashnitsa, P. Elumalai, Y. Fujio, N. Miura, Zirconia-based electrochemical gas sensors using nano-structured sensing materials aiming at detection of automotive exhausts, Electrochimica Acta, 54 (2009), 6099–6106

21 J.C. Yang, P.K. Dutta, High temperature amperometric total NOx sensors with platinum-loaded zeolite Y electrodes, Sensors and Actuators B: Chemical 123 (2007) 929–936.

22. M. Kleitz, M.C. Steil, Microstructure blocking effects versus effective medium theories in YSZ, Journal of the European Ceramic Society, 17 (1997), 819-829

23. L. Bultel, P. Vernoux, G, Gaillard, C. Roux, E. Siebert, Electrochemical and catalytic properties of porous Pt-YSZ composites, Solid State Ionics 176 (2005), 793-801

24. T. Wang, R. F. Novak, R. E. Soltis, A study of factors that influence zirconia/platinum interfacial impedance using equivalent circuit analysis, Sensors and Actuators B, 77 (2001), 132-138

25. L. Y. Woo, L. P. Martin, R. S. Glass, R. J. Gorte, Impedance characterization of a model Au/Yttria-Stabilized Zirconia/Au electrochemical cell in varying oxygen and NOx concentration, Journal of Electrochemical society, 154-4 (2007), J129-J135

26. L. Y. Woo, L. P. Martin, R. S. Glass, W. Wang, S. Jung, R. J. Gorte, E. P. Murray, R. F. Novak, J. H. Visser, Effect of electrode composition and microstructure of impedancemetric nitric oxide sensors based on YSZ electrolyte, Journal of Electrochemical society, 155 (2008), J32-J40

27. L. Y Woo, R. S. Glass, N. F. Robert. V. H. Jaco, Effect of electrode material and design on sensitivity and selectivity for high temperature impedancemetric NOx sensors, Journal of Electrochemical society, 157 (2010), 81-97

28. S. Pil Yoon, S. Woo Nam, K. Seung-Goo, H. Seong-Ahn, H. Sang-Hoon, Characteristic of cathodic polarization at Pt/YSZ interface without the effect of electrode microstructure, Journal of Power Sources, 115, (2003), 27-34

29. M. Mori, Y. Itagaki, Y. Sadaoka, S.-I. Nakagawa, M. Kida, T. Kojima, Detection of offensive odorant in air with a planar-type potentiometric gas sensor based on YSZ with Au and Pt electrodes, Sensors and Actuators B, 191 (2014), 351-355

30. L. Chevallier, E. Di Bartolomeo, M. L. Grilli, M. Mainas, B. White, E. D. Wachsman, E. Traversa, Non-Nernstian planar sensors based on YSZ with a Nb2O5 electrode Sensors and Actuators B, 129 (2008), 591–598

Chapter 4

Sensor responses in galvanostatic mode

Outline

Chapter 4 : Sensor responses in galvanostatic mode

Résumé

Ce chapitre décrit les propriétés électriques et électrochimiques ainsi que les réponses de capteurs à deux et trois électrodes en mode galvanostatique avec de faibles courants de l'ordre de dizaines de nA. Dans un premier temps, les propriétés électriques (chute ohmique) et électrochimiques des capteurs à deux électrodes ont été mesurées à la température de 450 °C dans le gaz de base (12% O_2, 2% H_2O, N_2). Deux types de capteurs à 2 électrodes ont été étudiés: Pt/YSZ/Pt et Pt/YSZ/Au. Les chutes ohmiques ont été déterminées pour des configurations de cellules différentes (distances entre les électrodes) par spectroscopie d'impédance. Ensuite, les surtensions des électrodes sensibles en or ont pu être estimées par comparaison entre les deux séries de capteurs. Il a été constaté que la surtension de l'or pour la réaction d'électrode à oxygène est beaucoup plus élevée que celle du Pt.

Nous avons ensuite étudié des capteurs à trois électrodes: Pt(CE), Pt(RE) et Au(WE). La mesure du signal du capteur est réalisée entre l'électrode sensible (WE) et l'électrode de référence. La valeur du signal est affectée par la position de l'électrode de référence, car elle est proportionnelle à la chute ohmique liée à la résistance de la couche d'électrolyte et à l'intensité du courant de polarisation. Nous avons choisi de placer l'électrode de référence au milieu des deux autres électrodes afin d'assurer une égale répartition des chutes ohmiques. En mesurant la résistance entre électrode de référence et électrode de travail par spectroscopie d'impédance, nous avons pu soustraire la chute ohmique et calculer la surtension de l'électrode sensible en or.

La forte dérive de la surtension de l'électrode sensible dans le temps perturbe la ligne de base du capteur et ne permet pas de réaliser des mesures très précises. En utilisant un matériau composite entre l'or et la zircone yttriée (chapitre 3), nous avons pu améliorer la stabilité de la ligne de base et abaisser la surtension de l'électrode sensible. Néanmoins, cette diminution de surtension baisse aussi la sensibilité au NO_2 qui passe de 290 mV/décade avec une électrode sensible en or à 35 mV/décade pour une électrode composite. Cependant, ce nouveau matériau d'électrode permettra d'augmenter le courant de polarisation et finalement la surtension afin d'augmenter la sensibilité au NO_2.

Summary

This chapter describes electrical and electrochemical properties as well as the responses of two- and three-electrode sensors in galvanostatic mode using low current intensity of the order of tens nA. First, electrical (ohmic drop) and electrochemical properties of two-electrode sensors have been carried out at 450 °C in the ba se gas (12% O_2, 2% H_2O, N_2 – balanced). Two kinds of 2-electrode sensors have been investigated: Pt/YSZ/Pt and Pt/YSZ/Au. Their ohmic drops were determined for different cell configurations (distances between electrodes) by impedance spectroscopy. Then, the Au and Pt sensing electrode overpotentials could be estimated by comparison between the overall overpotential between the two series of sensors. It was found that the Au overpotential for the oxygen electrode reaction is much higher than the one of Pt.

For three-electrode sensors, the measurement of the sensor response is recorded between the sensing electrode (WE) and the reference electrode The measured value of the sensor signal was found to be linked with the position of the reference which mainly alters the ohmic drop between the two electrodes. This latter depends on the electrolyte layer resistance and the bias current. EIS technique was used to measure the resistance between the reference electrode and the sensing electrode. Therefore, the ohmic drop voltage was subtracted to calculate the electrode overpotential of the sensing electrodes.

The high drift with time of the overpotential of the Au sensing electrode perturbs the sensor signal and does not allow to achieve accurate measurements. Using composite material (AuY) made of Au and Yttria-Stabilized Zirconia (YSZ) (Chapter 3), allowed us to improve the stability of the baseline and to decrease the sensing electrode overpotential. However, the sensitivity to NO_2 also decreases from 290 mV/decade with the Au electrode to 35 mV/decade with the composite one. Nevertheless, this composite electrode could allow working at higher polarization currents in order to reach higher overpotentials for which NO_2 sensitivity could be higher.

4.1. Two-electrode sensors: Pt/YSZ/Pt, Pt /YSZ/Au

4.1.1. Galvanostatic mode measurements

The galvanostatic measurements of the responses of two-electrode sensors were realized by using electrical connections described in figure 4.1. The first electrode, denoted as counter electrode (CE) and made of Pt was polarized as an anode, while the second one composed either of Pt (figure 4.1-A) or Au (Figure 4.1-B) was the working electrode (WE). This latter was negatively polarized as a cathode (see chapter 2). This is also the sensing one (SE). To reach the imposed polarization current i_{pol}, a polarization voltage V_{pol} ($V_{pol} = V_{CE}-V_{WE}$) was applied between the two electrodes. The resistance of the YSZ electrolyte between the two electrodes is denoted as R_{YSZ}.

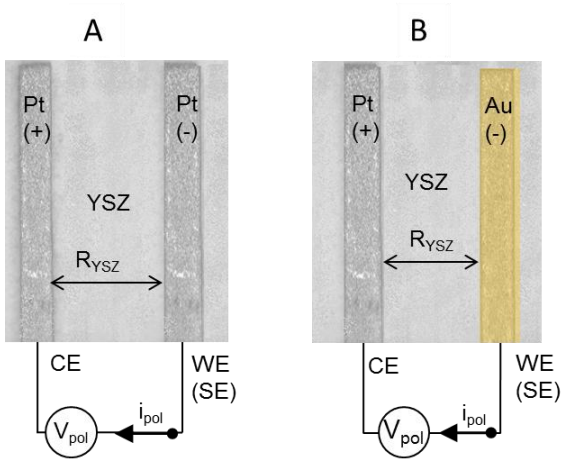

Figure 4.1: The electrical connection configuration of two-electrode sensors in galvanostatic mode measurements A – Pt/YSZ/Pt, B – Pt/YSZ/Au

As shown in chapter 2, according to equation 2.3, Vpol is linked to the open-circuit voltage (OCV = $\Delta V° = V°_{RE} - V°_{SE}$), the ohmic drop and the overpotentials of the two electrodes:

$$V_{pol} = \Delta V° + Ri_{pol} + \eta_{WE} + |\eta_{CE}|$$

Let us note that the ohmic drop induced by the electrodes was neglected since the electrode conductivity of both Pt and Au electrodes are assumed to be high. By using a two electrode cell configuration, this is impossible to separate the two overpotentials. Therefore, we have measured the overall overpotential (η_{total}), as follow:

$$\eta_{total} = V_{pol} - \Delta V° - Ri_{pol} \qquad (4.1)$$

where $\eta_{total} = \eta_{Pt\,WE} + |\eta_{Pt\,CE}|$ for Pt/YSZ/Pt sensor.
and $\eta_{total} = \eta_{Au\,WE} + |\eta_{Pt\,CE}|$ for Pt/YSZ/Au sensor.

As the material and the size of counter electrodes are identical for both sensors, one can assume that the η_{total} modifications between the two systems will be essentially due to the variation of the overpotential of the sensing electrode. To get insights into η_{WE} variations, OCV and V_{pol} values upon various i_{pol} have been measured. In addition, the electrolyte resistance between electrodes has been estimated by using impedance spectroscopy. Then, by using equation 4.1, one can calculate values of the total overpotential.

The OCV value of the Pt/YSZ/Pt sensor is normally equal to zero if the size of the two electrodes are perfectly identical. Practically, OCV values were between 0 and +5 mV in the temperature range 400 – 550°C whatever the composition of the feed gas. On the other hand, OCV values of the Pt/YSZ/Au sensor were found to be around +50, +60 mV at 450 °C and vanished to 0 mV above 550°C in the base gas (Table 4.1)

Table 4.1: The OCV variations of Pt/YSZ/Au sensor as a function of the temperature in base gas

Temperature	400 °C	450 °C	500 °C	550 °C	600 °C
ΔV° (OCV) / mV (This work)	62	49	25	10	3
ΔV°(OCV) / mV (Gao PhD 2011)	36	25	20	15	-

The OCV value of the Pt/YSY/Au sensor near 550°C is around +10 mV, this indicates that Pt and Au electrodes have almost identical potential, which is proportional to the activity of oxygen on electrodes. At this temperature, fast desorption of oxygen takes place on Pt as well on Au. Therefore, the oxygen coverage oxygen becomes low on both electrodes and potentials approaches one to each other.

Table 4.2 shows the OCV variations of two different Pt/YSZ/Au sensors with pO_2. The increase of the concentration of O_2 from 0.8 % to 19.7 % O_2 in base gas produces a slight decrease of OCV of -18 mV. The variation of the OCV of the Pt/YSZ/Au sensor with pO_2 was also used for the calculation of the overpotential as a function of pO_2 (Chapter 5). A quite good repeatability in the OCV values is observed between the two sensors.

Table 4.2: The OCV variations of two Pt/YSZ/Au sensors with pO_2 at 450°C

vol% O_2	0.8	4.7	12	19.7
Sample 1, mV	65	55	49	47
Sample 2, mV	64	53	48	45

When the electrode is exposed to oxygen, the potential is controlled by the partial pressure and the kinetic of oxygen electrode reaction. If the electrode is polarized, the difference between the equilibrium potential $V°_{SE}$ and the potential under polarization is called overpotential.

In the presence of CO, NO_2 or NO in the base gas, the OCV value of the Pt/YSZ/Au sensor at 450°C is positive of the order of +40-50 mV under CO (100 ppm) and NO (+30-40 mV) and negative under NO_2 (-50/-60mV upon 100 ppm of NO_2). These values correspond to the mixed potential [Gao 2011], [Somov 1996], [Sekhar 2010], which is controlled by the kinetic of two or more parallel electrode reactions [Y. Guan 2014]. As a consequence, the measurement of the OCV of the Pt/YSZ/Au is a difference between two mixed potentials (Au – as sensing and Pt – as reference) as described in chapter 3. In galvanostatic mode, this mixed potential disappears because of the external current. As the values of the overpotentials in galvanostatic mode are much higher than those of OCV, we have decided to only consider OCV values in base gas for the calculation of overpotentials in presence of CO, NO or NO_2. At the beginning of each tests, OCV values in base gas were measured and used for the calculation of overall overpotentials of sensors.

4.1.2. Measurements of the ohmic drop as a function of the distances between electrodes

Solid electrolyte is one of most important component of solid state electrochemical sensors. The detailed role of the YSZ layer is described in chapter 1. As mentioned in Chapters 2 and 3, the high porosity of the YSZ layer, made by screen-printing, induces large ohmic resistances, of the order of tens of MΩ at temperatures 450-550 °C (see Figure 5 in Chapter 3). Therefore, a small shift in the distance between the 2 electrodes can produce high modifications in the ohmic drop values. We have produced by screen-printing a series of symmetrical Pt/YSZ/Pt sensors with different spacing between the 2 electrodes: 0.31, 0.91, 1.51, 2.27 mm. The real distances between electrodes were measured by using an optic microscope (Figure 4.2).

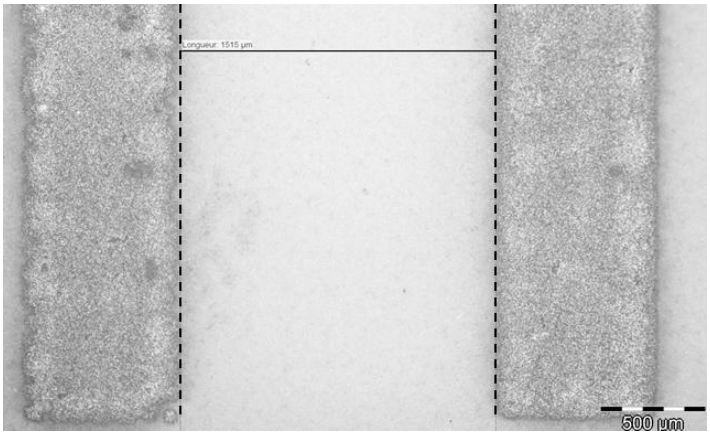

Figure 4.2: Image of Pt/YSZ/Pt sensor with measured inter-electrode distance

For EIS measurements of R_{YSZ}, AC signal amplitudes of 150 mV were applied between the two electrodes in the frequency range 10^5 Hz – 10^{-1} Hz. EIS measurements were performed between 450°C and 550°C with steps of 50°C after 3 h of annealing at each temperature. Figure 4.3 displays an example of Nyquist diagrams obtained at 500°C for 4 various inter-electrode distances. Values of R_{YSZ} were extracted from these diagrams by fitting the high-frequency part.

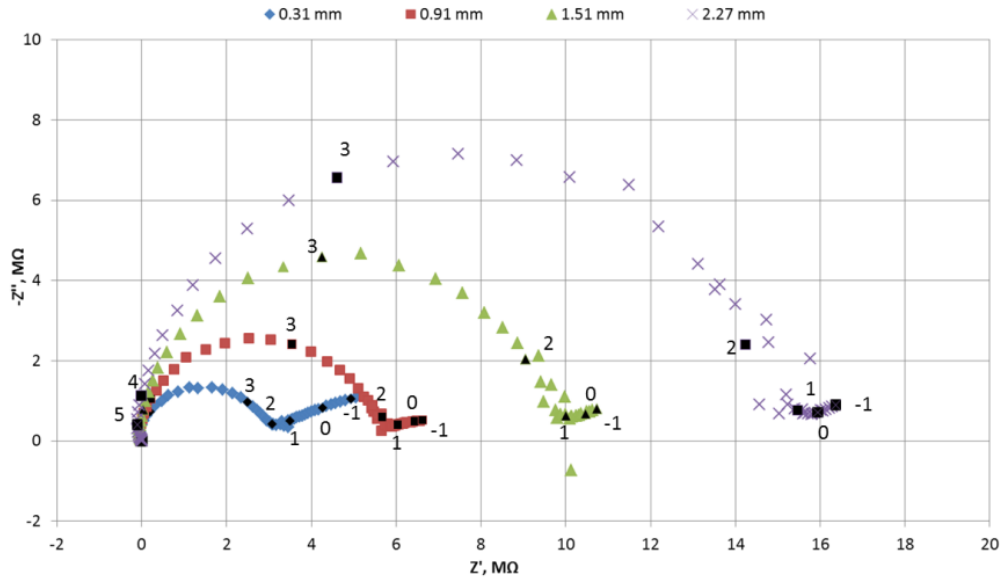

Figure 4.3: Nyquist plots of Pt/YSZ/Pt sensors with different spacing at 500 °C in base gas. Black dots indicate the log of frequency.

Figure 4.4 presents variations of R_{YSZ} as a function of the distance between the 2 electrodes for 3 temperatures.

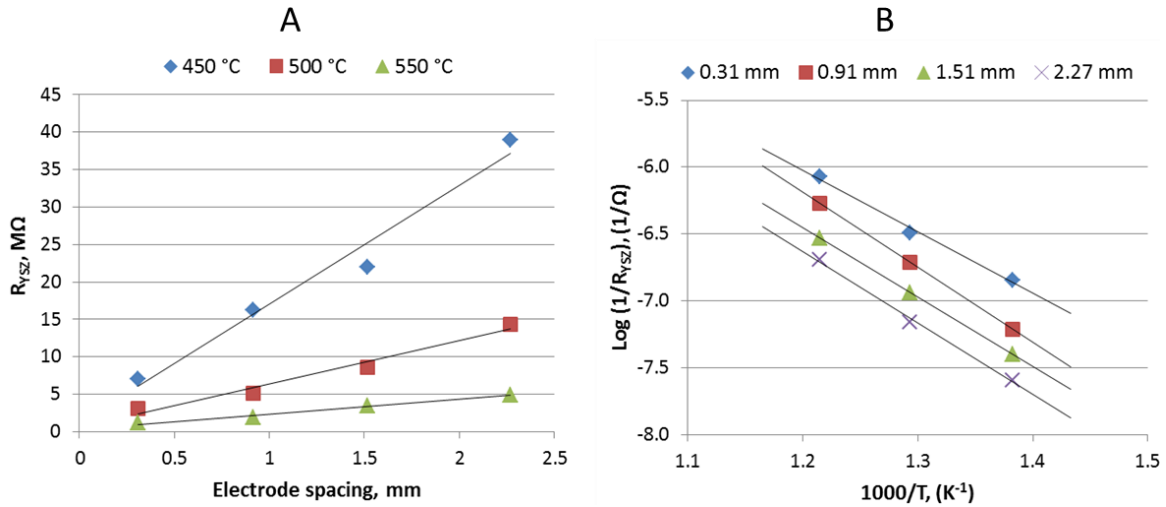

Figure 4.4: Resistance of the YSZ electrolyte layer as a function of the electrode spacing at different temperatures (A) and Arrhenius diagram (B).

As was shown previously in Chapter 3, thick YSZ layers present high values of resistance at 450-550°C of the order of MΩ. The linearity of the variations of R_{YSZ} values with the distance at three temperatures: 17.2 MΩ/mm at 450 °C, 6.3 MΩ/mm at 500 °C and 2,2 MΩ/mm at 550°C, indicates a good homogeneity of the electrolyte layers and a correct repeatability in the elaboration process of sensors. Activation energies calculated from the Arrhenius diagram (Figure 4.4-B) were found to be 1.07±0.03 eV. These values correspond to those reported for porous YSZ membranes in the literature. [Kleitz, 1997]

This study evidences the necessity to accurately control the sensor production. Indeed, a displacement of the electrode position of ±0.1 mm could produce a huge variation of R_{YSZ} of the order of ±1.5 MΩ at 450 °C and ±0.58 MΩ at 500 °C. This variation can be negligible for potentiometric mixed-potential sensors, but when a polarization current is applied, high modifications of R_{YSZ} can produce large deviations of the sensor responses. As example, for two-electrode sensor with 1 mm of spacing and R_{YSZ} = 15 MΩ at 450°C, a deviation of +0.1 mm can produce an increase of V_{pol} from +750 mV to +825 mV upon a polarization current of 50 nA.

4.1.3. Determination of overall overpotentials

Coupling equation 4.1 and the measurement of R_{YSZ} values in galvanostatic mode, one can calculate the overall overpotential for both 2-electrode sensors: Pt/YSZ/Pt and Pt/YSZ/Au.

Assuming that values of $\eta_{Pt\ CE}$ are similar for both sensors, the overall overpotential variations between the 2 systems are only due to the difference between the overpotentials of the two working electrodes. Therefore, we can compare the electrochemical properties of Au and Pt working electrodes.

First, we have measured the overall overpotentials of the two electrode sensors. As an example, the procedure is described for a Pt symmetrical sensor with a distance between the 2 electrodes of 0.31 mm. Different cathodic currents, in the range 0 – 50 nA, were applied according to Figure 4.5 at 450°C in the base gas. The polarization voltage, V_{pol}, is the sensor response. It was measured as a function of time upon successive constant current applications of 2 hours, starting from the lowest intensity up to the highest (Figure 4.5). The first two hours without any polarization allows measuring the ΔV° in base gas for Pt/YSZ/Pt sensor, which was equal to 4 mV.

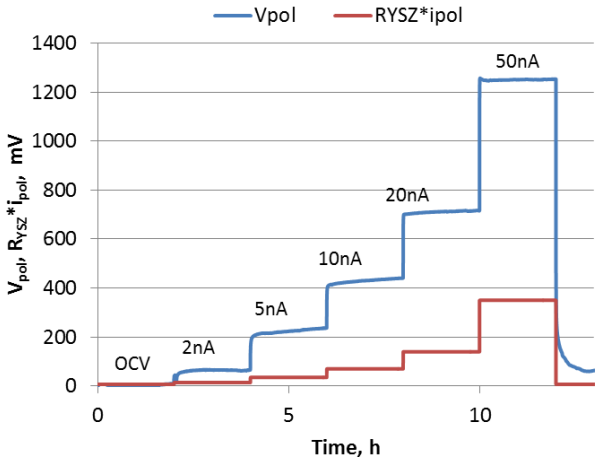

Figure 4.5: Variations of the Ohmic drop ($R_{YSZ}i_{pol}$) and the polarization voltage Vpol as a function of time at different polarization currents. Two-electrode sensor: Pt/YSZ/Pt cell (0.31 mm spacing). Temperature: 450 °C in base gas.

The ohmic drop was calculated by using EIS data presented in figure 4.4-B. As expected, the ohmic drop linearly increases with the current according to the Ohm's law, confirming that it can be easily measured from EIS data. Figure 4.6 shows that the ohmic drop represents a significant part of the polarization voltage: 22.5% upon 2 nA, 18.6% upon 5 nA 17.8% upon 10 nA 20.7% upon 20 nA and 28% upon 50 nA.

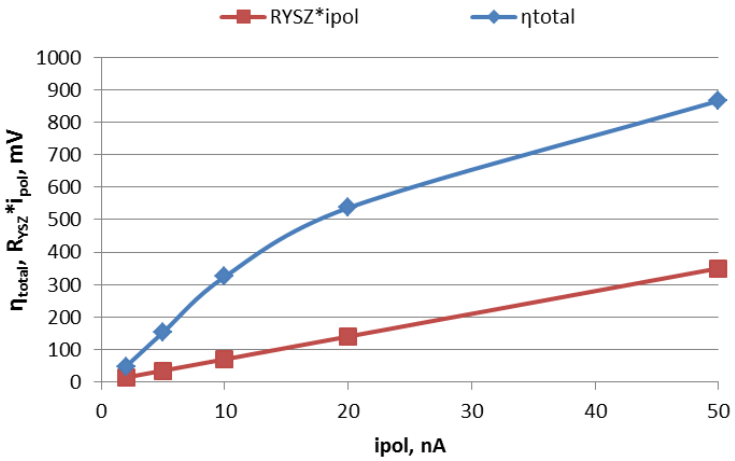

Figure 4.6: Variations of the Ohmic drop (R_{YSZ}*i_{pol}) and of the overall overpotential (η_{total}) as a function of the applied current. Two-electrode sensor: Pt/YSZ/Pt cell (0.31 mm spacing). Temperature: 450 °C in base gas.

The overall overpotential was found to follow a logarithmic variation with the applied current, as described by the Tafel equation (Figure. 4.7). We have also calculated the overall overpotential of Pt/YSZ/Au electrodes by using equation 4.1. The total overpotential of Pt/YSZ/Au sensor was calculated from the measurements of R_{YSZ} and OCV ($V°_{CE} - V°_{WE}$) which was found to be 45 mV at 450°C in base gas.

Figure 4.7 depicts logarithmic variations of overall overpotentials of Pt/YSZ/Pt and Pt/YSZ/Au systems with the applied current. Overall overpotentials of the Au/YSZ/Pt sensor are much higher than those of the symmetrical Pt sensor. This indicates that the electrochemical properties of Au for the oxygen electrode reaction are poor compared to those of Pt at 450°C, in good agreement with literature data [Razniak 2011], [Van Hassel 1991]. The linearity of overpotential for each electrode indicates a charge transfer limiting step. Further investigations of electrode kinetic have been performed with a 3-electrode sensor and are presented in chapter 5.

The total oxygen electrode reaction taking place at Au/YSZ or Pt/YSZ interface is the following:

$$O_2 + 2V_O^{\bullet\bullet} + 4e^- \leftrightarrow 2O_O^x$$

where, in Kroeger Vink notation, $V_O^{\bullet\bullet}$ is an oxygen vacancy of YSZ and O_O^x is a normal O^{2-} ion in the YSZ lattice.

According to literature data, the nature of this difference between Au and Pt in previous reaction can be related to the low activity of gold to adsorb oxygen and then to a low coverage of gold by oxygen [Kishimoto 2008], [Van Hassel 1991]. The different morphology between a porous Pt electrode and a dense Au electrode can also explain these different electrochemical behaviors since the number of tpb is much higher on Pt [Rezniak 2011].

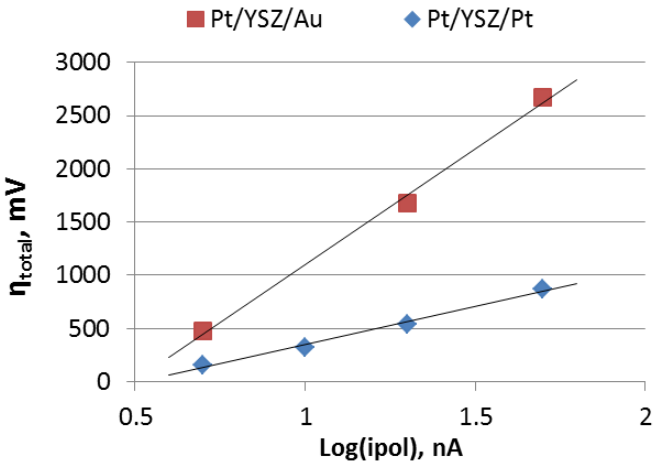

Figure 4.7: Logarithmic variations of the overall overpotential of Pt/YSZ/Au and Pt/YSZ/Pt sensors with the applied current. T=450°C in base gas.

The SEM micrographs (chapter 3) evidence these different morphologies between Au and Pt electrodes. The platinum electrode is highly porous, contains micrometric Pt particles (1 - 5 µm) and pores (1 - 5 µm). Contrary to Pt, the Au electrode is dense and totally covers the surface of the electrolyte. The interactions between the gold film and the porous YSZ layer are poor. In this case, TPB (electrode/electrolyte/gas) is limited by the perimeter of the Au dense film.

To evaluate the difference in electrochemical efficiency for the oxygen electrode between Au and Pt, we have calculated the ratio of overall overpotentials η_{total}(Pt/YSZ/Au)/ η_{total}(Pt/YSZ/Pt) as a function of temperature and applied current (Figure 4.8). The highest ratio at around 3.7 is observed at 550 °C upon 50 and 100 nA. Below 550°C, the ratio is about 2.25-3 for 5, 20 and 50 nA. Whatever the temperature and the applied current, the ratio is larger than 2. Therefore, for all studied temperatures and current ranges investigated in this study, the overall overpotential of the Pt-Au system is, at least, 2 times higher than that of the symmetrical Pt sensor.

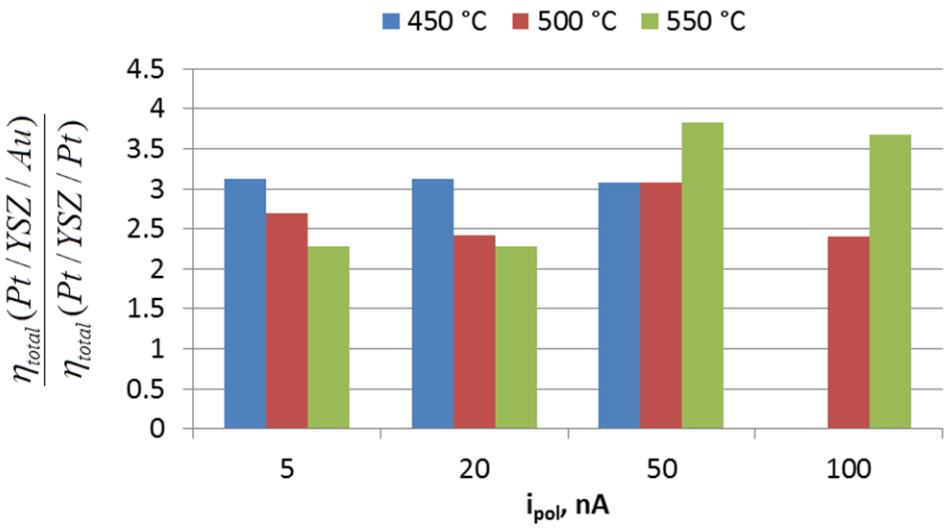

Figure 4.8: Ratio between the overall overpotentials of Pt/YSZ/Au and those of Pt/YSZ/Pt sensor at 450, 500 and 550 °C in base gas.

4.1.4. Two-electrode sensor responses

The responses of the two sensors in galvanostatic mode have been measured in presence of CO, NO and NO_2 in the base gas. The sensors responses were monitored for three different applied current (5, 20 and 50 nA). The ohmic drop of each sensor was measured by using EIS. The OCV values of the two sensors in the base gas were found to be 4 mV and 45 mV for Pt/YSZ/Pt and Au/YSZ/Pt, respectively.

Total overpotentials of the 2 sensors have been calculated according to the equation 4.1. Figure 9, 10 and 11 show overall overpotentials variations of Pt/YSZ/Pt and Pt/YSZ/Au cells during successive injections at 450°C of CO, NO_2 and NO. During the first hour of experiments, the sensors were not polarized in order to measure OCV values in the base gas. Then, three successive currents were applied for 5 hours from the lowest intensity up to the highest one (5, 20 and finally 50 nA). For each current, the pollutant injection sequence was the following: 1 h in base gas / pulse of pollutant (CO, NO_2 or NO) of 10 ppm for 1 h / 1 h in base gas / pulse of pollutant (CO, NO_2 or NO) of 100 ppm for 1 h / 1 h in base gas. The first sequence was performed with CO injections, then with NO_2 and finally with NO. After each sequence of measurements, sensors were cooled down to room temperature by convection and then again heated up 450°C in 2 minutes.

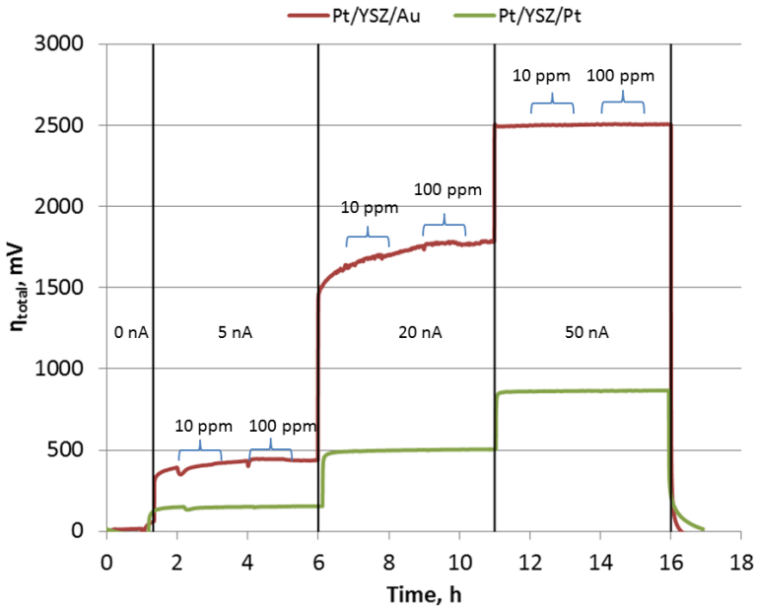

Figure 4.9: Variations of the overall overpotential of the two electrode sensors at 450°C during pulses of CO (10 and 100 ppm) in the base gas for three different currents 5, 20 and 50 nA.

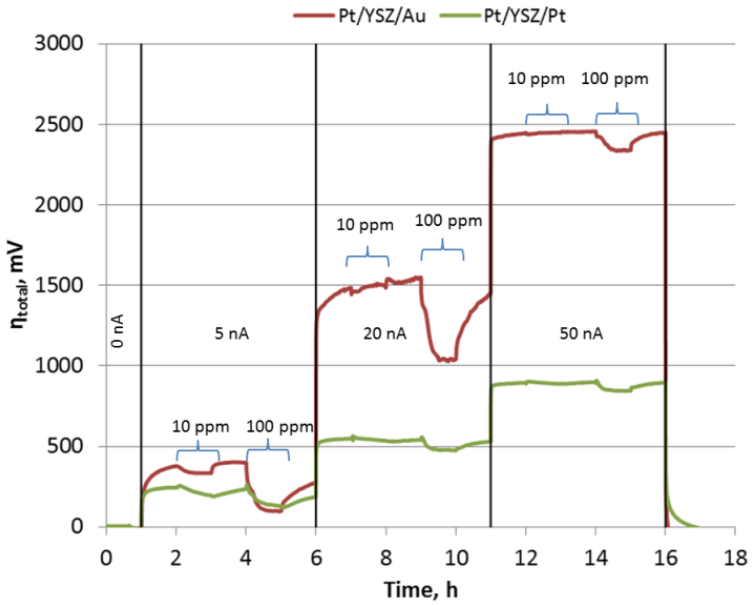

Figure 4.10: Variations of the overall overpotential of the two electrode sensors at 450°C during pulses of NO_2 (10 and 100 ppm) in the base gas for three different currents 5, 20 and 50 nA.

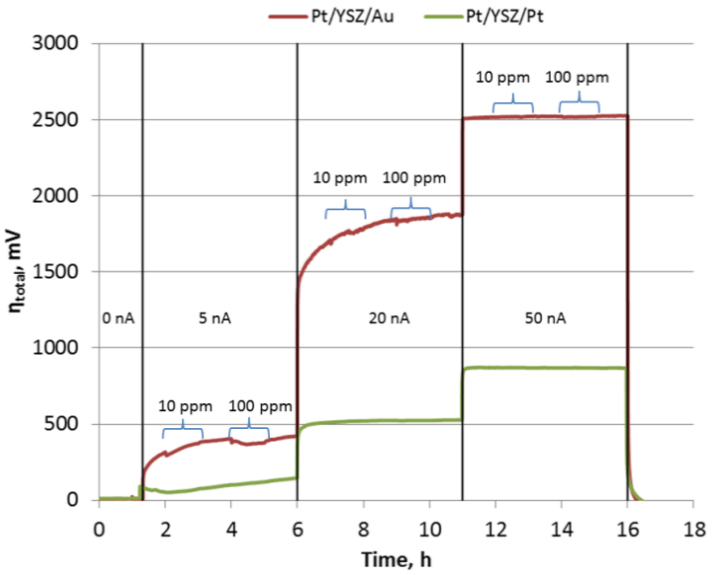

Figure 4.11: Variations of the overall overpotential of the two electrode sensors at 450°C during pulses of NO (10 and 100 ppm) in the base gas for three different currents 5, 20 and 50 nA

As can be noticed, overall overpotentials of the Pt/YSZ/Au sensor are much higher than those recorded on Pt/YSZ/Pt. During pulses of NO_2, overall overpotentials of the sensor with the Au sensing electrode dramatically decrease. For instance, a pulse of 100 ppm NO_2 produces a drop in η_{total} of 300-450 mV, 500-600 mV and 80-100 mV upon 5, 20 or 50 nA, respectively. For the Pt/YSZ/Pt sensor, the overall overpotential also decreases in presence of NO_2 but in much less extend: 100, 80 and 50 mV upon 5, 20 and 50 nA, respectively. The difference in the responses to NO_2 of the two sensors is much more pronounced for low current intensities, i.e. 5 and 20 nA. As NO_2 is an oxidizing gas, the galvanostatic mode can only produce the electrochemical reduction of NO_2 at the working electrode. These results clearly indicate that this electrochemical reaction strongly decreases the Au overpotential for low current intensities.

No variation of overpotentials for the two sensors upon 20 and 50 nA during injections of CO or NO (figures 4.9 and 4.11) have been observed.

The CO is a reducing gas; it can only produce electrochemical oxidation of CO at the Pt counter-electrode. This reaction does not seem to affect strongly the overall overpotential. This indicates that the predominant contribution is the electrochemical reduction of O_2 at the working and counter electrodes. Only small variations, less than 20 mV in presence of 100 ppm CO have been detected on Pt/YSZ/Au sensor that could be linked to a slight decrease of the oxygen coverage due the competitive adsorption between CO and O_2.

Similar conclusions can be proposed during pulses of NO. Possible electrochemical reactions that can occur in presence of NO, either the electrochemical reduction of NO at the working electrode or the electrochemical oxidation of NO at the counter electrode does not modify the kinetic of the electrochemical reduction of O_2 at the working and counter electrodes.

In presence of NO, we can expect the chemical transformation of NO into NO_2 on the Pt sensing electrode as Pt is an effective catalyst for the NO oxidation reaction [Benard 2005]. Therefore, this as-produced NO_2 may be detected by the sensor. However, the two sensors (Figure 4.11) did not detect any traces of NO_2 (no significant drop of the overpotential). This effect can be explained by the low catalytic activity of Pt electrode for NO oxidation since it presents an extremely low Pt dispersion [Gao 2010]. Then, the catalytically produced quantity of NO_2 could be too low to be detected by the sensor. However, only a slight decrease of the overpotential was observed upon 5 nA in presence of 100 ppm NO which is probably due to the catalytic activity of Pt for NO oxidation.

The comparison of Pt/YSZ/Au with Pt/YSZ/Pt sensors in polarization mode clearly indicates that the sensor signal is driven by the overpotential of Au electrode. At the same time, the increase with time of the total overpotential is related to the gold overpotential drift.

The results were reproduced with two different Pt/YSZ/Au sensors. The sensors responses during injection of CO, NO_2 and NO are presented in figures 4.12-14. The values of the overall overpotential in base gas of the two Pt/YSZ/Au sensors are not similar during the measurement sequences. Collected data of overpotential is presented in table 4.4.

Despites, these 2 sensors have been stabilized for 800°C during 120 h in air, important deviations in the overpotential measurements have been observed from one test to another one. The time drift of the overall overpotential is also observed for both sensors at 5, 20 and 50 nA. This could be due to the high overpotentials over 1.5 V which can modify strongly the interfacial resistance and produce the rearrangement of tpb number [Mutoro 2008] or, even the composition around the electrode [Razniak 2008].

Table 4.4: The overall overpotential of Pt/YSZ/Au sensor in base gas at 450°C before pulses of 100 ppm of pollutant gas

Test	i_{pol}, nA					
	5	20	50	5	20	50
	Sensor 1, η_{tot}, mV			Sensor 2, η_{tot}, mV		
Before 100 ppm CO	350	1660	2560	430	1742	2500
Before 100 ppm NO_2	510	1760	2635	400	1548	2450
Before 100 ppm NO	550	1880	2670	400	1833	2550

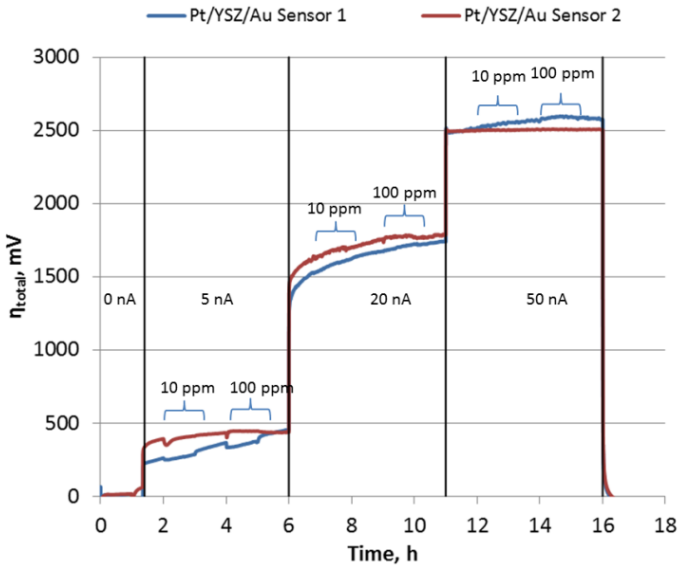

Figure 4.12: Variations of the overall overpotential of the two electrode sensors at 450°C during pulses of CO (10 and 100 ppm) in the base gas for three different currents 5, 20 and 50 nA

The reproducibility of overpotential between two Pt/YSZ/Au sensors is far to be perfect (Figure 4.12). However, we observed similar trends in the overpotential variations with time: gradual increase with time and similar sensing properties to NO_2 pulses for both sensors at different i_{pol}. The highest response was observed upon 20 nA of polarization. Deviations of the response between two sensors can reach around 150 mV at 5 nA, 200 mV for 20 and 50 nA. This difference can be explained by variations of the YSZ thickness layer and thermal properties of used material.

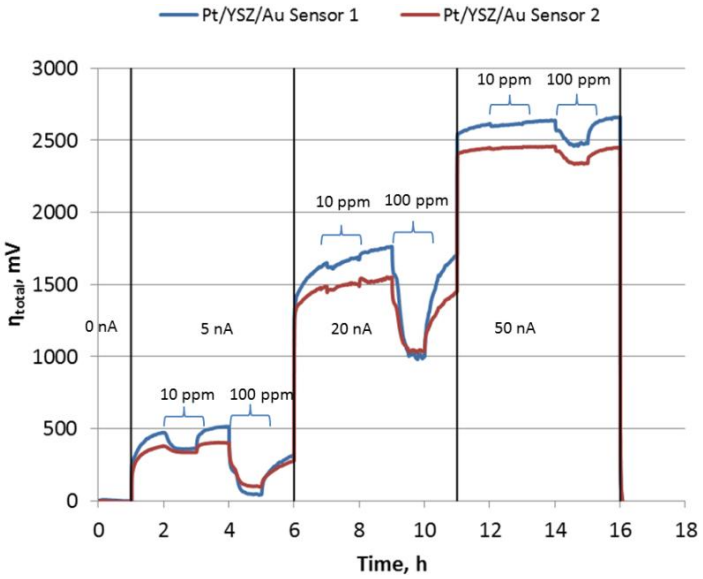

Figure 4.13: Variations of the overall overpotential of the two electrode sensors at 450°C during pulses of NO_2 (10 and 100 ppm) in the base gas for three different currents 5, 20 and 50 nA

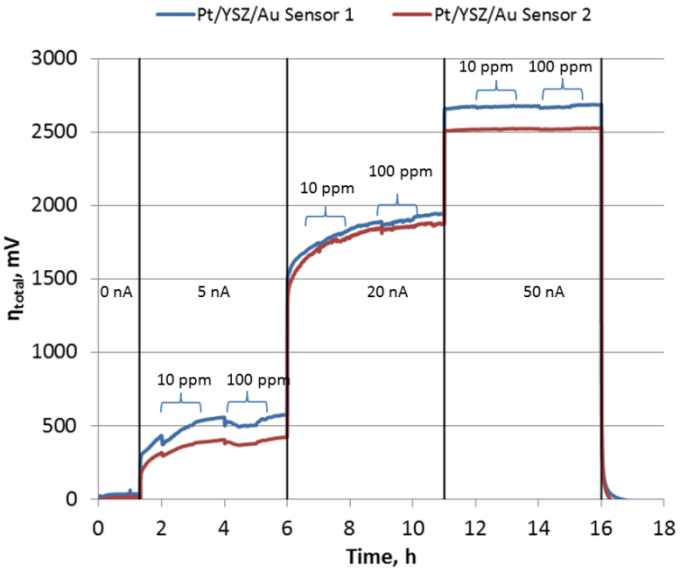

Figure 4.14: Variations of the overall overpotential of the two electrode sensors at 450°C during pulses of NO (10 and 100 ppm) in the base gas for three different currents 5, 20 and 50 nA

The simultaneous test Pt/YSZ/Au with Pt/YSZ/Pt sensors in polarization mode indicates clearly that the source of the sensor signal is overpotential of Au electrode. The instability of the sensor responses are clearly observed for Pt/YSZ/Au sensor and is probably due to the Au/YSZ interface. Relatively fast heating from room temperature to operating 450°C until 120 seconds and free cooling to room temperature after the test could produce the thermal cracking due to different TEC (Thermal Expansion Coefficients) between Al_2O_3, YSZ, and Au. Deeper investigations of the YSZ layer and the electrode/electrolyte interface during thermal cycling and polarizations should be performed to better understand the evolution with time of the sensor responses.

By using this two electrode configuration of the sensors, we cannot measure the overpotential of the working electrode but only of the overall overpotential of the two electrodes. Therefore, we have made a series of 3-electrode sensor, including a reference electrode, to evaluate the overpotential of the working electrode (Pt or Au).

4.2. Three-electrode sensors

4.2.1. Impact of the position of the reference electrode

In aqueous electrochemical system, the position of the reference electrode plays an important role in the electrochemical measurements. For accurate potentiometric measurements, the reference electrode must be located far from the active zone. This principle is not critical when the conductivity of liquid electrolytes is high. However, as shown in paragraph 4.1, the resistance of the porous YSZ electrolyte layer is quite high, of the order of tens MΩ at 450°C. Therefore, the position of the reference electrode can play an important role in the overall electrical properties. In addition, the home-made potentiostat, we used for these experiments, cannot compensate the ohmic loss. For this reason, this is preferable to study the influence of the position of the reference electrode on the measured potential.

A series of Pt-based three-electrode sensors were made by screen printing with different WE-RE distances (Figure 4.15).

Minimal size of RE was chosen to decrease the perturbation possibly provoked by the electrical field induced by the polarization between WE and CE. All electrodes were made from the same Pt paste. The working and counter electrodes are 4 mm length and 0.5-0.6 mm width. The inner reference electrode is about 2-2.5 mm length and 0.5-0.6 mm width. The distance d_{WE-CE} and d_{RE-WE} were measured by using an optical microscope (Table 4.5).

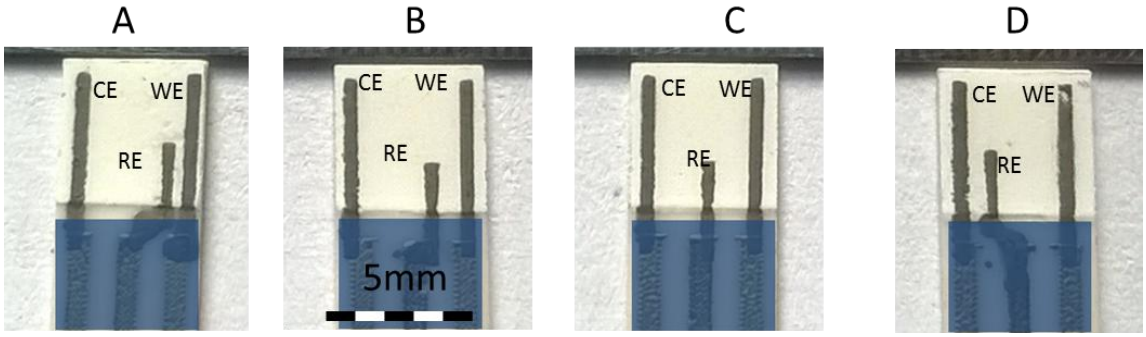

Figure 4.15: 3-electrode electrochemical sensors with different RE-WE spacing (d_{WE-RE}): Sensor A with d_{WE-RE}=0.25 mm, sensor B with d_{WE-RE}=0.75 mm, sensor C with d_{WE-RE}=1.25 mm, and sensor D with d_{WE-RE}=2 mm.

Table 4.5: Geometrical parameters of 3 electrode cells.

Sensors	A	B	C	D
d_{WE-CE}, ±0.01 mm	3.25	3.5	3.25	3.1
d_{RE-WE}, ±0.01 mm	0.25	0.75	1.25	2

The electrical connections of the three-electrode sensors have been realized according to the setup presented in chapter 2 (Figure 4.16).

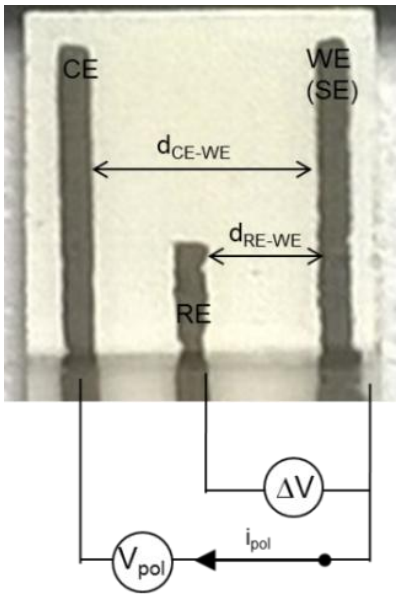

Figure 4.16: Connection setup of three-electrode sensors.

As usual, the polarization voltage is applied between CE and WE ($V_{pol}=V_{CE}-V_{WE}>0$) to generate cathodic current $i_{pol}>0$, the sensor output signal $\Delta V>0$ is measured between RE and WE.

Figure 4.17 depicts variations of the polarization voltage at 450 °C as a function of the applied current. V_{pol} values are in the range 3.8-4.8 V upon 50 nA depending on $d_{WE-RE.}$ It was not possible to apply 100 nA because the polarization voltage exceeds 5 V which is the limit of the electronic card. Theoretically, values of V_{pol} should be constant whatever values of d_{WE-RE}. However, this is not the case probably because the sensor elaboration process did not produce identical thicknesses of electrodes and distances between WE and CE (d_{WE-CE}). The variation in the electrode spacing is present in table 4.5 for all samples. The maximal deviation of d_{WE-CE} is 0.4 mm (observed between sensor B and D) which induces the maximal variability in Vpol of around 1 V upon 50 nA (Figure 4.17). This result underlines that the sensor elaboration process has to be strongly improved to deliver identical sensors with similar signals.

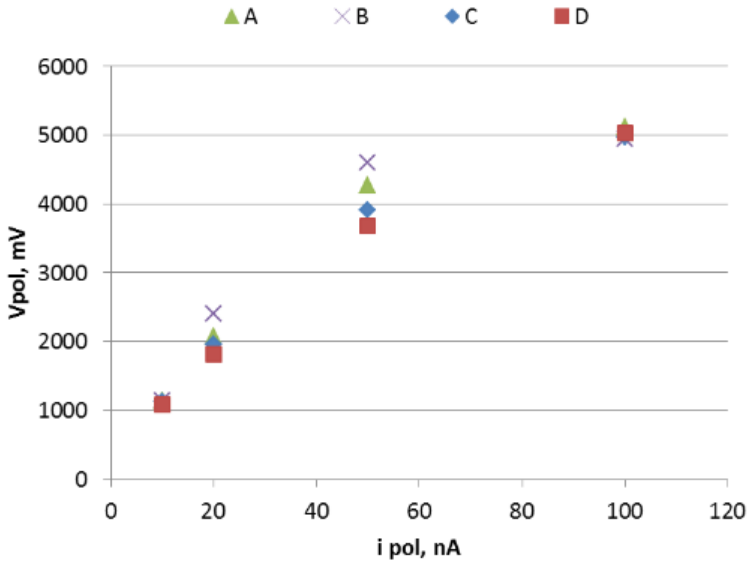

Figure 4.17: Variation of the polarization voltage as a function of the applied current for different WE-RE distances. Sensor A with d_{WE-RE}=0.25 mm, sensor B with d_{WE-RE} =0.75 mm, sensor C with d_{WE-RE}=1.25 mm, and sensor D with d_{WE-RE}=2 mm. T= 450°C, base gas

The figure 4.18 displays values of the polarization voltage normalized with d_{WE-CE}, expressed in mV/mm. These latter are fairly constant, except for the highest current. This is probably due to the error in the measurement of the d_{WE-CE} distance. Indeed, upon 50 nA, an error of 10 µm approximately induces a deviation in the polarization voltage of 10 mV.

In a three-electrode configurations, the response of the sensor is measured between the working and the reference electrodes ($\Delta V = V_{RE} - V_{WE}$). The working electrode, which is also the sensing

one, is affected by the applied cathodic current while the potential of the reference electrode is supposed to be constant and not altered by the polarization.

Figure 4.19 illustrates variations of the sensor base line in the base gas upon successive steps of currents of 10, 20 and 50 nA and for different values of d_{WE-RE}. Whatever, the intensity of the applied current, the baseline increases with the distance between the working and the reference electrodes.

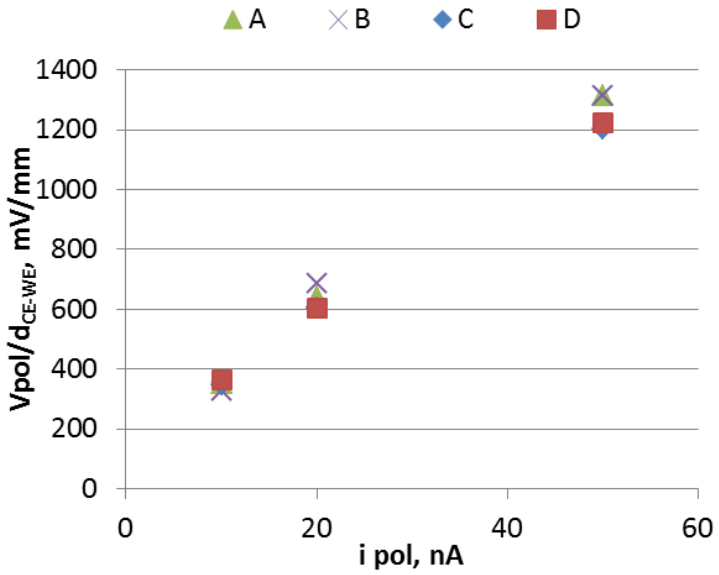

Figure 4.18: Variation of the normalized polarization voltage with d_{WE-CE} as a function of the applied current for different WE-RE distances. Sensor A with d_{WE-RE}=0.25 mm, sensor B with d_{WE-RE}=0.75 mm, sensor C with d_{WE-RE}=1.25 mm, and sensor D with d_{WE-RE}= 2 mm. T= 450°C, base gas.

The sensor baseline ΔV (Figure 4.19), contains both the overall overpotential and the ohmic drop between RE and WE (2.6). At constant i_{pol} (10, 20 or 50 nA), ΔV increases with the distance. This indicates the influence of the ohmic drop in the measured signal. Upon 10 nA, an increase of d_{WE-RE} from 0.25 mm up 2 mm induces an enhancement of 320 mV of the signal due to a huge increase of the ohmic drop (32 MΩ). The increase of the ohmic drop upon 20 and 50 nA corresponds to an increase of the signal of 540 and 1290 mV, respectively.

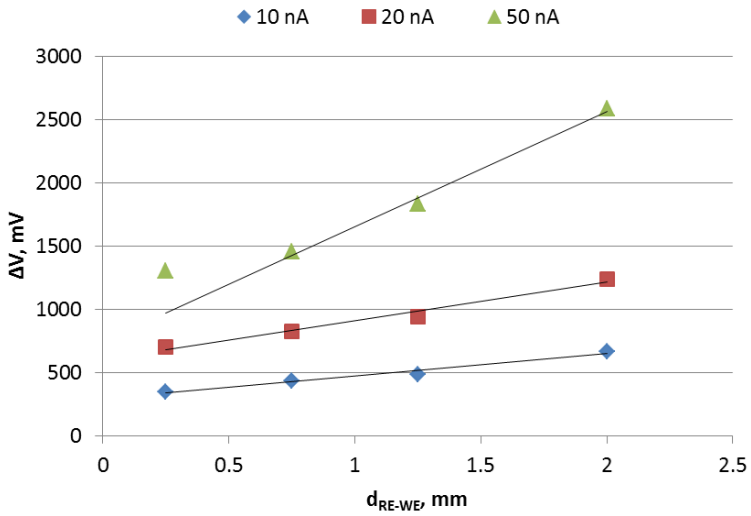

Figure 4.19: Variations of the sensor baseline as a function of the distance RE-WE in a 3-electrode configuration at 450 °C in the base gas

Theoretically, the calculated R_{YSZ} values according to the Ohm law must be identical. However, we have observed a some deviations from 32 MΩ at 10 nA to 26 MΩ at 50 nA. As the width and length of RE are not identical, we can suppose that measured potential vs RE is affected by current. We have tried to measure, by using EIS, the ohmic drop between RE and WE. Unfortunately, different size and shape of the reference electrode compared with those of WE seem to perturb the measurements.

Good exploitable data were only achieved for sensors with parallel and identical electrodes, as used in paragraph 4.1. Therefore, for correct measurements of the ohmic drop, a next series of 3-electrode sensors were made with similar size (length and width) electrodes.

These measurements confirm the influence of the position of the reference electrode on the sensor response (ΔV). For low current intensities (10 and 20 nA, Figure 4.19), the signal responses varies linearly with d_{RE-WE}. This suggests that variations of ΔV is mainly due the increase of the ohmic drop (resistance between RE and WE). On the opposite, upon 50 nA, the variations of the response with d_{RE-WE} are no more linear, indicating a deviation of the potential of the reference electrode. It also seems than the shape of the reference electrode has an impact. Using a reference electrode with similar size and shape than WE and CE seems to avoid inhomogeneity in the current distribution through the sensor. The necessity of high precision during the sensor production is confirmed.

4.2.2. Determination of the working electrode overpotential

Previous paragraph has shown that the position of RE has an impact on the sensor baseline. Therefore, we made a series of 3-electrode sensors with constant distances between the reference and the working electrodes but different spacing between the counter and the reference electrodes (Figure 4.20). Exact distances (±0.01 mm) were measured from optical microscope images. The length (3.8-4 mm) and the width (0.25-0.3 mm) were slightly similar for the three electrodes. The working electrode was made with the Au paste. After annealing at 800°C the sensors were tested in the base gas at 450 °C. As usual, the voltage polarization V_{pol} was applied between CE and WE to reach applied i_{pol} while the sensor response, ΔV, was measured between RE and WE. Results are presented on figure 4.21.

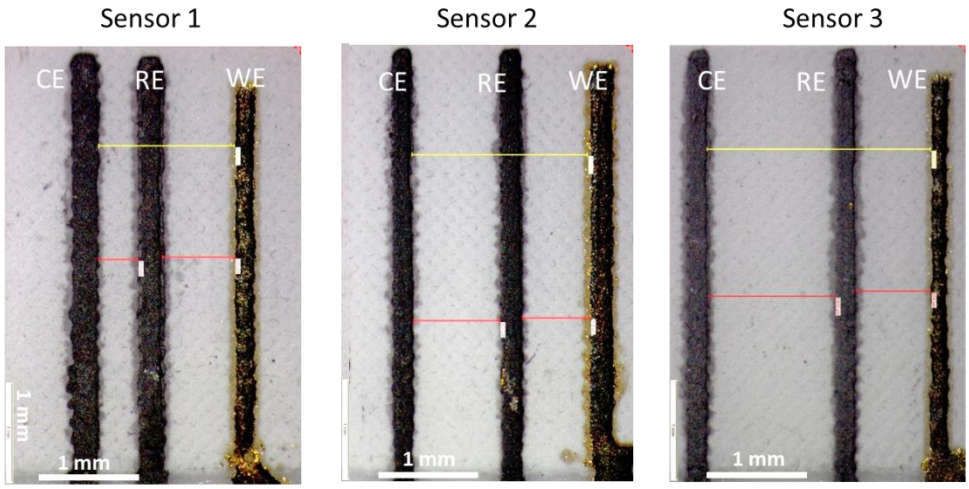

Figure 4.20: Photos obtained by an optical microscope of three-electrode sensors WE(Au)/RE(Pt)/CE(Pt): Sensor 1 with d_{WE-CE}=1.53 mm, d_{RE-WE}=0.81 mm; Sensor 2 with d_{WE-CE}=1.97 mm, d_{RE-WE}=0.75 and Sensor 3 with d_{WE-CE}=2.52 mm, d_{RE-WE}=0.83.

As expected (Figure 4.21), the polarization potential increases with d_{WE-CE}, due to the enhancement of the ohmic drop. For instance, increasing the CE-WE spacing from 1.53 mm (Sensor 1) to 2.52 mm (Sensor 3) enhances the polarization voltage from 2.2 V to 3.7 V upon 100 nA. As obtained with 2-electrodes sensors, the normalization of the polarization resistance with the distance (d_{WE-CE}) (Figure 4.22) removes the deviations for low currents. For high currents, the observed differences are linked with the error in the optical measurement of the distance, with the inhomogeneity of the YSZ layer thickness and the modification of the reference potential

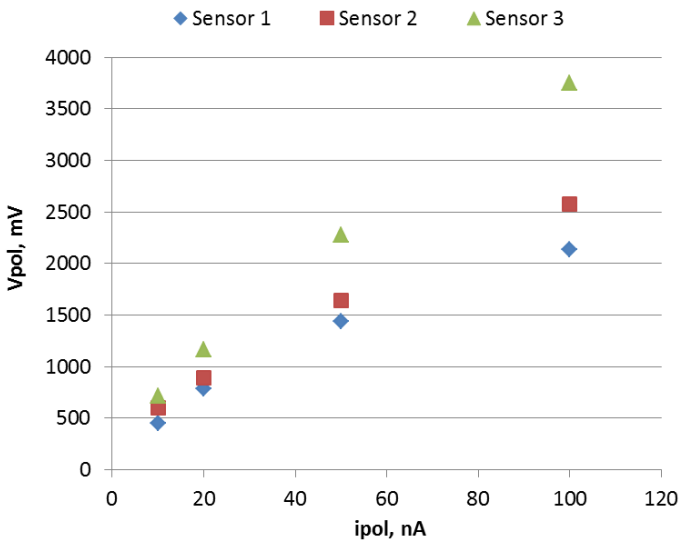

Figure 4.21: Variations of the polarization voltage of sensors as a function of the applied currents. T=450°C in the base gas. Three-electrode sensors WE(Au)/RE(Pt)/CE(Pt): Sensor 1 with d_{WE-CE}=1.53 mm, Sensor 2 with d_{WE-CE}=1.97 mm and Sensor 3 with d_{WE-CE}=2.52 mm.

Values of OCV are measured when i_{pol}=0 nA at 450°C between the Pt counter and the Au working electrode: Sensor 1, OCV = 39 mV, Sensor 2 OCV = 50 mV, Sensor 3 OCV =62 mV at 450 °C in the base gas.

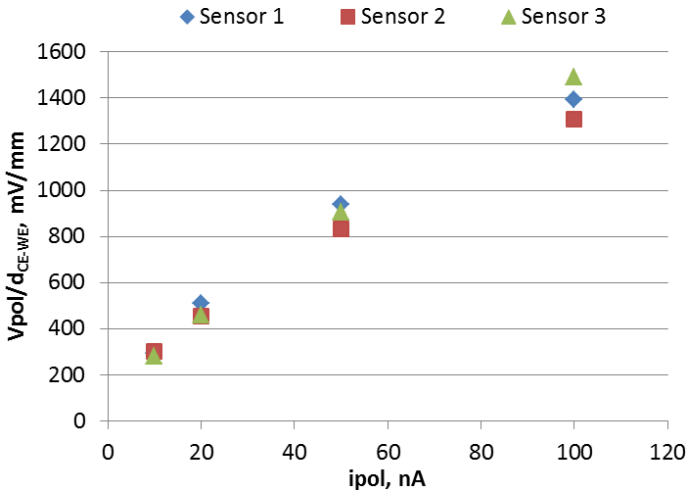

Figure 4.22: Variations of the normalized polarization voltage of sensors as a function of the applied currents. T=450°C in the base gas. Three-electrode sensors WE(Au)/RE(Pt)/CE(Pt): sensor 1 with d_{WE-CE}=1.53 mm, Sensor 2 with d_{WE-CE}=1.97 mm and Sensor 3 with d_{WE-CE}=2.52 mm.

The resistance of the electrolyte layer of this series of sensors is around of tens of MΩ (Figure 4.23). This value is smaller than that previously observed (~40 MΩ) for two-electrode Pt-Pt sensors (distance =2.27 mm). Such difference can be again related to the manufacturing of different series of sensor. A better reproducibility in the YSZ layer elaboration can be solved in mass production with straightly controlled reproducible conditions (humidity, temperature, viscosity of ink, etc).

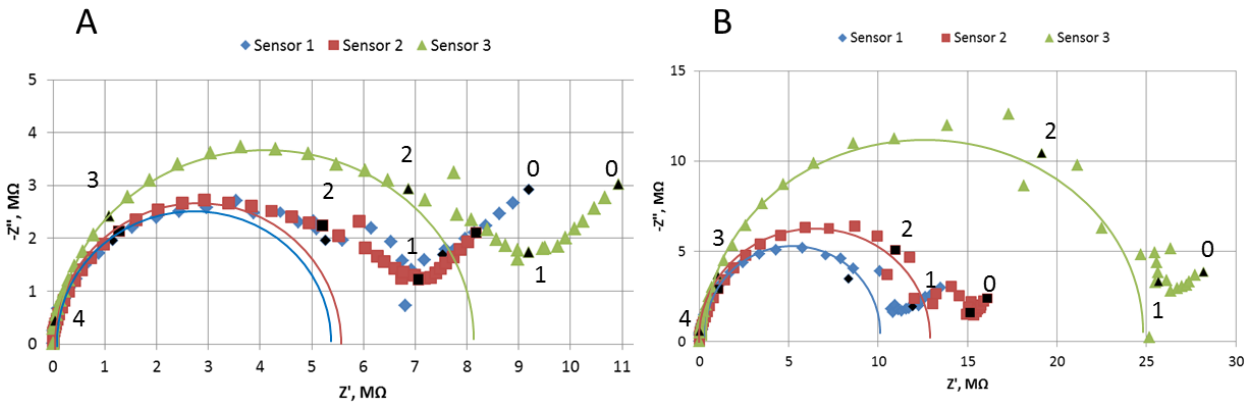

Figure 4.23: Experimental and fitted Nyquist diagrams of WE(Au)/RE(Pt)/CE(Pt) three-electrode sensors: A – measurements of $R_{YSZ\ RE\text{-}WE}$: Sensor 1 with $d_{RE\text{-}WE}$=0.81 mm, Sensor 2 with $d_{RE\text{-}WE}$=0.75 mm, Sensor 3 with $d_{RE\text{-}WE}$=0.83 mm and B measurements of – $R_{YSZ\ CE\text{-}WE}$: Sensor 1 with $d_{WE\text{-}CE}$=1.53 mm, Sensor 2 with $d_{WE\text{-}CE}$=1.97 mm and Sensor 3 with $d_{WE\text{-}CE}$=2.52 mm in base gas at 450 °C.

Using the three-electrode configuration (Figure 2.14-C), we have measured the resistance of the YSZ porous layer between WE and CE electrodes (R) as well as between WE and RE electrodes (R'). Figure 4.23 displays the impedance spectra recorded at 450°C in base gas for various positions of the CE as well as the fitted high frequency contribution. On the impedance diagrams, we were only interested on R_{YSZ} values. Below 100 Hz, the resistivity part is difficult to separate from the electrode reaction kinetic contribution. To exclude this possibility, fittings were realized mostly in a frequency range from 10^5 Hz down to $5*10^2$ Hz. As expected, the resistance (R) of layer between CE and WE increases with $d_{CE\text{-}WE}$ distance: 10.3, 13.5 and 24.3 MΩ for sensor 1, 2 and 3, respectively. At the same time, R' value is not identical for all sensors. It increases also from 5.35 MΩ to 5.6 MΩ between sensor 1 and 2 and reaches high value of 8.23 MΩ for sensor 3. Such difference shows the importance of the inhomogeneity of the YSZ layer during production.

Figure 4.24 presents conductance Arrhenius diagrams of the electrolyte layer of the sensors both between CE and WE as well as between RE and WE electrodes in the temperature range 450-550 °C (589°C for sensor 1). As expected, the conductance between CE and WE is lower than that

between RE and WE because of higher distances. The activation energies of YSZ conductance calculated from the Arrhenius diagrams were found to be in the range 1.08-1.20 eV for CE-WE spacing and 1.12-1.18 eV for RE-WE spacing. These values are higher of around 0.05-0.13 eV than those measured on porous YSZ layers in paragraph 4.1.2.

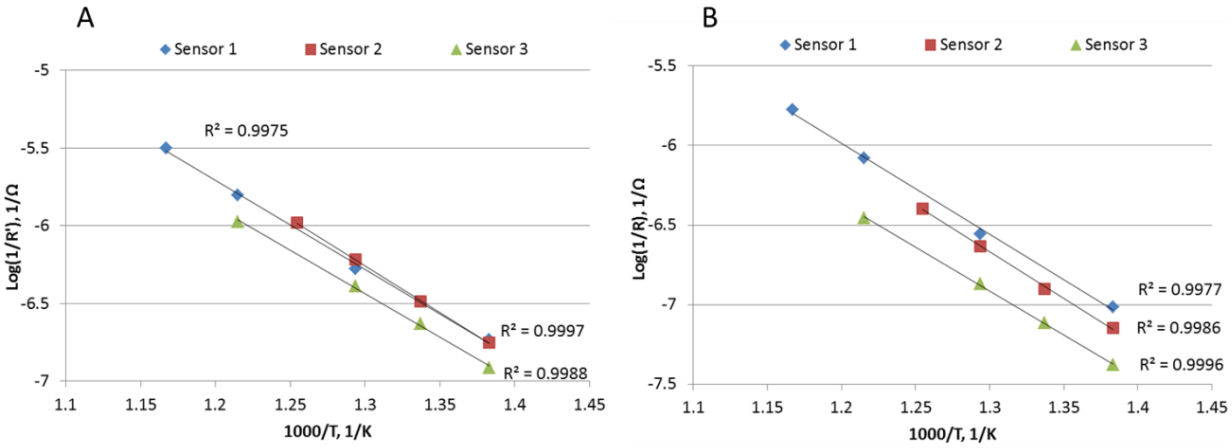

Figure 4.24: Arrhenius diagrams of the YSZ layer conductance in the base gas of WE(Au)/RE(Pt)/CE(Pt) three-electrode sensors: A – R': Sensor 1 with d_{RE-WE}=0.81 mm, Sensor 2 with d_{RE-WE}=0.75 mm, Sensor 3 with d_{RE-WE}=0.83 mm and B – R: Sensor 1 with d_{WE-CE}=1.53 mm, Sensor 2 with d_{WE-CE}=1.97 mm and Sensor 3 with d_{WE-CE}=2.52 mm

Values of these ohmic drop between CE and WE have been used to calculate the overall overpotentials of all sensors (Figure 4.25). The linear logarithmic dependency of the overpotential with the current is still valid, as in previous tests with 2 electrode sensors. However, the overall overpotentials, η_{total} ($\eta_{CE}+\eta_{WE}$), are lower than those observed in two electrode sensors configurations (Pt/Au) but stay higher than overall overpotential for Pt-Pt sensor (Figure 4.26). These variations (between Pt-Au couples in 2 and 3 electrode devices) are linked with the poor reproducibility of the sensor elaboration despite stabilization at 800°C during 120 h as well as with variability in electrode size.

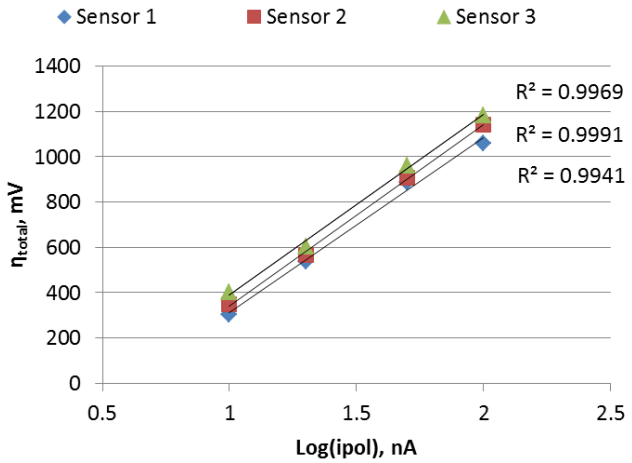

Figure 4.25: Logarithmic variations of the overall overpotential with applied current for different WE-CE distances, three-electrode sensors WE(Au)/RE(Pt)/CE(Pt): sensor 1 with d_{WE-CE}=1.53 mm, Sensor 2 with d_{WE-CE}=1.97 mm and Sensor 3 with d_{WE-CE}=2.52 mm.

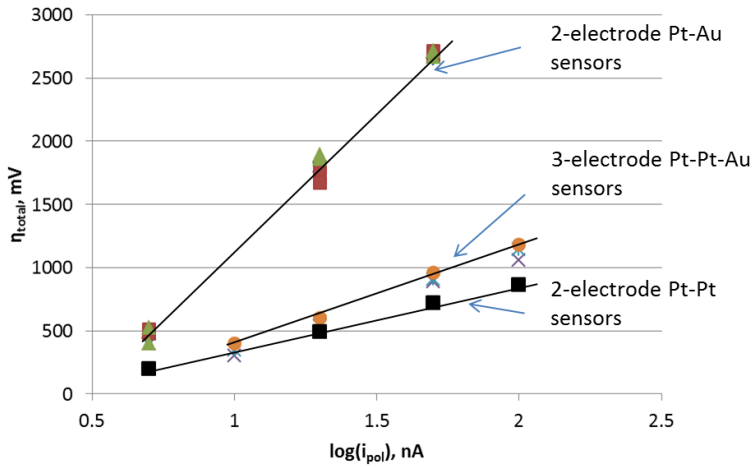

Figure 4.26: Logarithmic variations of the overall overpotential η_{total} ($\eta_{CE}+\eta_{WE}$) with applied current for 2 - CE(Pt)-WE(Au) and 3 - WE(Au)/RE(Pt)/CE(Pt) electrode sensors in base gas at 450 °C.

Sensors responses and OCV values have been measured at 450°C upon 10, 20, 50 and 100 nA (Figure 4.27). Values of $\Delta V°$ ($V°_{RE} - V°_{WE}$) were 20 mV for sensors 1 and 2 and 40 mV for sensor 3. These values were used for the calculation of the overpotential of the gold sensing electrode according to the following equation:

$$\eta_{WE} = \Delta V - \Delta V° - R' i_{pol} \qquad (2.9\text{-B})$$

Values of the baseline, i.e. ΔV, depend on the intensity of the applied current as shown in paragraphs 4.1. and 4.2.1. One can estimate that, for a constant position of the reference electrode, ΔV will not depend on CE-WE spacing and shall be only fixed by i_{pol}. Figure 4.27 partially confirms this hypothesis considering the resistivity of electrolyte layer identical for all sensors (which is not the case as shown in Figure 4.24). Indeed, the output sensor signal ΔV of the three sensors as a function of the polarization current is fairly identical for sensors 1 and 2. Important deviations of the baseline have been observed for sensor 3: (in comparison with sensors 1 and 2) around 300, 200, 100 and 90 mV upon 100, 50, 20 and 10 nA, respectively. These data are in good agreement with the highest ohmic drop of the sensor 3.

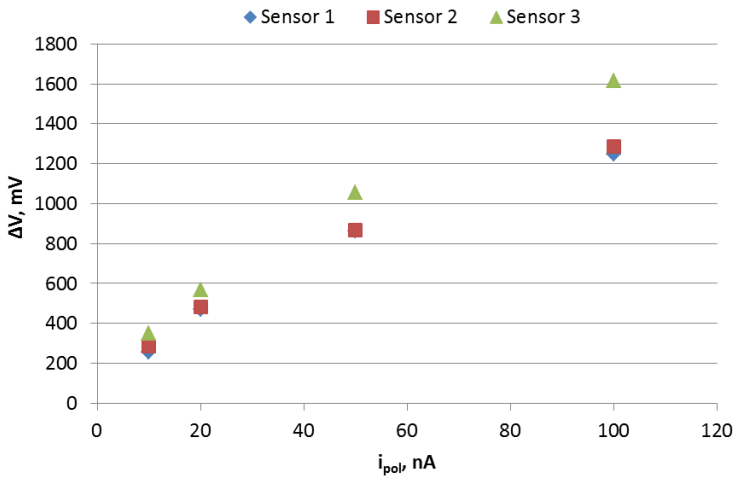

Figure 4.27: Variation of the sensors baseline as a function of the applied current. T=450°C in the base gas. Three-electrode sensors WE(Au)/RE(Pt)/CE(Pt): sensor 1 with d_{WE-CE}=1.53 mm, Sensor 2 with d_{WE-CE}=1.97 mm and Sensor 3 with d_{WE-CE}=2.52 mm.

On figure 4.28, both the Au working electrode overpotential and the ohmic drop are presented at 450°C in the base gas as a function of the applied current. As expected, the fraction of ohmic losses in the sensor response increases with the current, from around 20% up to 40-50% between 20 and 100 nA.

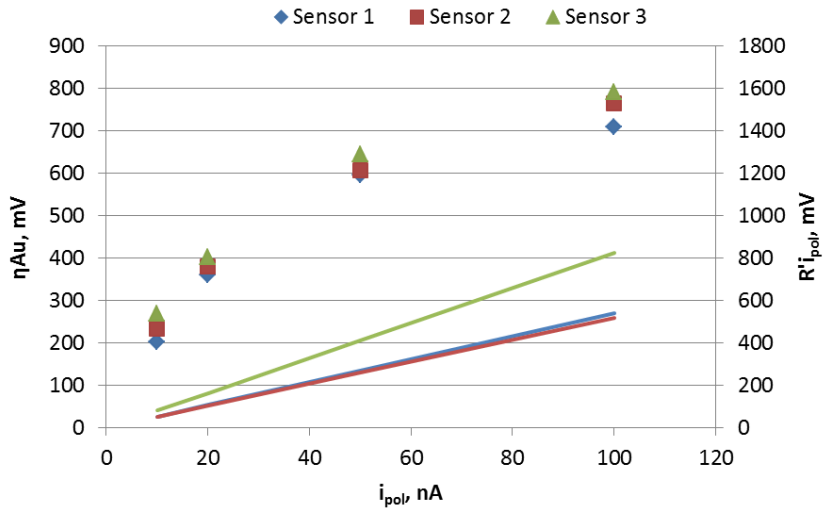

Figure 4.28: Variations of the working Au electrode overpotential as well as the ohmic drop as a function of the applied current at 450°C in the base gas. Three-electrode sensors WE(Au)/RE(Pt)/CE(Pt): sensor 1 with d_{WE-CE}=1.53 mm, Sensor 2 with d_{WE-CE}=1.97 mm and Sensor 3 with d_{WE-CE}=2.52 mm.

The highest ohmic drop calculated for Sensor 3 represents the largest deviation linked to different YSZ layer thickness observed in this study. At the same time, the values of calculated overpotentials are close and confirm independence of overpotential from ohmic drop. This result allows using the equation 2.9 in further calculations.

The Au overpotential values follow a linear logarithmic dependence with the applied current at 450°C according to Tafel equations (Figure 4.29). This suggests that the oxygen electrode reaction on Au is limited by the charge transfer in this current intensity range and for this oxygen partial pressure. Nevertheless, van Hassel et al. have shown that apparent Tafel behaviors can also be observed when a competition exists between charge transfer and oxygen mass transport along the Au, O_2 (g) /YSZ interface [Van Hassel B.A., 1991], The limiting step can be determined by studying the influence of pO_2 on the equilibrium exchange current. Details of this study are presented the chapter 5.

All these results show that ohmic losses are high and have an important influence on measured signal (ΔV). In addition, the reference electrode is probably affected by the polarization between WE and CE upon high current (up to 50 nA) The realization of a reference electrode isolated from gaseous environment and current lines to achieve a real constant potential can be one important perspective.

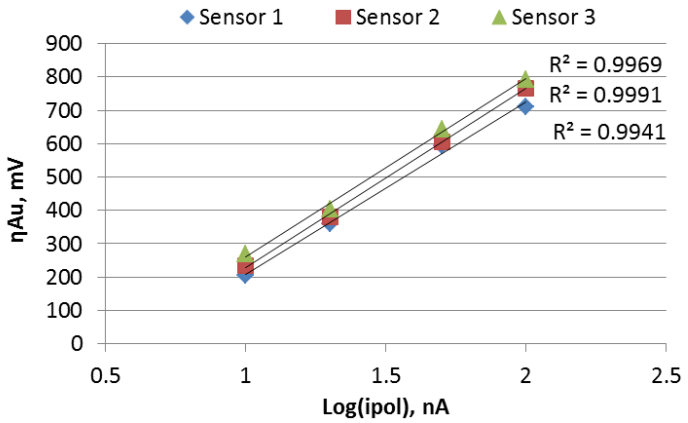

Figure 4.29 Logarithmic variations of the Au working electrode overpotential versus the applied current at 450°C in the base gas. Three-electrode sensors WE(Au)/RE(Pt)/CE(Pt): Sensor 1 with d_{WE-CE}=1.53 mm, Sensor 2 with d_{WE-CE}=1.97 mm and Sensor 3 with d_{WE-CE}=2.52 mm.

We have decided to locate the reference electrode at the middle between WE and CE. This configuration, in a first approximation, allows to divide the ohmic drop in two almost identical parts and to work with similar values of R and R' (Figure 4.30). It allows avoiding the presence of Pt electrode (RE) too close to WE. Indeed, the catalytic activity of the Pt (RE) may perturb the gas composition in the surrounding of the working electrode. Regarding the industrial prototypes made by MEAS, the reference was located on position distant on 1/3 of d_{CE-WE} from WE because of the presence of a fourth electrode.

At the same time, the weak reproducibility of sensors between different series of production is a key problem and may parasite the interpretation of results. The measurement of inter-electrode resistance R (CE-WE), R' (RE-WE) of series of sensors could help to control the reproducibility and the homogeneity of the YSZ layer.

4.2.3. Three-electrode sensors responses to pollutants

The sensors response to pollutant gases were measured in galvanostatic mode by using three electrode sensors. As usual, the gold working electrode was as cathode whereas the counter electrode was anode (Figure 4.30). The reference electrode was placed at the middle between WE and CE.

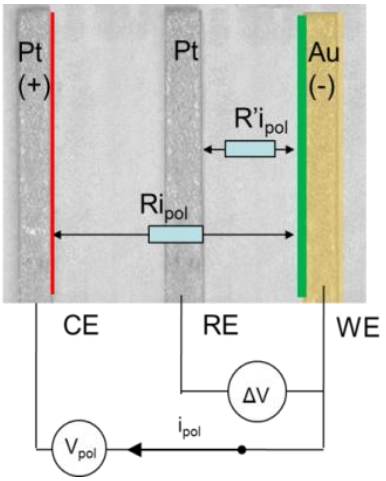

Figure 4.30: Connection of three-electrode cell for galvanostatic investigations

The measurements were made in periodic mode, with firstly injections of NO_2, then tests with pulses of CO and finally of NO. Four sensors were installed in the test bench and heated from the room temperature up to the working one (450 °C) in 120 seconds. Then, OCV values were measured in the base gas for 1-1.5 h upon i_{pol} =0. Then, four successive currents were applied for 5 hours from the lowest intensity up to the highest one (5, 20, 50 and 100 nA). For each current, the pollutant injection sequence was the following: 1 h in base gas / pulse of pollutant (NO_2, CO or NO) of 10 ppm for 1 h / 1 h in base gas / pulse of pollutant (NO_2, CO or NO) of 100 ppm for 1 h / 1 h in base gas. After each test (NO_2, CO, NO) sensors were heated to working temperature in 120-180 seconds. At the end of each test, the sensor heating was turned off and sensors were cooled down to room temperature. Figures 4.31-34 depict the variations of absolute values of electrodes overpotentials – cathodic for Au (ηAu) and anodic for Pt (ηPt) of one sensor. This data can be compared with total overpotential variations described in section 4.1.3 for polarized 2-electrode Pt/YSZ/Au sensors.

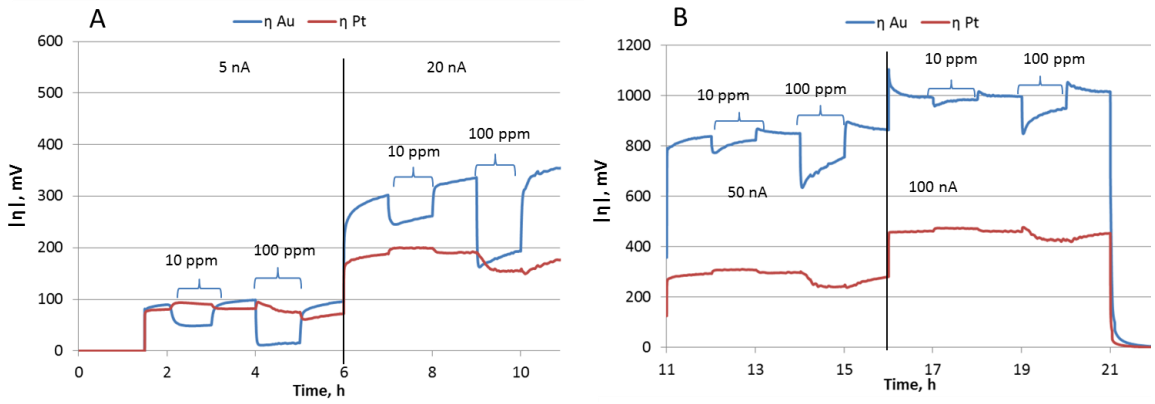

Figure 4.31: Variations of absolute values of Au (WE) and Pt (CE) overpotentials with time of 3-electrode cell upon A) 5, 20 nA, and B) 50 and 100 nA at 450°C in base gas during 10 or 100 ppm injections of NO_2.

During the first part of the measurement sequence (1.5 h), the polarization current is 0 and the overpotential of each electrode is equal to 0. Then i_{pol}=5 nA is applied and overpotentials increases – cathodic for Au and anodic for Pt (the absolute values).

During pulses of NO_2, the overpotential of the Au sensing electrode dramatically decreases. As can be noticed, the overpotential of gold electrode is not stable during the NO_2 injection upon 20, 50 and 100 nA. For instance, upon 5, 20, 50 and 100 nA, a pulse of 100 ppm NO_2 produces a maximal drop in ηAu of 85, 155, 190 and 115 mV during the 2 first minutes of pulse, respectively. After this initial response, the Au overpotential gradually increases with time. This signal increase reaches 140, 100 and 60 mV upon 20, 50 and 100 nA, respectively.

The polarization current of 20 nA can be defined as optimal since it produces the highest sensitivity to NO_2.

Slight changes of the Pt counter electrode overpotential (ηPt) also occur during NO_2 pulses but in a much less extend. For instance, during 10 ppm NO_2 pulses, it increases to 15-18 mV for all ipol values. Upon 100 ppm NO_2 pulses, the Pt overpotential decreases of -20, -40 and -25 mV upon 20, 50, and 100 nA, respectively. Let us note that for low applied currents (5 nA) and low NO_2 partial pressures (10 ppm), the Pt overpotential slightly increases.

As NO_2 is an oxidizing gas, the galvanostatic mode can only produce the electrochemical reduction of NO_2 at the working electrode. These results clearly indicate that this electrochemical reaction strongly decreases the Au overpotential for low current intensities.

As the NO oxidation reaction into NO_2 is an equilibrium, NO is also probably present in the feed. The Pt electrode is polarized as an anode, meaning that only oxidation reactions can take place. The electrochemical oxidation of NO into NO_2 at the Pt/YSZ interface is not probable in

these conditions. Indeed, during tests with two electrode cells, we did not observe any important influence of NO on the overall overpotential (Figure 4.14). Therefore, we can assume that potential of the Pt reference electrode can be slightly affected by NO_2 by modification of his potential according to the mixed potential theory.

Figures 4.32-33 depict calculated cathodic and anodic overpotentials at different polarizations during CO/NO injections at 450°C.

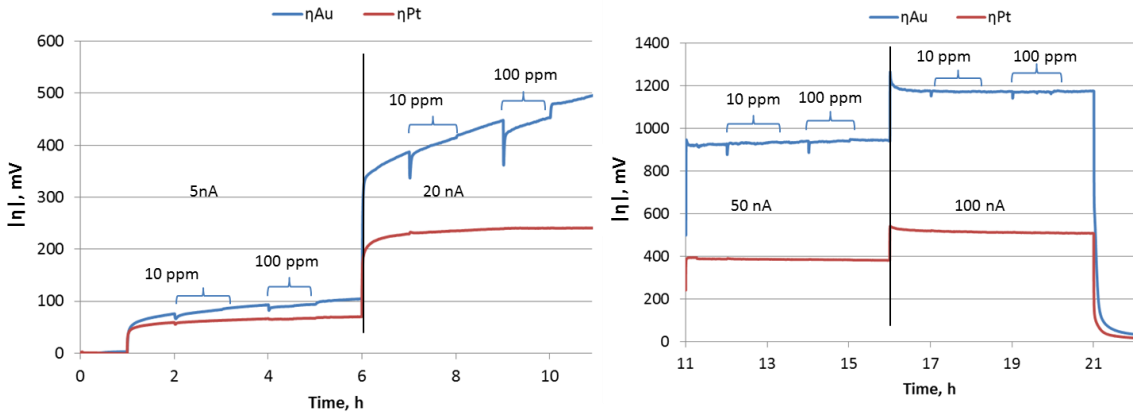

Figure 4.32: Variation of the absolute values of Au (WE) and Pt (CE) overpotential with time of 3-electrode cell upon A) 5, 20 nA, and B) 50 and 100 nA at 450°C in base gas during 10 or 100 ppm injections of NO.

Any variation of overpotentials upon 50 and 100 nA in presence of CO or NO (figures 4.32-33) has been observed. Only small variations, -10 mV at 5 nA and -25 mV in presence of 100 ppm NO have been detected (figure 4.32-A) on Au. The NO and CO are two reducing gases. They can produce electrochemical oxidation at the Pt counter-electrode. These reactions do not seem to affect strongly the overall overpotential. This indicates that the predominant contribution is the electrochemical reduction of O_2 at the working electrode. Let us note also that the electrochemical reduction of NO into N_2O or N_2 does not seem to take place at the Au/YSZ interface.

Before each injection of 10 or 100 ppm of CO or NO, upon 5 and 20 nA, a fast and short drop of the Au overpotential was observed. This is more pronounced for NO upon 20 nA (around -50 mV for 10 ppm and -100 mV for 100 ppm). The source of this drop can be related to possible oxidation of NO to NO_2 in the pipes in case of NO pulses before the injection into the sensor. Injections of CO were performed after those of NO_2. One can assume that traces of NO_2 could be still present in the pipes during the first injections of CO as the same mass-flow meter and pipe are used to inject the three pollutants. This could explain why this initial sharp drop of the signal is only observed during the first injections in the case of CO.

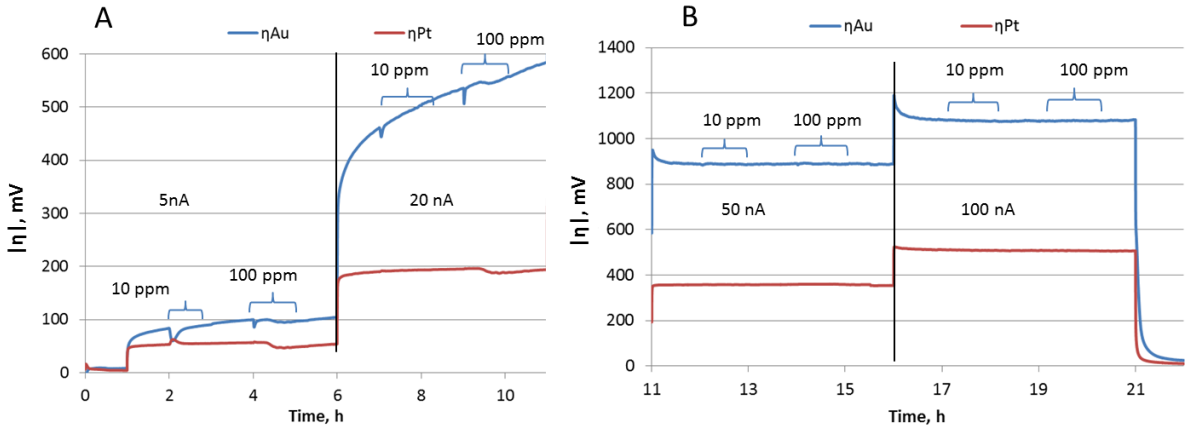

Figure 4.33: Variations of the absolute values of Au(WE) and Pt(CE) overpotentials with time of 3-electrode cells upon A) 5, 20 nA, and B) 50 and 100 nA at 450°C in base gas during 10 and100 ppm injections of CO.

As already observed, the stability with time of Au and Pt overpotentials is different. The anodic overpotential of Pt counter electrode is much stable than the overpotential of Au working electrode for all investigated valued of i_{pol}. The overpotential of Au electrode increases with time upon 5 and 20 nA and becomes more stable for 50 and 100 nA. This trend is valid whatever the nature of the injected pollutants (Figures 4.32, 4.33 and 4.34). When the polarization is stopped, Vpol gradually decreases to around 0. The initial and final OCV are presented in table 4.6.

The values of the overpotential in the base gas are not identical at fixed i_{pol} during the three successive sequences. The figure 4.34 shows the variation of overpotentials measured before injections of 100 ppm of NO_2, CO and NO.

Table 4.6: Variation of the absolute values of cathodic (ηAu) and anodic (ηPt) overpotentials during the different sequences

Sequence rank	ΔV°, mV before/after the sequence	ηAu, mV before injection of 100 ppm of pollutant				|ηPt|, mV before injection of 100 ppm of pollutant			
		i_{pol}, nA				i_{pol}, nA			
		5	20	50	100	5	20	50	100
1/ NO_2	50/60	100	333	857	1000	81	190	351	517
2/ CO	45/50	95	532	888	1075	60	200	362	508
3/ NO	39/55	105	450	944	1169	63	240	384	511

The overpotential of Au electrode in the base gas has a tendency to increase along the sequences. This enhancement is around +5, + 117 +87 and + 169 mV upon 5, 20, 50 and 100 nA, respectively. In opposite to Au, the overpotential of Pt (CE) is more stable with time with variations of the order 18, +50, +33 and – 6 mV upon5, 2, 50 and 100 nA, respectively. OCV values are always higher at the end of the sequence, most probably they need more times to go back to their initial value. Interesting point is the initial value of the OCV for the three different sequences. Values slightly decrease from 55 down to 39 mV. This indicates a morphological modification of the Au/YSZ interface, confirmed by the strong modification with time of the overpotential.

The figure 4.35 depicts the variation of cathodic (ηAu) and anodic (ηPt) overpotentials during the different sequences. The anodic overpotentials of Pt are lower than cathodic of Au electrode. In addition, the Pt overpotential deviations are extremely low. Despite the high variation of the Au overpotential the linearity of ηAu as a function of $\log(i_{pol})$ can still be observed.

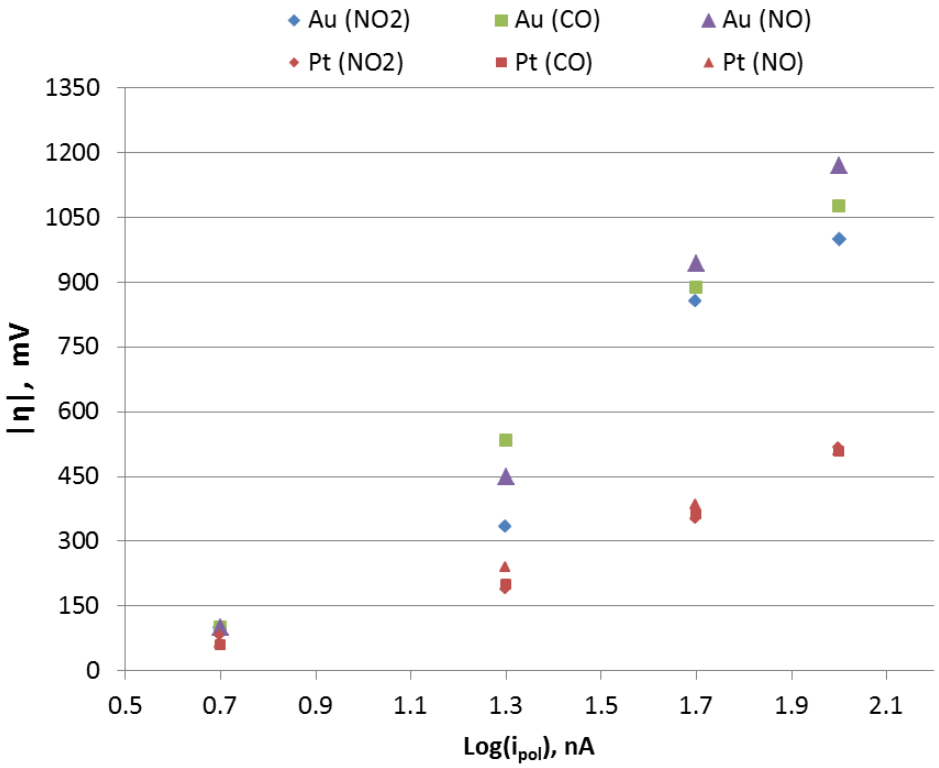

Figure 4.34: Variations of the absolute values of the overpotential of electrodes of three-electrode sensor measured before injections of 100 ppm of pollutant (NO_2, CO and then NO) as a function of the applied current during the successive measurements sequences. T=450°C in the base gas.

Similar results with high variations of the Au overpotential along the sequences were reproduced on four different sensors. Results for three of them, denoted as 1-Au, 2-Au and 3-Au are reported in Table 4.7 for each pollutant gas injection: (NO_2), (CO) or (NO). From a general point of view, the Au overpotential increases with time. However, the first values upon 5 nA are quite similar. This could indicate that low applied currents (5 nA) do not induce strong modifications on the Au/YSZ interface. Another key point is that, upon 20 nA, we have observed strong variation of overpotentials in all sequence tests. This could be related to a non-stationary reaction at this i_{pol}. However, a similar value of ηAu before the 100 ppm injection of NO_2 (820-857 mV) for the 3 sensors is observed. The NO_2 sequence is the first one. This could indicate that before any temperature cycling (fast cooling and heating between the first and second measurement sequence), the baseline of the 3 sensors are quite similar. Upon 100 nA, the baseline before the 100 ppm NO_2 injection is different according to the sensors, meaning that this high intensity rapidly modifies the morphology of the Au/YSZ interface. On the other hand, high deviations of the Au overpotential for the second and third sequences are observed from 20 nA. This drift of the Au overpotential with time varies between the 3 sensors. For instance, upon 50 nA, the Au overpotential in base gas at 450°C increases from 857 mV (1st sequence – NO_2) up to 944 mV, 1055 mV and 1000 mV (3rd sequence – NO) for sensor 1-Au, 2-Au and 3-Au, respectively.

Table 4.7: Variations of cathodic (ηAu) overpotential during the different sequences recorded on 3 various sensors at 450°C in base gas.

i_{pol}, nA	before injection of 100 ppm of pollutant								
	1-Au, mV			2-Au, mV			3-Au, mV		
	Sequence rank								
	NO_2	CO	NO	NO_2	CO	NO	NO_2	CO	NO
5	100	100	100	110	112	111	145	155	149
20	333	532	450	460	290	600	470	345	666
50	857	888	944	821	890	1055	840	894	1000
100	1000	1075	1169	1065	1180	1340	1112	1185	1160

Therefore, we can definitively conclude that in 3-electrode polarized sensor, the Au overpotential is a major part of the baseline. The behavior of the Au electrode must be improved to achieve a better stability. The polarization current must also be chosen to achieve the highest stability. The optimal values of i_{pol} with better sensitivity to NO_2 were determined at around 20 nA. Unfortunately, the sensor response is not stable upon this intensity. Higher stability combined with high sensitivity can probably be achieved for current intensities of the order of 25-30 nA. High

polarizations (larger than 50 nA) have to be avoided as they seem to provoke fast and non-reversible damages of the Au/YSZ interface.

4.2.4. Baseline stability of composite working electrode based sensor

The instability of the overall overpotential of the sensors is related to the overpotential of the Au electrode. The variation of the Au overpotential with time can affect the measurements of the baseline. Therefore, this is an important problem for a long-term utilization of sensors. To increase the stability of signals, composite sensing electrodes were developed and tested, as described in chapter 3. The gold electrode was replaced by composite materials consisted of Au commercial paste (ESL 8880-H) mixed with 10 wt % handmade YSZ ink, denoted as AuY. This material has lower interface resistance and advanced morphology (higher porosity and number of triple phase boundaries). The test of two sensors with AuY sensing electrode material named AuY–1 and AuY–2 are presented in this section. Results are compared with those of sensors Au-1 and Au-2 which contain a pure Au sensing electrode. The variation of overpotentials of different SE as a function of polarization currents is shown on figure 4.35.

According to figure 4.35-B, the overpotential of the composite electrode AuY is much lower than that of Au pure: ~7 times at 5 nA, 3.5 times at 20 nA and 2.5 times at 50 nA. At the same time, we can estimate the drift of the WE overpotential in base gas with time for each polarization current: 5, 20, 50 nA during 2h. The results are presented in table 4.8.

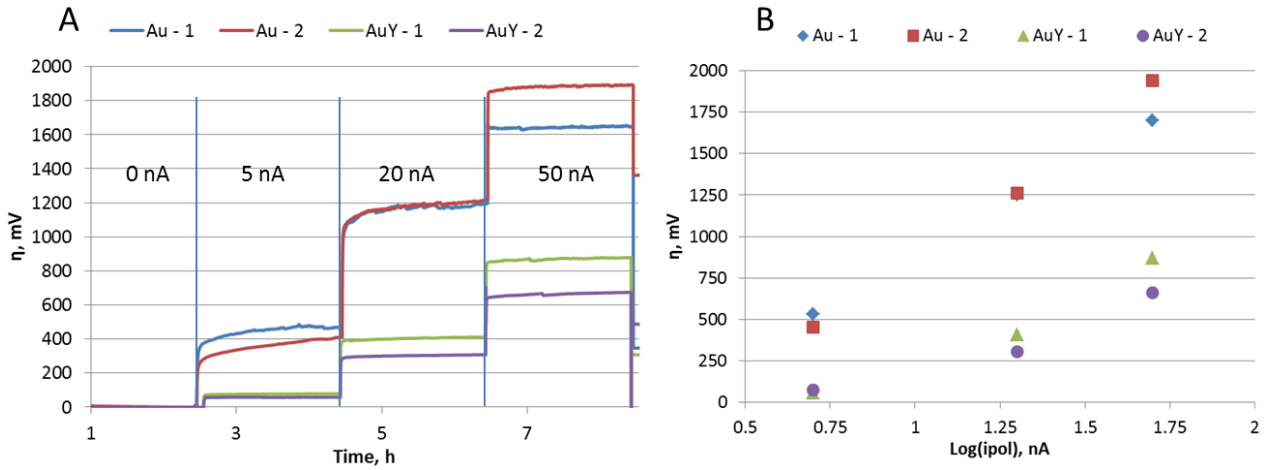

Figure 4.35: A - variation of the overpotential of different SE of three-electrode sensor as a function of applied currents with time and B - variation of the overpotential of SE of 3-electrode sensor as a function of electrode material and the applied current (5, 20 and 50 nA). T=450°C in the base gas.

The drift with time of the AuY overpotential is much lower than that of Au, especially for low current intensities (5 and 20 nA). The lower overpotential and better stability under polarization could indicate a more stable interface electrode/electrolyte morphology and a higher number of tpb. These results are in good agreement with the different morphologies of the electrodes presented in chapter 3 (figure 4).

Table 4.8: Drift with time of the cathodic (ηAu) overpotential upon different polarization.

Sensor	Drift of the Au overpotential, mV/h		
	i_{pol}, nA		
	5	**20**	**50**
Au-1	30	43	15
Au-2	35	46	16
AuY-1	0.5	8	10
AuY-2	0.7	8	10

4.2.5. Sensitivity to CO/NO_2/NO – comparison with Au, response time, stability, recovery time.

Sensing properties of the composite AuY electrode in galvanostatic mode is shown on figure 4.36. The data was obtained by using an industrial prototype shown on figure 2.6 of chapter 2. Sensor prototypes manufactured in Toulouse (Figure 2.6) by MEAS were made by screen printing on Al_2O_3 substrate of 52 mm length, 5 mm wide and 0.6 mm thickness. The three electrodes are around 0.1-0.15 mm of width and 4 mm of length. The sensors are equipped with a catalytic filter. The main aim of this filter is to maintain the thermodynamic equilibrium between NO_2 and NO while NO or NO_2 is present in exhaust. The secondary function is the oxidation of hydrocarbons and carbon monoxide [Gao 2011] to avoid any cross-sensitivity.

The properties of two sensors with different sensing electrodes (Au and AuY) have been carried out at 450°C. The output signal ΔV of sensors in presence of CO and NO/NO_2 are plotted in figure 4.37

The Au-based sensor exhibits a non-stable baseline (ΔV), which is increasing with time from 1150 mV before 100 ppm of CO pulse, to 1250 before 100 ppm NO and 1275 mV before 100 ppm pulse NO_2.

During the first pulse of 100 ppm CO, the sensor response presents a fast and sharp initial drop as already observed in figures 4.33. As already explained, this is probably to the presence of traces of NO_2 in the pipes before the first CO injection.

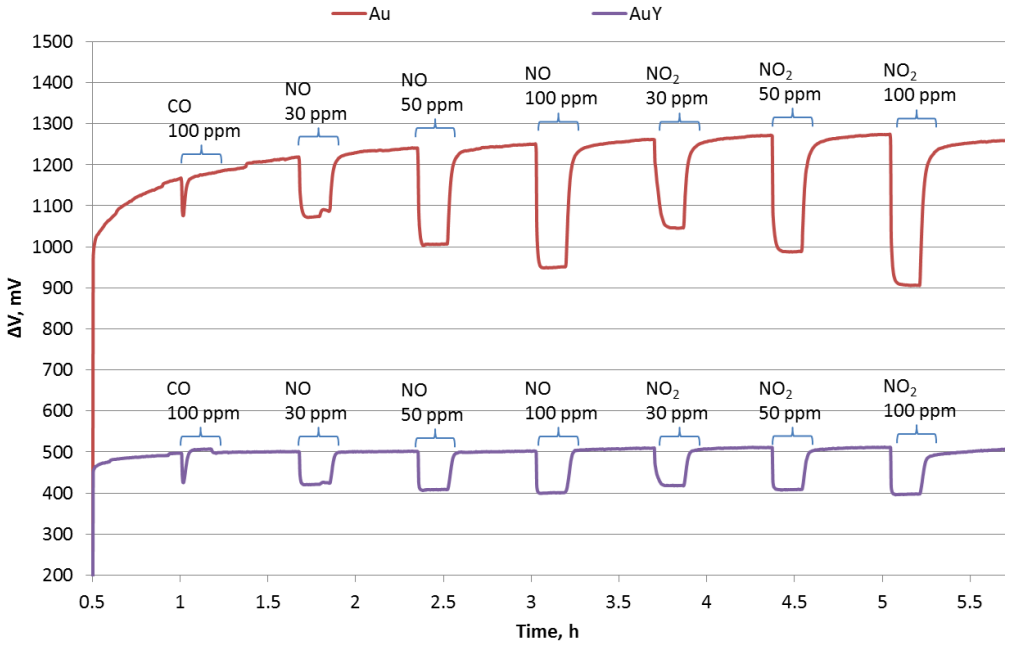

Figure 4.36: The three-electrode sensor response to pollutant pulses ($CO/NO/NO_2$) as a function of time upon ipol = 25 nA at 450°C. Comparison between a pure Au SE (Au) and an AuY electrode.

As the sensor has a catalytic filter, the thermodynamic equilibrium of the NO oxidation reaction should be reached. Considering the partial pressure of O_2 in the base gas, the thermodynamic equilibrium corresponds at this temperature to a NO/NO_2 ratio closed to 1.

Table 4.9: Variations of the baseline (ΔV) and of the overpotential drop (ΔVgas) of output signal of sensors with Au and AuY sensing electrode at 450°C and for i_{pol}=25 nA.

Sensing material	ΔV, mV	Gas pulse, ppm						
		CO	NO			NO_2		
		100	30	50	100	30	50	100
Au	Base line	1150	1215	1241	1248	1260	1270	1274
	ΔVgas, mV	-	142	235	299	213	286	369
AuY	Base line	500	500	501	502	508	509	511
	ΔVgas, mV	-	80	94	103	91	101	105

In case of composite sensing electrode, the baseline is almost constant during measurements. Expect the initial drop due to the presence of NO_2 in the pipeline, the sensors response to CO is negligible. The injections of NO/NO_2 have identical effect on the measured signal. The

overpotential drop is in the range 80/91, 94/101and 103/105 mV under 30, 50 and 100 ppm, respectively. These results confirm that the catalytic filter reaches the thermodynamic equilibrium NO/NO_2 and then produces at 450°C in the base gas similar concentrations of NO and NO_2

The response and recovery times were calculated for a pulse of 50 ppm of NO_2 (Figure 4.37).

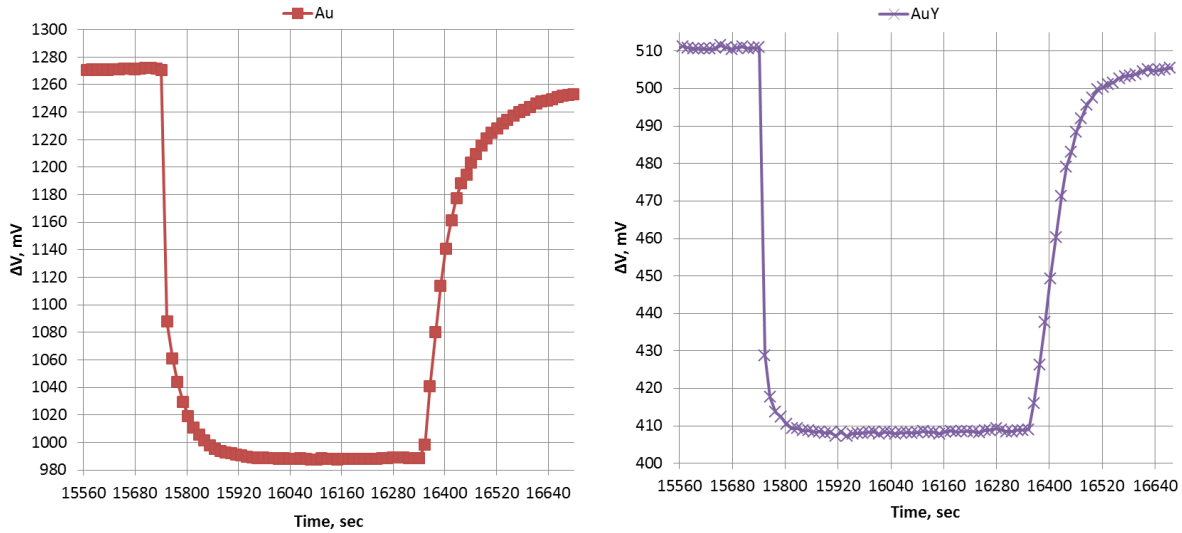

Figure 4.37: The three-electrode sensor response to a 50 ppm NO_2 pulse upon i_{pol} = 25 nA at 450°C in base gas.

The response and recovery times for all concentrations are presented in the table 4.10.

Table 4.10: Response and recovery time of sensors with Au and AuY sensing electrode (T=450°C, i_{pol}=25 nA).

Sensing material	T_{09}	Gas pulses					
		NO, ppm			NO_2, ppm		
		30	50	100	30	50	100
Au	response, sec	60	60	60	120	65	60
	recovery, min	2.5	3	3.5	4	4	6
AuY	response, sec	30	15	10	80	15	60
	recovery, min	1.5	1	2	3	2	8

The composite based sensing electrode present faster response and recovery times for all concentrations. The sensitivity can be calculated according to table 4.10. The sensitivity of the sensor with Au sensing electrode is 290 mV per decade, while it is only 35 mV/decade for the

AuY-based sensor. Meanwhile the higher stability, the sensor with the composite electrode has a lower sensitivity to NO_2. The increase of sensitivity of AuY-based sensor can be reached by using higher polarization currents and as consequence highest operated overpotential.

For a better understanding of the sensor mechanism, the current – voltage curves were recorded for different WE materials in working conditions as well as various oxygen and NOx concentrations. These results are presented in chapter 5.

Conclusions

The different components of the sensor signals as overpotential, OCV and ohmic drop have been determined at 450°C for three-electrode polarized sensors: Pt(CE)/Pt(RE)/Au(WE=SE). A large part (between 20 and 40%) of the measured signals of sensors is due to the ohmic drop linked with the high resistivity of the YSZ porous layer. This contribution is proportional to the intensity of the applied current and to the geometrical position of the reference electrode (resistance of electrolyte between RE and WE).

In galvanostatic mode, the Pt/Pt/Au sensor is very sensitive to NO_2. This sensitivity is linked to the decrease of the Au overpotential in presence of NO_2. The Au overpotential values follow a logarithmic dependence with the applied current at 450°C according to Tafel equations Cross-sensitivity toward CO and NO is rather limited without a catalytic filter. Sensitivity up to 290 mV/decade can be achieved at 450°C. These values are more than six times higher than those measured (52 mV/decade) for the AuY sensing electrode in the potentiometric sensor at 450°C [Chapter 3]. Recently, polarized sensor based on lambda probe has been reported to achieve a selectivity to NO_2 of 112 mV/decade (0.5-50 ppm NO_2), which is more than two times lower than that reported in this present study [Fischer 2012].

Our proposed sensor is sensitive and selective to NO_2 in galvanostatic mode in a temperature range 400 – 500°C (suitable with Diesel exhausts). However, some drawbacks have to be solved before considering a real application:

- These sensors present high ohmic drops (10 – 50 MΩ) due to the high porosity of the YSZ layer. Therefore, the position of the reference electrode (RE) strongly influences the sensor response. We have decided to locate RE between (at the middle) CE and WE electrodes because :
    - Similar (or proportional) ohmic drop between WE-RE and CE-RE can be achieved
    - To avoid the modification of the gaseous atmosphere at the surrounding of the WE
- The baseline is not stable with time for different reasons:
    - Evolution with time and with thermal cycling of the morphology of the YSZ layer
    - Evolution with time and thermal cycling of the Au/YSZ interface
- Bad reproducibility of the sensor elaboration process induces different signals between two series of sensors :
    - Size and position of electrodes must be strictly identical
    - A better reproducibility in the process of the deposition of the YSZ layer is necessary.

AuY composite electrode can solve the problem of the instability of the baseline. However, the sensitivity strongly decreases. However, sensors can be operated at highest polarization currents

The mechanism of the selective detection of NO_2 of the three electrode Pt/Pt/Au sensor is presented in chapter 5.

Bibliography

Benard S., Retailleau L., Gaillard F., Vernoux P., Giroir-Fendler A., 2005, Supported platinum catalysts for nitrogen oxide sensors, *Applied Catalysis B: Environmental*, 55(1), p.11-21.

Fischer S., Schönauer-Kamin D., Pohle R., Magori E., Farber B., Fleischer M., Moos R., NOx-Detection by Pulsed Polarization of Lambda Probes, 2012, communication on 14th International meeting on Chemical sensors, doi 10.5162/IMCS2012/P1.6.4

Gao J., Viricelle J-P., Pijolat C., Vernoux P., Boreave A., Giroir-Fendler A., 2011, Improvement of the NOx selectivity for a planar YSZ sensor, Sensors and Actuators B: Chemical, 154(2), p.106-110.

Gao J., 2011. Etude et mise au point d'un capteur de gaz pour la détection sélective de NOx en pot d'échappement d'automobile. *Thèse de doctorat. École Nationale Supérieure des Mines de Saint-Étienne.*

Guan Y., Chunhao Li, Xiaoyang Cheng, Biao Wang, Ruize Sun, Xishuang Liang, Jihong Zhao, Hong Chen, Geyu Lu, 2014, Highly sensitive mixed-potential-type NO_2 sensor with YSZ processed using femtosecond laser direct writing technology*, Sensors and Actuators B: Chemical,* 198, p.110-113.

Kishimoto H., Sakai N., Yamaji K., Horita T., Manuel E. Brito, YokokawaH., Amezawa K., Uchimoto Y., 2008, Visualization of oxygen transport behavior at metal electrode/oxide electrolyte interface using secondary ion mass spectrometry, Solid State Ionics, 179(9–10), p.347-354.

Kleitz, M., Steil M.C., 1997, Microstructure blocking effects versus effective medium theories in YSZ, *Journal of the European Ceramic Society*, 17, p819-829.

Mutoro E., Günther S., Luerßen B., Valov I., Janek J., 2008, Electrode activation and degradation: Morphology changes of platinum electrodes on YSZ during electrochemical polarisation, *Solid State Ionics*, Volume 179(33–34), p.1835-1848.

Razniak A., Dudek M., Tomczyk P., 2008, Reduction of oxygen at the interface M|solide oxide electrolyte (M=Pt, Ag and Au, solid electrolyte=YSZ, GDC); Autocatalysis or artifact? *Catalysis today*, 176, p.41-47.

Sekhar P.K., Brosha E.L., Mukundan R., Li W., Nelson M. A., Palanisamy P., Garzon F.H., 2010, Application of commercial automotive sensor manufacturing methods for NOx/NH_3 mixed

potential sensors for on-board emissions control, *Sensors and Actuators B: Chemical*, 144(1), p.112-119.

Somov S., Reinhardt G., Guth U., Göpel W., 1996, Gas analysis with arrays of solid state electrochemical sensors: implications to monitor HCs and NOx on exhaust, *Sensors and Actuators B*, 35-36, p.409-418.

Striker T., Ramaswamy V., Armstrong E. N., Willson P. D., Wachsman E. D., Ruud J. A., Effect of nanocomposite Au–YSZ electrodes on potentiometric sensor response to NOx and CO, *Sensors and Actuators B,* 181 (2013), 312-318.

Van Hassel B.A. 1991, Electrode polarization at the Au, O_2(g)/YSZ interface Part 1: Theoretical consideration of reaction model, *Solid State Ionics,* 48, p.155-171.

Romanytsia I., Viricelle J.-P., Vernoux P., Pijolat C., Application of advanced morphology Au–X (X = YSZ, ZrO_2) composites as sensing electrode for solid state mixed-potential exhaust NOx sensor, *Sensors and Actuators B*, 2015, Pages 391-397.

Chapter 5

Investigations of the oxygen electrode reaction on Au and Au/YSZ composite sensing electrodes in presence of NO_2

Outline

Chapter 5

Résumé

Ce chapitre est écrit sous forme d'un article et reporte l'étude du mécanisme du capteur à savoir la réaction d'électrode à oxygène (réduction) et la détection de NO_2 à 450 °C dans des conditions proches de celles d'un pot échappement d'un moteur diesel.

Des mesures systématiques de courbes courant-potentiel en présence de différentes pressions partielles en oxygène ont été réalisées à 450°C sur des capteurs à trois électrodes. Deux types d'électrodes sensibles ont été étudiées : l'or pur et le composite entre l'or et YSZ (AuY). Les droites de Tafel nous ont permis de déterminer les lois de variations des courants d'échange en fonction de la pression partielle en oxygène et d'en déduire des hypothèses sur le mécanisme de la réaction d'électrode à oxygène. Nous avons montré que la réduction électrochimique de l'oxygène sur l'électrode en or est limitée par le transfert de charge entre l'oxygène atomique adsorbé et l'ion O^-, ce qui se caractérise par une surtension élevée. Les surtensions mesurées sur AuY sont plus faibles et l'étape limitante est différente puisqu'elle semble être liée à l'incorporation des ions O^- dans le réseau d'YSZ. En présence de NO_2, la surtension baisse fortement. Cette baisse a été reliée à la réduction électrochimique de NO_2 en NO qui produirait également des espèces O^- adsorbées.

La sensibilité à NO_2 du capteur polarisé équipé d'un filtre catalytique et d'une électrode sensible AuY est de l'ordre de 130 mV/décade dans la gamme 10-100 ppm. Cette valeur est plus élevée que celles récemment présentées dans la littérature. Le temps de réponse et le temps de recouvrement ont été mesurés pour différentes concentrations en oxygène et en NO_2

Summary

This chapter is written in the form of a publication and deals with the study of the mechanism of the oxygen electrochemical reduction on the sensing electrode at 450°C in presence of NO_2, i.e. under conditions near to diesel engine exhausts.

Systematic measurements of I-V curves have been performed at 450°C for different oxygen partial pressures on 3-electrode sensors at 450°C. Two kinds of sensing electrodes have been investigated: the pure Au one and the composite electrolyte between Au and YSZ (AuY). From the Tafel plots, we have extracted the relationships between the exchange current and the oxygen partial pressure in order to propose some assumptions regarding the mechanism of the oxygen electrochemical reduction on the sensing electrode. We have shown that the rate-determining step on Au is linked with the charge transfer between adsorbed atomic oxygen and ionic O^- species, resulting in very high overpotentials. These latter are smaller on AuY as the limiting step was found to be different since linked with the incorporation of O^- species into the YSZ network. In presence of NO_2, the overpotential drops dramatically. We assumed that this is linked with the electrochemical reduction of NO_2 into NO that could also produce adsorbed O^- species.

The sensitivity to NO_2 of the sensor equipped with a catalytic filter and a AuY sensing electrode was found to be 130 mV/decade in the NO_2 concentration range 10-100 ppm. This value is higher than those recently reported in the literature. The response time and recovery time were also recorded for different concentrations of oxygen and NO_2.

Investigations of the oxygen electrode reaction on Au and Au/YSZ composite sensing electrodes in presence of NO_2

1 Introduction

Modern legislations in automotive exhaust [1] oblige the car manufacturers to equip the diesel light-duty vehicles with an after treatment system to remove pollutants such as nitrogen oxides. One of the effective NOx (NO and NO_2) aftertreatment process is the selective catalytic reduction (SCR). A post-injection of urea produces, via hydrolysis, NH_3 which is used as a reducing agent for NOx conversion into N_2 [2, 3]. The NOx conversion depends on various factors as the oxygen partial pressure, NH_3/NO and NO/NO_2 ratios and temperature. In modern SCR systems, NOx conversions can reach 99% at 573 K [3]. In this context, fast and accurate on-board diagnostics of NOx concentrations in the exhaust are strongly required

For NOx on-board detection in light and heavy duty vehicles, potentiometric gas sensors are currently developed. They are composed of a solid electrolyte such as β-alumina ($2Na_2O–11Al_2O_3$) [4], yttria-stabilized zirconia (YSZ) [5-9], as well as two electrodes, a reference one and a sensing one. These two electrodes must present different electrocatalytic activity to detect NOx such as the couples Pt-Au [4, 5], Pt-$MnCr_2O_3$ [8], $ZnFeO_4$ [9] or Pt – (Au-oxide) [10, 11].

In a complex gas environment, the signal of a two electrode potentiometric sensor shows a non-Nernstian behavior due to the establishment of a mixed potential [5, 6, 8] on the sensing electrode. This latter is linked to the superposition of parallel electrode reactions occurring at the triple phase boundaries (tpb) [8, 9, 11, 12], such as the oxygen electrode reaction and the electrochemical reduction (oxidation) of NO_2 (NO). The sensitivity to NO_2 is always higher than that of NO. In addition, by using the Au/Pt couple of electrodes interfaced on YSZ, NO_2 and NO exhibit opposite responses, positive for NO and negative for NO_2 [5]. At the same time, the cross sensitivity to NH_3, CO or hydrocarbons can take place [5, 6, 10-12] and strongly interfere on the sensor signals. For this reason, the metrological characteristics of mixed-potential sensors must be improved in terms of selectivity and calibration.

The modification of sensitivity and selectivity can be enhanced by the polarization of the sensing electrode [13, 14]. For instance, in the galvanostatic mode, the selectivity of the sensing electrode depends on the polarization direction. If the electrode is polarized negatively as a cathode, only reducible gas can modify its potential and then can be detected. On the opposite, if

the electrode is polarized positively as an anode, the sensor becomes only selective to gases that can be electrochemically oxidized [13, 15]. In addition, the kinetic of oxidation or reduction electrochemical reactions depends also on the nature of the electrode material. Different sensing electrode compositions are reported in the literature such as $CdCrO_4$ [13, 14], $La_{0.8}Sr_{0.2}CrO_3$ [15] or Pt [16] in order to modify its chemisorptive properties.

The oxygen is always present in diesel exhausts in much higher concentrations (2 – 15%) than NO or NO_2 (10 – 500 ppm). Using polarized sensors in galvanostatic mode, O_2, NO and NO_2 can be electrochemically reduced on the cathodically polarized working electrode:

$$1/2\,O_2 + 2e^- + V_O^{\cdot\cdot} \longleftrightarrow O_O^x \quad (1)$$

$$NO + 2e^- + V_O^{\cdot\cdot} \longleftrightarrow 1/2\,N_2 + O_O^x \quad (2)$$

$$2NO + 2e^- + V_O^{\cdot\cdot} \longleftrightarrow N_2O + O_O^x \quad (3)$$

$$NO_2 + 2e^- + V_O^{\cdot\cdot} \longleftrightarrow NO + O_O^x \quad (4)$$

$$NO_2 + 4\,e^- + 2V_O^{\cdot\cdot} \leftrightarrow 1/2N_2 + 2O_O^x \quad (5)$$

$$2NO_2 + 6e^- + 3V_O^{\cdot\cdot} \longleftrightarrow N_2O + 3O_O^x \quad (6)$$

Where $V^{\cdot\cdot}_O$ is an oxygen vacancy and O^x_O is a normal position of O^{2-} ion in the YSZ lattice.

The rate of the electrochemical process is determined by the applied current which generates overpotentials. The magnitude of these latter will depend on rate-limiting steps of the different electrochemical reactions that are taking place in parallel. The sensitivity of the sensor will be fixed by the variations of these overpotentials. A high sensitivity and selectivity to NO_2 of polarized sensors can be achieved if the rate of electrochemical NO_2 reduction at the interface electrolyte/sensing electrode is much higher than the rate of the oxygen electrochemical reduction. The oxygen electrochemical reduction rate and the associated mechanism depend on the nature of the electrode material. Several oxygen electrodes are reported in the literature such as Pt [7, 17-19, 21, 22, 23], Pd [20], Au [17-19, 22, 23], Pt+5%Ga_2O_3 [7] or Ag [19]. The electrochemical performance is mainly linked with the ability of the cathode material to chemisorb oxygen. Gold electrode is known to present the smallest activity for the oxygen electrochemical reduction reaction [17, 18, 19, 23] in the temperature range 300-600°C mainly because of the low coverage of oxygen on gold [17, 18] as well as small oxygen exchange rates [22, 23].

Our aim is to achieve a sensor with a high sensitivity to NO_2 in a galvanostatic mode. The strategy was to implement a poor electrode for the oxygen electrochemical reduction in order to

induce significant drops of the overpotential of the sensing electrode in presence of NO_2. Therefore, we have selected Au-based sensing electrode.

A series of three-electrode planar sensors has been prepared by using YSZ as an electrolyte. The counter and the reference electrodes were composed of Pt. Recently, we have shown that the addition of YSZ in the composition of the Au electrode can significantly decrease the polarization resistance in air [24]. In addition, it was found that the (Au+10 wt% YSZ)/YSZ/Pt sensor has a shorter response time and higher sensitivity to NO_2 (range 20-100 ppm) at 450-550 °C in comparison with a pure Au electrode. Therefore, two kinds of Au-based sensing electrodes were investigated: a pure Au electrode (denoted as Au) and a Au-YSZ composite one (denoted as AuY). The kinetic of the oxygen electrode reaction on both types of Au sensing electrodes has been carried out at 450°C by using Electrochemical Impedance Spectroscopy (EIS) and I-V curves. In addition, the impact of the presence of NO_2 on the electrochemical properties of the AuY composite was investigated at 450°C for various O_2 and NO_2 partial pressures. Finally, responses to NO_2 of the AuY-based sensor were measured at 450°C in galvanostatic mode.

2. Experimental

2.1. Elaboration of 3-electrode sensors

Sensor prototypes with the configuration Pt(CE)/Pt(RE)/Au(WE) on YSZ (Figure 1) were fabricated by screen-printing (DEK) on alumina substrates of 52 mm length, 5 mm wide and 0.6 mm thick (CoorsTek). First, a functional and porous layer (5x5 mm) of solid electrolyte (YSZ: $(ZrO_2)_{0.92}(Y_2O_3)_{0.08}$ provided by Superconductive) was deposited by screen-printing (200 mesh) from a home-made ink. This latter was containing 4 g of YSZ powder, 1.7 g of organic binder (ESL V400A) and 1 g of solvent (ESL 404). These elements were mixed for 10 min in a three-roll mill (Exakt 80E).

After deposition of the YSZ layer, sensors were dried for 15 min in air at 120°C and sintered at 1380 °C in air for 2 hours with a ramp of 5°C/min. The second step consists in the deposition of the electrodes. Platinum and pure gold-electrodes (0.2 mm width and 3-4 mm length) were then screen-printed on the surface of the YSZ layer using a commercial paste of Pt (ESL 5545) and Au (ESL 8880-H). The distance between the electrodes was approximately 2 mm. The deposited electrodes were further dried for 15 minutes at 120°C and then sintered at 850°C for 2 hours in air with a ramp of 5°C/min. Gold based composite electrodes were also prepared by mixing the Au commercial paste (ESL 8880-H) with 10 wt% handmade YSZ (denoted as AuY). The calcination procedure was similar than for the pure Au electrode. Final amount of the ceramic fraction in the

AuY composite electrode is around 9.5 %wt. Details in the preparation and characterization of this AuY electrode material is described in [24] (chapter 3).

A top layer of a dielectric material was deposited onto the Au (ESL 8880-H) current collectors to prevent any short circuit or contamination On the reverse side, the heating element was made of Pt (ink Pt ESL 5545) and is also protected by the same dielectric layer (ESL 4917).

As a third step, a catalytic layer was deposited to cover the three electrodes. This catalytic filter is based on Pt-supported alumina. Details of its preparation and composition are given in reference [5]. The calcination procedure was identical (850°C, 2 h in air).

The gold-based electrode was deposited at the right place and was defined as the working electrode (WE). The reference electrode was placed between the counter (CE) and the working electrode (Figure 1). The three electrodes have a similar size.

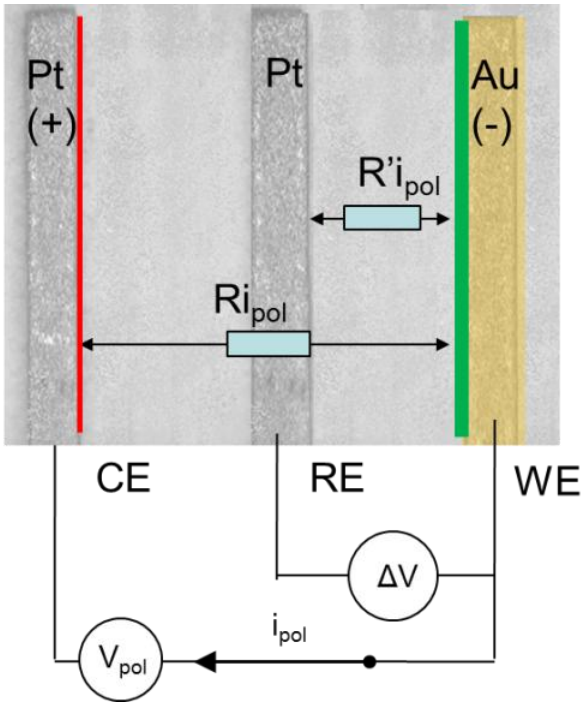

Figure 1: Schematic drawing of the 3-electrode sensor.

The polarization voltage V_{pol} is applied between CE and WE to reach the maintained current i_{pol}, the sensor output signal ΔV is measured between RE and WE. The ohmic drop (Ri_{pol}) between CE and WE depends on the electrolyte resistance R between CE and WE The ohmic drop between RE and WE is linked with the resistance R' between the working electrode and the reference one.

2.2. Electrochemical measurements

The 3-electrode sensors were tested in the test bench described in figure 2 and in more details in [5, 24]. The sensors were heated by passing current in the heating element. The temperature was automatically regulated with a precision of 0.1 °C from 450 °C to 600 °C.
Electrochemical Impedance Spectroscopy was used to investigate the resistance of the electrolyte between the electrodes. Two parameters were measured: R and R', and the apparent activation energy which was extracted from Arrhenius diagrams. These data were recorded in the synthetic gas bench with a "base gas" flow of 15 l/h containing 12 vol% O_2 and 1.5 vol% H_2O. A AC signal amplitude of 150 mV was applied between the two electrodes in the frequency range 10^5 Hz – 10^{-1} Hz. EIS measurements were performed between 450°C and 600°C with a step of 25°C both during heating and cooling down. The fitting of the Nyquist plots was performed with the ZView software. The obtained resistance values (both R and R') were of the order of tens MΩ at 450°C. Such high values can be explained by the high porosity of the electrolyte layer, as reported in [24]. The apparent activation energy (Ea) values are in the range 1.13-1.16 eV. These values are close to those representative of the grain boundaries at temperatures around 400 °C [25]

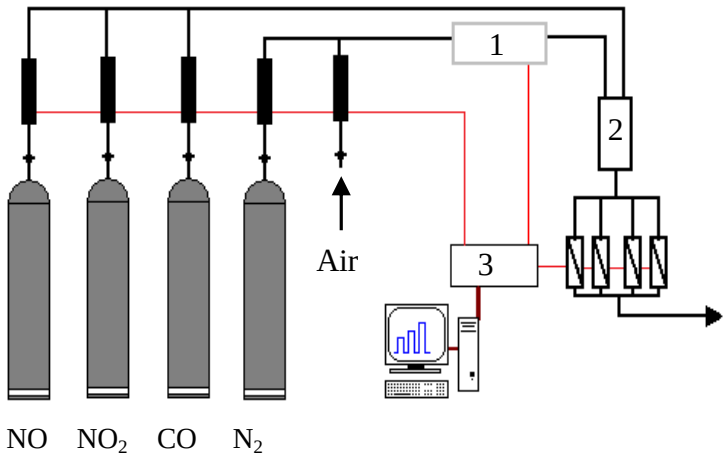

Figure 2: Test bench: 1 – Humidifier, 2 – Mixing chamber, 3 –Control card/potentiostat Versastat3.

The electrochemical properties for the oxygen electrode reaction of the sensing electrodes (Au and AuY) have been investigated at 450°C. Polarization measurements were performed in galvanostatic mode in base gas for different concentrations of O_2 (from 0.7 to 19.7 vol%) in

presence of 1.5 vol% H_2O in N_2. Various currents (from ± 2 to ±50 nA) from the lowest to the highest intensity were applied to monitor I-V curves. For each gaseous composition, each applied current was applied for 30 min to reach a steady-state. First, the cathodic zone was studied and then the anodic one. High anodic and cathodic overpotentials were achieved between ±200 and ±900 mV. Values of both cathodic currents and overpotentials were arbitrary fixed as positive to simplify the presentation of the results as the studied sensing Au-based electrode is the cathode.

In galvanostatic mode, the measured signal, ΔV, which is the sensor response, is defined as follow:

$$\Delta V = V_{RE} - V_{WE} \tag{7}$$

where V_{RE} and V_{WE} are the potentials of the working Au-based electrode and that of the reference upon the applied current (i_{pol}). Value of ΔV can express as follow:

$$\Delta V = \Delta V^0 + R' i_{pol} + \eta_{WE} \tag{8}$$

where R' is the electrical resistance of solid electrolyte between RE and WE;

i_{pol} is the polarization current between WE and CE,

ΔV° is the open-circuit voltage ($\Delta V° = V°_{RE} - V°_{SE}$= OCV),

η_{WE} is the electrochemical overpotential of the working electrode;

Therefore, the overpotential of the working electrode can be calculated using the following equation:

$$\eta_{WE} = \Delta V - \Delta V^0 - R' i_{pol} \tag{9}$$

The variations of the sensing electrode overpotential were recorded upon various applied currents in a wide range of oxygen partial pressure. In addition, the impact of injections of NO_2 (10 to 100 ppm) on the WE overpotential was also investigated for different oxygen partial pressures. The experimental study of interfacial reaction is made by current – potential characteristics often named (i-η), where (i) is a current and (η) is an overpotential. According to Butler-Volmer equation, the current which passes through the cell (i) at small overpotentials (η) close to the equilibrium potential (E_{eq}) is:

$$i = i_0 \left(\exp\left(\frac{\alpha_a n_a F \eta}{RT} \right) - \exp\left(\frac{-\alpha_c n_c F \eta}{RT} \right) \right) \tag{10}$$

where $\eta=E_{pol}-E_{eq}$ is the overpotential, (i_0) is the equilibrium exchange current, α_a, α_c are the anodic and cathodic charge transfer coefficients respectively, n_a and n_c are the number of electrons in anodic and cathodic reaction, respectively, F is the Faraday constant, R is the ideal gas constant, T is the absolute temperature. At high overpotentials, equation 10 is transformed into the Tafel relationship:

$$\eta = \frac{2.303RT}{\alpha_c n_c F}\log(i_0) + \frac{2.303RT}{\alpha_c n_c F}\log(i_{pol}) \quad (11)$$

or into Tafel plots in a more simple representation:

$$\eta = a + b\log(i_{pol}) \quad (12)$$

with i_{pol} is the polarization current, $a=(2.303RT/\alpha_c n_c F)\log(i_0)$ and $b=2.303RT/\alpha_c n_c F$..

According to equation 11, the apparent values of the i_o (equilibrium exchange current) and corresponding charge transfer anodic or/and cathodic coefficients can be extrapolated from the slope and the intercept of a linear relationship between $\log(i_{pol})$ and η.

2.3. Sensor response measurements.

The sensor responses were monitored during injections of 15 minutes of NO_2 (10, 50, 100 ppm) at 450°C. These operating conditions were selected to match those of diesel exhausts and for specific thermodynamic properties of the NO/NO_2 equilibrium. The increasing of temperature decreases the fraction of NO_2 produced by the catalytic filter. At 450°C, the fraction of NO_2, predicted by the thermodynamic equilibrium is around 40-50% for 5-15% of O_2. Short injections during 15 min of 50ppm NO and 50 ppm NO_2 in presence of 5-15% of O_2 were used to check that the catalytic filter can achieve the thermodynamic equilibrium, leading similar sensor responses.

3. Results and discussions

3.1. Oxygen electrode kinetic on Au and AuY working electrodes

The Tafel plots from anodic and cathodic polarization curves obtained on Au electrode at 450°C in 9.8% O_2 in the base gas are presented on figure 3. One can observe a correct linearity of the overpotential as a function of $\log(i_{pol})$. A small current of 10 nA produces +400 and -230 mV of cathodic and anodic overpotential, respectively. Upon 40 nA, these values increase up to +600 and -400 mV. This indicates that the rate of the electrochemical reduction of oxygen on Au is lower than the one for the electrochemical oxidation.

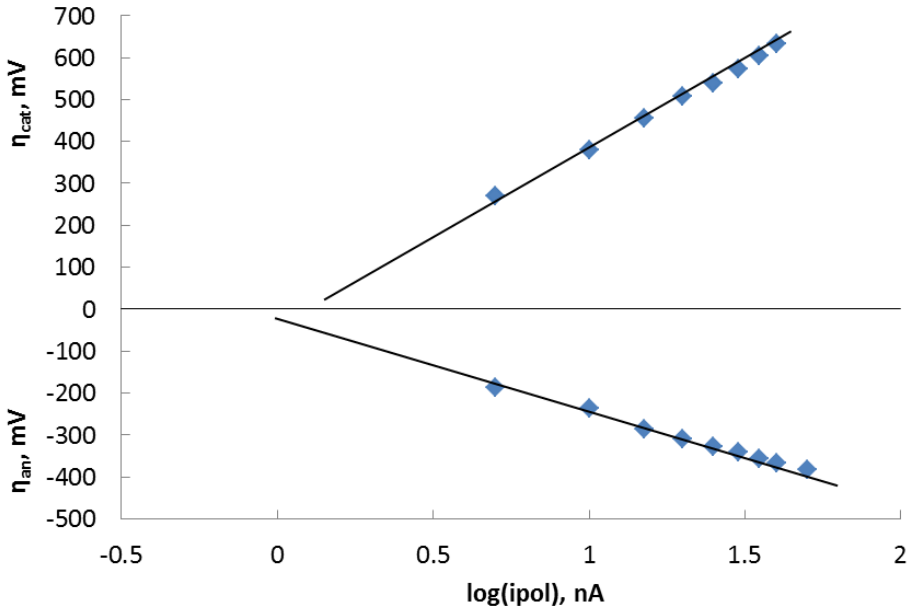

Figure 3: Tafel plot of current-overpotential curves of the Au working electrode in 9.8 % O_2 at 450°C

Figure 4 depicts variations of Au cathodic (η_{cat}) and Pt anodic (η_{an}) overpotentials with partial pressure of oxygen at 450°C. The cathodic overpotential decreases with increasing of pO_2 while the anodic overpotential is almost constant.

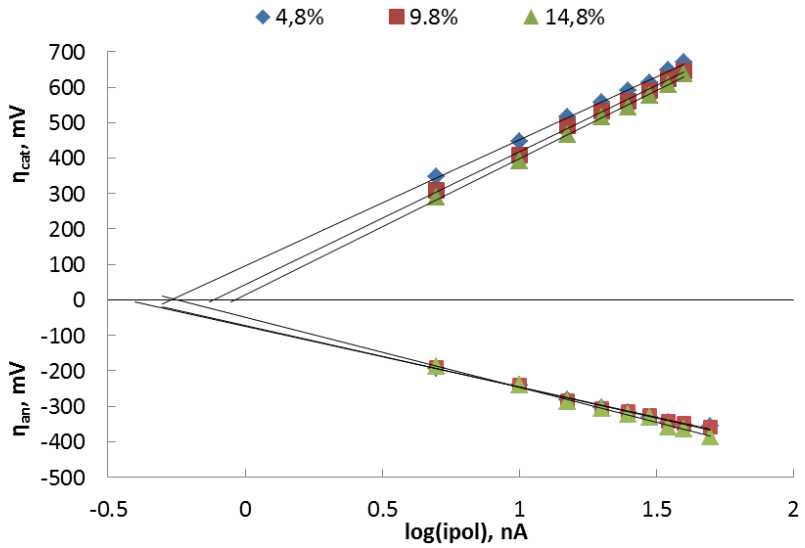

Figure 4: Tafel plots of current-overpotential curves of Au working electrode at 450°C as a function of the oxygen concentration

The Tafel plots of the AuY composite electrode are presented on figures 5 and 6. Upon 10 nA, the cathodic overpotential is lower than 50 mV. This value is much lower than that obtained on the Au electrode. At same time, the anodic overpotential is extremely high, of the order of -150 mV. Variations with pO_2 are similar that those obtained with pure Au: the cathodic overpotential increases with pO_2 while the anodic overpotential is constant (Figure 6).

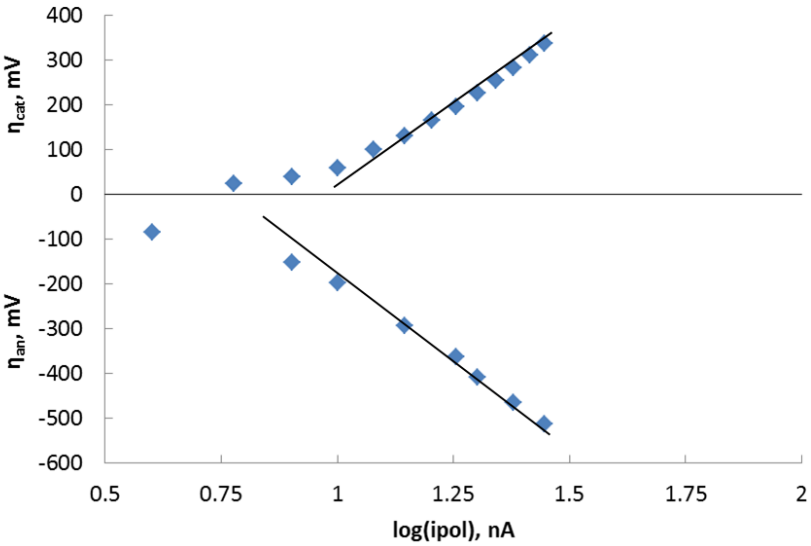

Figure 5: Tafel plot of current-overpotential curve of AuY working electrode in 9.7 % O_2, 1.5 %H_2O, N_2 at 450°C

In the linearity part of the $\eta=f(\log(i_{pol}))$ curves, one can calculate the exchange current (i_o) and then compare the electrochemical behaviors of the two electrodes.

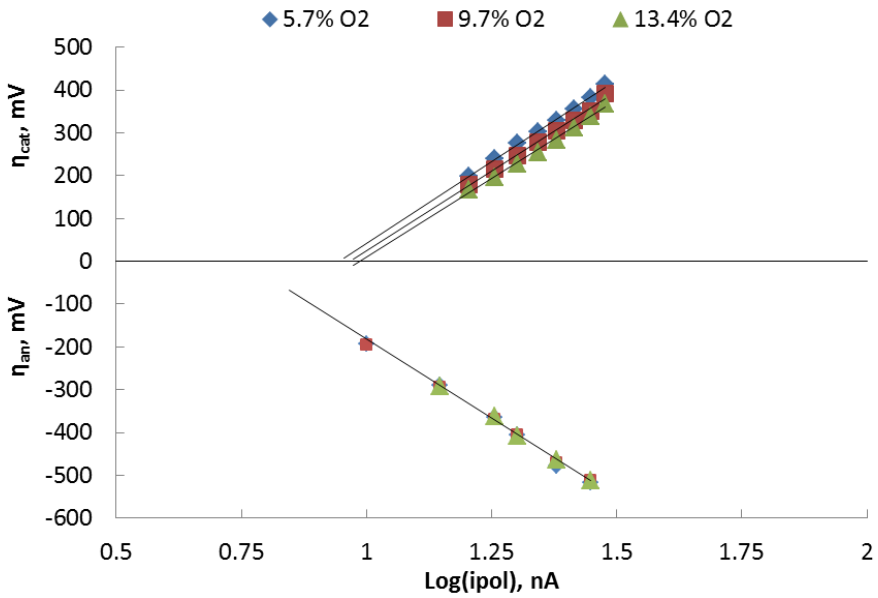

Figure 6: Tafel plots of current-overpotential curve of AuY working electrode at 450°C as a function of the oxygen concentration in base gas.

The exchange current depends on pO_2 according to the following equation:

$$i_0 \propto (P_{O_2})^m \tag{13}$$

The variation of (i_0) as a function of pO_2 is presented on figure 7. According to this proposed mechanism [17, 18], the value of "m" indicates the pathway of charge transfer limiting step of the electrochemical reaction. The value of 0.35 for Au electrode is close to 3/8 indicating a limiting reaction due to the charge transfer between atomic and ionic oxygen species according to reaction 14.

$$O_{ad} + e^- \longleftrightarrow O_{ad}^- \tag{14}$$

where O_{ad} is the adsorbed oxygen, O^-_{ad} is the reduced oxygen species on YSZ.

The value of "m" of 0.13 for AuY composite electrode is lower and closer to 1/8. This may indicate another limiting reaction pathway according to the model presented in [17] which corresponds to the incorporation of O^-_{ad} inside the YSZ network:

$$O^-_{ad} + e^- + V^{\cdot\cdot}_O \longleftrightarrow O^x_O + ad \qquad (15)$$

where O^-_{ad} is the reduced oxygen species on YSZ, $V^{\cdot\cdot}_O$ is an oxygen vacancy, O^x_O is a normal position of O^{2-} ion in the YSZ lattice, and "ad" is an adsorption site.

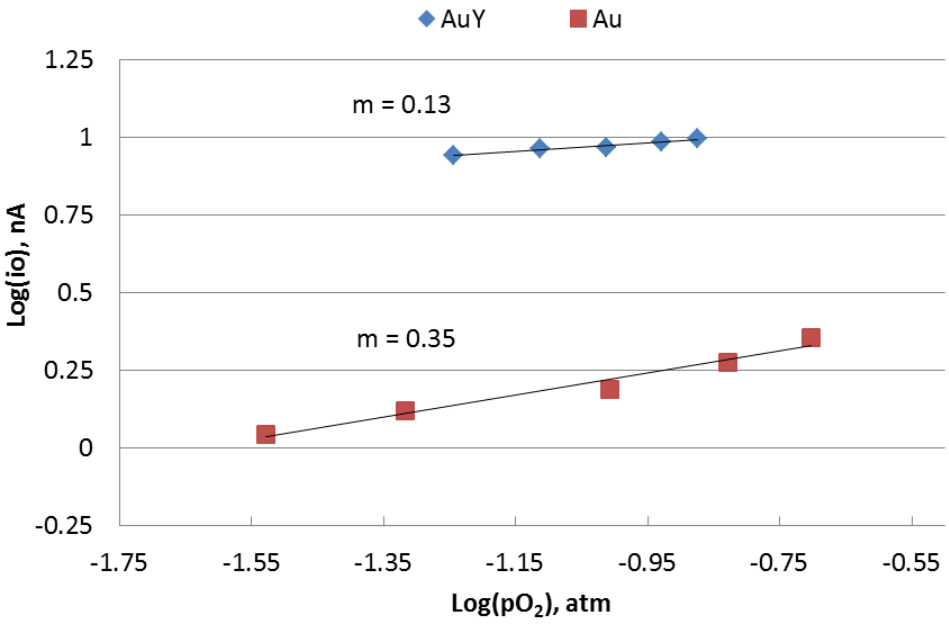

Figure 7: Equilibrium exchange current variations recorded on Au and AuY as a function of the oxygen partial pressure at 450°C in the base gas

The exchange current for the composite electrode AuY is almost 10 times higher than for dense Au electrode. This result correlates with conclusions presented in paper [24] which have shown that the composite electrode has a higher number of tpb and a lower interface resistance. This study [24] also has described the better stability and sensitivity of AuY as a sensing electrode to NO_2 in comparison with pure Au. Therefore, we have decided to deeply investigate the electrochemical performances of this composite electrode.

The variations of the AuY cathodic overpotential with $\log(pO_2)$ is shown in figure 8. For each value of the applied current, a different linear relationship is established. The slope of these equations is fairly similar. As the AuY overpotential is the main component of the sensor response,

this latter can be linked with the oxygen partial pressure. Therefore, without NO_2 in the feed, the sensor can measure the oxygen partial pressure at a constant temperature.

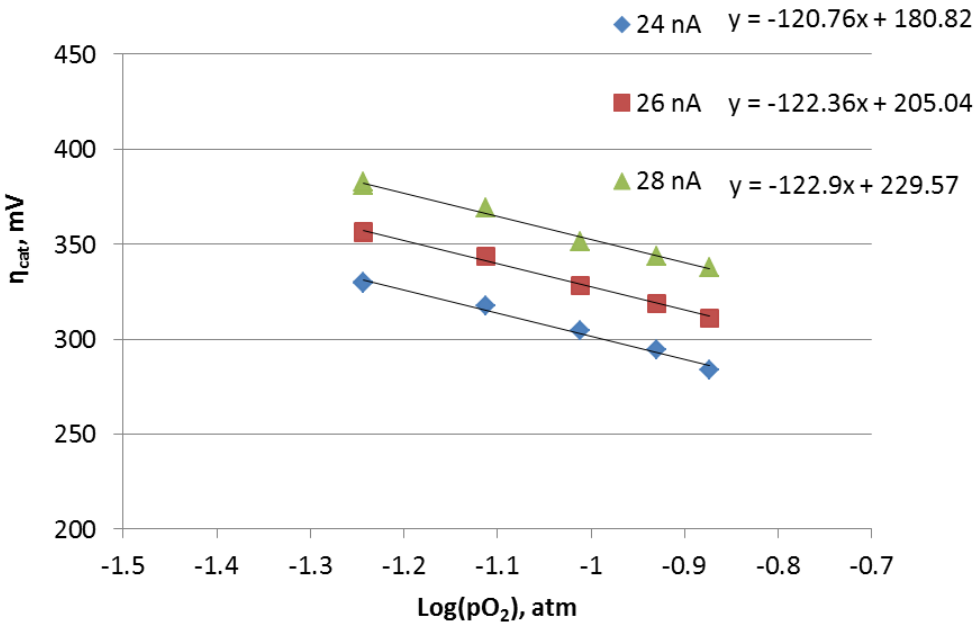

Figure 8: The variations of cathode overpotential as a function of log(pO_2) at 450 °C upon various values of i_{pol} 24, 26, 28 nA)

3.2. Oxygen electrode kinetic on AuY in presence of NO_2

The sensitivity to NO_2 was tested upon four applied currents i_{pol} 24, 26, 28 and 30 nA and three concentrations of oxygen: 5.7, 9.7 and 13.7%. The overpotential variation in presence of different concentrations of NO_2 is presented on figure 9. The overpotential at 0 ppm of NO_2 is much higher than that presented in the previous paragraph. This deviation can be the result of a long-term anodic polarization at anodic overpotentials up to -700 mV during previous tests at different pO_2. The high polarization can produce the modification of interface electrolyte/electrode where electrochemical reaction takes place [19] as already discussed in chapter 4.

The calculated values of the exchange current are higher than those previously observed: 12.1, 11.9, 10.7 under 5.7%, 9.7% and 13.7% of O_2, respectively. This increase of i_0 after anodic polarization was reproduced with other identical sensors. The average increase of i_0 was around +30±3% and has a tendency to decrease with of the partial pressure of O_2. The value of m from

equation 13 was found to be -0.13. This negative slope after an anodic polarization was reproduced on similar sensors at around -0.135±0.05.

In presence of NO_2, the overpotential strongly decreases, as shown on figure 9 in all studied range of i_{pol}. At the same time, the linear Tafel behavior is still observed. Upon i_{pol}=24 nA, the overpotential decreases from 487 mV in 5.7%O_2 to 337 mV when 10 ppm of NO_2 is injected to the base gas. The drop of cathodic overpotential slightly depends on the value of i_{pol}: -150 mV upon 24 nA, -163 mV upon 26 nA, -155 mV upon 28 nA and -153 mV upon 30 nA (Table 1).

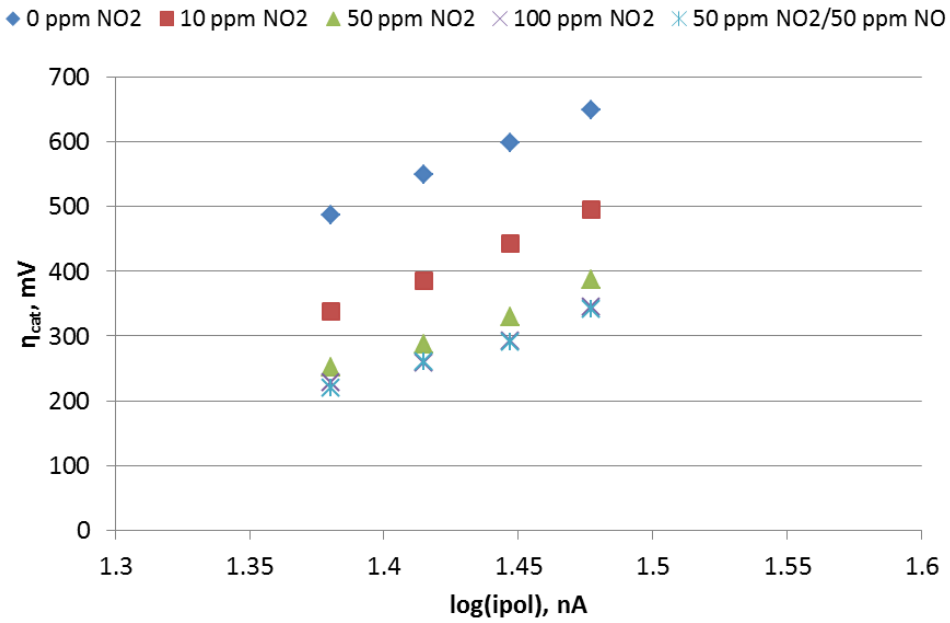

Figure 9: Overpotential variations as a function of the polarization current of AuY electrode at different concentrations of NO_x at 450 °C and for an oxygen partial pressure of 5.7% O_2.

The variation of the overpotential in presence of different NO_x concentrations and different oxygen partial pressures at constant i_{pol}=28 nA is shown on figure 10. The sensors are equipped with catalytic filter that can achieve the thermodynamic equilibrium of the NO oxidation reaction into NO_2. Therefore, injected concentrations of NOx are transformed to a NO/NO_2 mixture according to the thermodynamic equilibrium [3, 5] (Table 2)

Table 1: The overpotential drop during NO_2 pulsed as a function of pO_2 and i_{pol}.

i_{pol}, nA	Injected $[NO_2]/[NO]$, ppm/ppm	Baseline and overpotential drop, $\Delta V_{basegas}$-ΔV_{NO_2}, mV		
		pO_2, %		
		5.7	9.7	13.7
24	0 (baseline)	487	473	461
	10/0	150	141	132
	50/0	235	222	214
	100/0	259	250	239
	50/50	268	250	239
26	0 (baseline)	548	548	526
	10/0	163	143	106
	50/0	262	235	213
	100/0	290	264	245
	50/50	288	265	246
28	0 (baseline)	597	566	557
	10/0	155	146	135
	50/0	268	247	235
	100/0	305	274	265
	50/50	308	275	259
30	0 (baseline)	648	636	593
	10/0	153	141	98
	50/0	261	250	238
	100/0	304	290	272
	50/50	307	292	280

To simplify the presentation, only the injected concentrations are presented on figures 10 and 11. However, the sensitivity, expressed in mV/decade, to NO_2 and i_0 variations were calculated according to the real concentration of NO_2 estimated from the thermodynamic equilibrium

Table 2: Values of the injected and theoretical thermodynamic concentrations of NO_2 after passing through the catalytic filter at 450 °C at different pO_2.

injected [NO_2]/[NO], ppm/ppm	Thermodynamic concentration of NO_2, ppm		
	pO_2, %		
	5.7	9.7	13.7
10/0	2.5	3	3.5
50/0	12.5	15	17.5
100/0	25	30	35
50/50	25	30	35

The slopes of the η_{cat}=log(pO_2) curves vary from -108 (no NO_2), to -56 (10 ppm NO_2), -20 (50 ppm NO_2) and +21-22 mV/decade (100 ppm NO_2 and NO/NO_2 50 ppm/50 ppm), for i_{pol}=28nA. The presence of NO_2 strongly decreases the cathodic overpotential, suggesting that the NO_2 electrochemical reduction is faster than that of oxygen. The same trend is also valid for other currents, 24, 26 and 30 nA. Nevertheless, additional experimental (intermediate NO_2 concentrations) points would be required to obtain more accurate relationships.

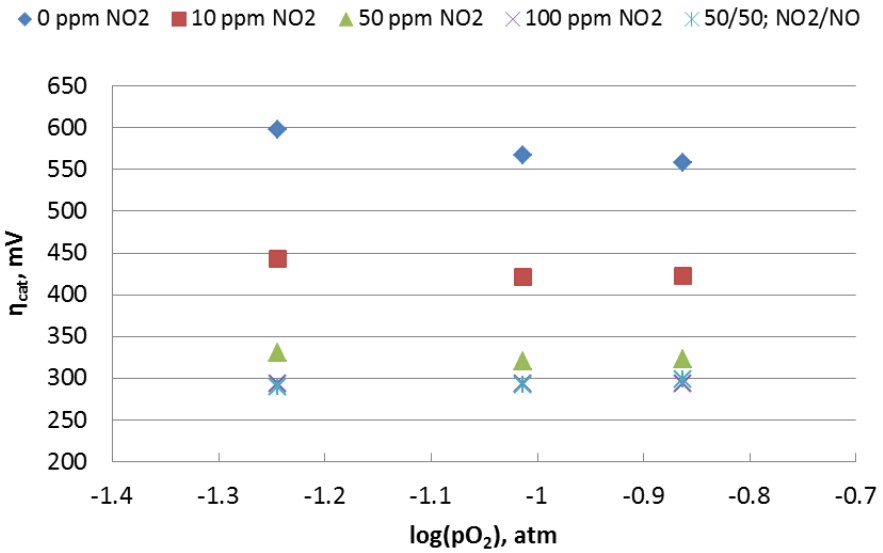

Figure 10 : Overpotential variations of the AuY electrode as a function of log(pO_2) at different concentrations of NO_2 upon i_{pol}=28 nA and T=450 °C.

As previously observed, the cathodic overpotential decreases with pO_2 (Figure 10 at 0 ppm NO_2). The overpotential slightly decreases from 600 mV at 5.7% O_2 to 560 mV in 13.7% O_2. This drop is much higher than the decrease of OCV of -7 mV observed between 5.7 and 13.7 % O_2. This OCV variation was subtracted to calculate the overpotential.

The presence of small amounts of NO_2 at the AuY/YSZ interface (2.5 ppm for 10 ppm injected) produces a strong decrease of the overpotential under 5.7% O_2 from 597 mV to 447 mV. Injections of 50 ppm and 100 ppm of NO_2 produce a stronger drop of overpotentials of 330mV and 290 mV, respectively. The similarity of results recorded for 100 ppm of NO_2 and 50/50 ppm NO/NO_2 indicates that the catalytic filter is working properly as identical concentration of NO_2 reaches the sensing electrode.

The influence of the oxygen concentration on the exchange current in presence of NO_2 is presented on figure 11. A significant increase of i_0 in presence of NO_2 is observed whatever the NO_2 concentration. At the same time, i_0 slightly decreases with pO_2 but remains at around 15±1 nA, value which is not affected by different NO_2 concentrations in the range 10 – 100 ppm. One can conclude that electrochemical reaction of NO_2 on AuY electrode is favored within 5.7-13.7 $\%O_2$, but that simultaneous reductions of NO_2 and O_2 electrochemical reduction take place.

The variations of i_0 with the theoretical thermodynamic concentration of NO_2 are shown on figure 12. It seems, that the value of i_0 has a tendency to increase with pNO_2 for oxygen partial pressures equal to 5.7% and 9.7% with m=0.02 and to decrease at 13.7% O_2 with m=-0.03. However, the linearity cannot be proved with only three points.

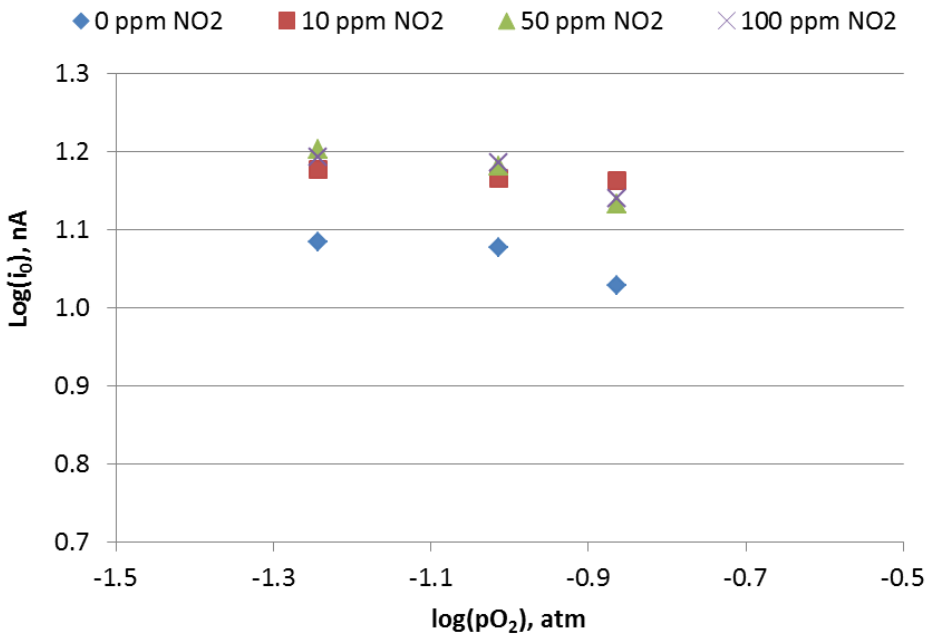

Figure 11: Variations of the equilibrium exchange current as a function of the logarithm of the oxygen partial pressure at 450°C for different concentrations of NO_x for the AuY electrode.

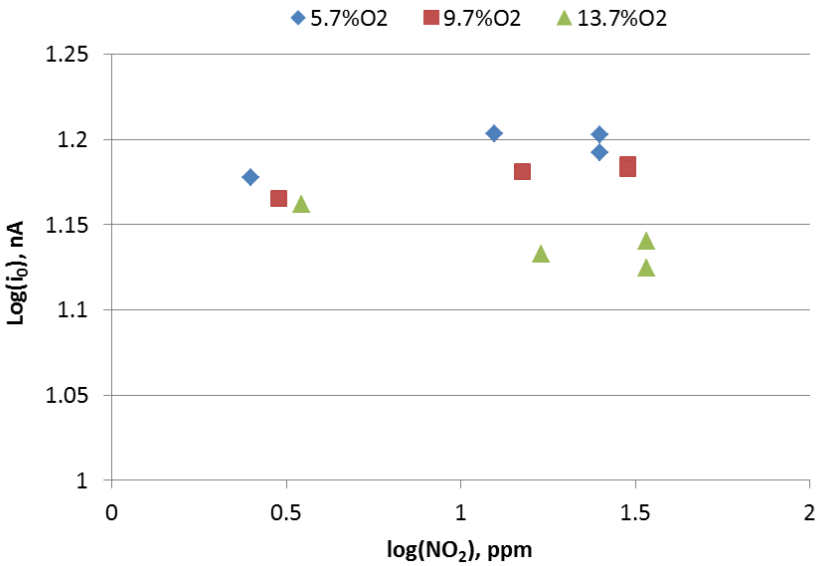

Figure 12: Variation of the equilibrium exchange current as a function of the logarithm of the theoretical thermodynamic NO_2 concentration at 450°C in 5.7%, 9.7% and 13.7 % of O_2 for AuY electrode.

As a conclusion, we can confirm that the linearity of η-log(i_{pol}) curves indicates a charge transfer limiting step of the oxygen electrode reduction on AuY. The similar Tafel behavior in presence of pulses of NO_2 suggests a similar one-electron mechanism (reactions 14 and 15) with a preliminary adsorption step (reaction 16). Reaction 15 is supposed to be the rate determining step according to the relationships between the exchange current and pO_2.

$$O_2 + 2ad \longleftrightarrow 2O_{ad} \quad (16)$$

In parallel, the electrochemical reduction of NO_2 could proceed via an adsorption step (17), following by a one-electron step (18) to produce NO and the same intermediate O^-_{ad} as for the oxygen electrode reaction (14). Then, the final step is similar (15).

$$NO_2 + ad \longleftrightarrow NO_{2ad} \quad (17)$$

$$NO_{2ad} + e^- \longleftrightarrow O^-_{ad} + NO \quad (18)$$

The main process of the electrochemical reaction takes place at the interface electrode/electrolyte and depends on the catalytic activity of electrode material. For instance, according to the literature data, the mechanism of the oxygen reaction on Pt and Au electrodes is different because of different activity between Pt and Au in the temperature range 300-600°C, mainly because of the low coverage of oxygen on gold [17, 18].

Before charge transfer reactions at the electrode/electrolyte interface, the steps of diffusion and adsorption of gas on the adsorption sites ("ad") have to take place (reactions 16 and 17). One can suggest that NO_2 adsorption is easier on Au than O_2 adsorption. Therefore, our assumption is that reaction (15), which is the rate limiting process on AuY, is strongly accelerated because NO_2 provides O^-_{ad} intermediate species.

3.3. Responses to NO_2 of the AuY-based sensor

Figures 13-15 show the typical sensor response, ΔV, at i_{pol} =28 nA to injections of 10, 50, 100 ppm of NO_2 as well as 50/50 ppm NO/NO_2 in presence of 5.7, 9.7, 13.7% of O_2. The baseline level of the AuY-based sensor was chosen as the value of ΔV before the first injection of 50 ppm of NO_2

As it was noticed previously, the sensor is equipped with a catalytic filter and concentrations of NO_2 on the electrode are fixed by the thermodynamic equilibrium, i.e. the temperature and the partial pressure of oxygen. At 450°C in presence of 9.7 % O_2, the calculated concentrations of NO_2 are 3, 15 and 30 ppm for 10, 50 and 100 ppm of injected NO_2, respectively. For a simplest presentation, only injected concentrations are presented. After stabilization of the baseline during 45 minutes in base gas with 5.7% O_2, 1.5% H_2O and N_2, a pulse of 10 ppm NO_2 into the base gas was injected. After 15 minutes, the pulse was stopped. This sequence was repeated for 50, 100 ppm of NO_2 and 50/50 ppm NO/NO_2 pulses in 9.7 and 13.7 % O_2 upon i_{pol}=24, 26, 28, 30 nA.

The decrease of ΔV during the injection of 10 ppm of NO_2 is relatively fast. Values of the response times ($T_{0.9}$ res, defined in chapter 2) are 123, 129 or 119 seconds for 5.7%, 9.7% and 13.7 % of O_2, respectively. The recovery time is much higher and is presented in minutes: 5, 8 and 3 minutes for 5.7%, 9.7% and 13.7 % of O_2, respectively. When 50 ppm of NO_2 was injected, the response time is much shorter, less than 60 seconds for all concentrations of O_2. The recovery time for higher pNO_2 is also few minutes (Table 3). The evolution with time of the signal recovery can be divided into two zones: a first fast step following by a slow process. During the first fast step, signal recovers 70-80% of its initial overpotential in 60-120 seconds. On the other hand, the slow process duration is of the order of ten minutes. This time increases with the injected concentration

of NO_2, from 5 minutes for 10 ppm to 28 and 44 minutes for 50 and 100 ppm, respectively in 5.7% O_2. These results were reproduced with identical sensors.

Table 3: Response ($T_{0.9}$ res) and recovery ($T_{0.9}$ rec) times of the AuY-based sensor at 450°C, ipol=28 nA at different pO_2.

injected $[NO_2]/[NO]$, ppm/ppm	pO_2, %								
	5.7			9.7			13.7		
	Calc $[NO_2]$, ppm	T_{09} res, sec	T_{09} rec, min	Calc $[NO_2]$, ppm	T_{09} res, sec	T_{09} rec, min	Calc $[NO_2]$, ppm	T_{09} res, sec	T_{09} rec, min
10/0	2.5	123	5	3	129	8	3.5	119	3
50/0	12.5	45	28	15	45	12	17.5	30	21
100/0	25	35	44	30	30	38	35	45	33
50/50	25	35	33	30	30	23	35	30	15

The increase of the recovery time with NO_2 and decrease with O_2 is observed for high NO_2 (from 50 ppm). This phenomenon can indicate a competitive adsorption between NO_2 and O_2 on the sensing electrode.

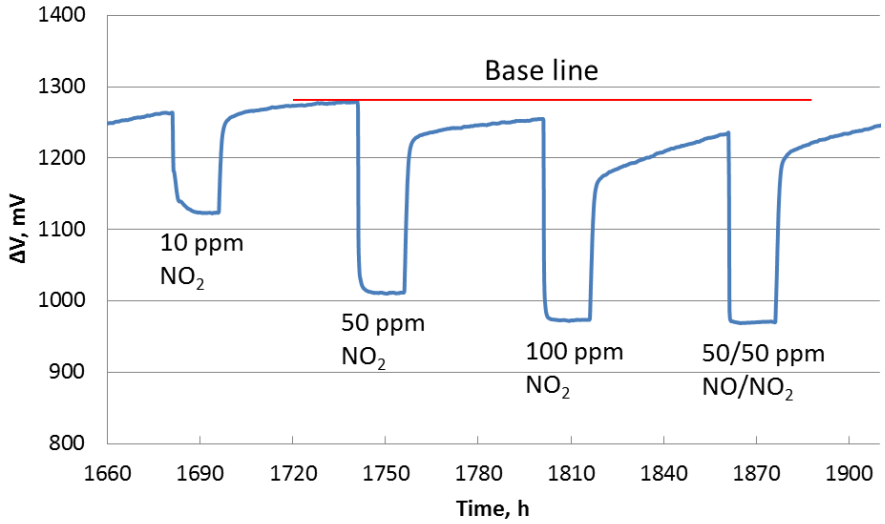

Figure 13: Sensor with AuY sensing electrode responses to NO_2 in 5.7 %O_2, ipol=28 nA, T=450°C.

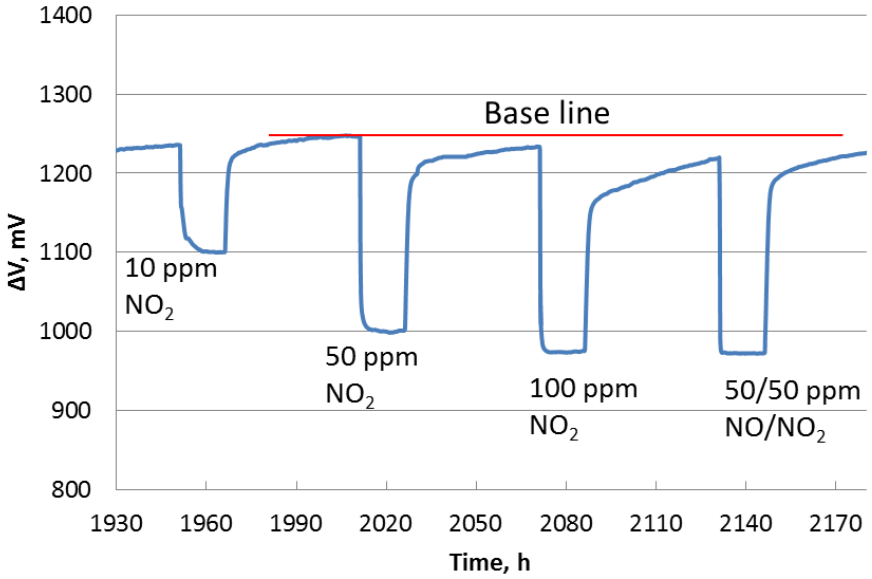

Figure 14: Responses of the AuY sensing electrode to NO_2 in 9.7 $\%O_2$, ipol=28 nA, T=450°C.

The mechanism in presence of NO_2 has to be clarified using adsorption and desorption techniques of NO/NO_2 from YSZ, AuY and porous catalytic filters. The fast response and slow recovery was also observed in potentiometric measurements for Pt/YSZ/AuY sensor without catalytic filter [24].

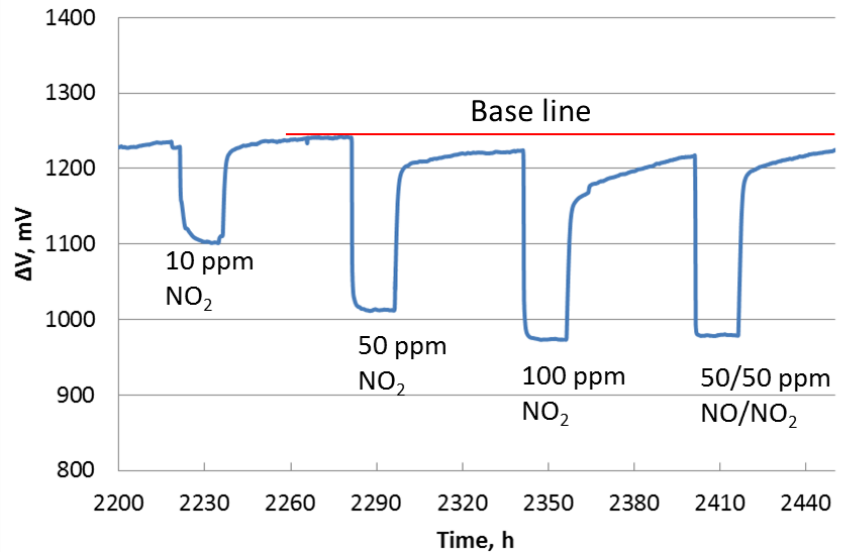

Figure 15: Responses of the AuY sensing electrode to NO_2 in 13.7 $\%O_2$, ipol=28 nA, T=450°C

The variation of the sensing electrode overpotential with log(NO_2) (theoretical concentrations according to the thermodynamic equilibrium) is presented on figure 16. The overpotential linearly depends on the logarithm of the NO_2 partial pressure. The slopes are respectively 151, 129 and 129 mV/decade for 5.7%, 9.7% and 13.7% O_2. These values are more than two times higher than those measured for the AuY sensing electrode in the potentiometric sensor: 52 mV/decade at 450°C [24], or 35 mV/decade at 500 °C [5]. They are also higher than the ones reported (112 mV/decade for (0.5-50 ppm NO_2) for a polarized device based on lambda probe [26]

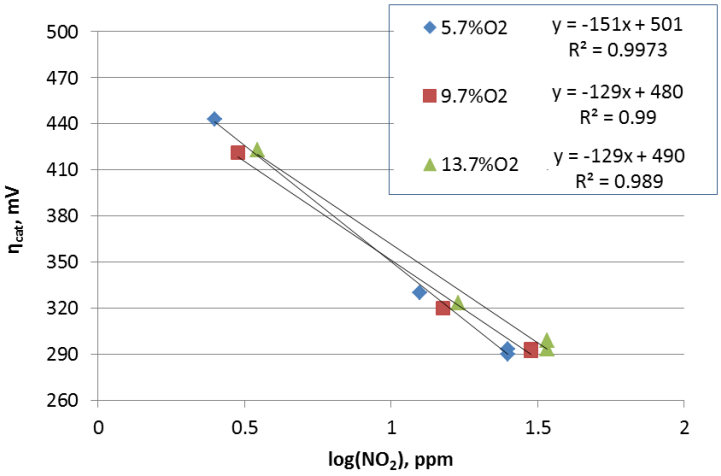

Figure 16: Variations of the cathodic overpotential of the AuY sensing electrode as a function of log(NO_2) at 450°C at i_{pol}=28 nA.

Such high sensitivity to NO_2 is related to the effect of polarization. In potentiometric mode, the mixed potential of the electrode [5, 8, 24] is mainly linked with the difference in electrocatalytic properties of the two electrodes. In galvanostatic mode, the sensitivity is only driven by the overpotential of the sensing electrode. In case of polarized sensing electrodes, the applied current fixes the rate of the electrode reactions, both the electrochemical reduction of oxygen and NO_2. As was shown by values of the exchange current i_0, the rate of the NO_2 electrochemical reduction is higher than that of the oxygen one. NO_2 can be more easily electrochemically reduced than O_2. The strong decreasing of the overpotential is a consequence of the fast electrochemical reduction of NO_2 and is proportional to the logarithm of the NO_2 concentration.

The impact of pO_2 on the sensitivity is not significant in the range 9.7-13.7%. (Figure 16).Furthermore, the variation of pO_2 in the exhaust could be determined with variation of the baseline of the sensor (if there is no NO_2) and compare with OBD lambda probe data.

4. Conclusions

The proposed system of thee-electrode solid state sensor with polarized Au-based sensing electrode allows comparing the oxygen electrochemical reaction on different sensing materials. The composite sensing electrode (Au+10 wt% YSZ) shows higher activity to oxygen electrochemical reduction than simple Au electrode.

The electrochemical reduction of oxygen on AuY composite with different oxygen concentrations and in presence of 10-100 ppm of NO_2 seems to follow a one electron charge transfer-step. The reduction may occur in two consecutive reactions with one electron transfer. The presence of NO_2, in range of 10-100 ppm, under 5.7-13.7 % O_2, increases the equilibrium exchange current. This indicates that the electrochemical reduction of NO_2 is faster than that of oxygen.

The results indicate that the limiting step of the oxygen reduction is the production of adsorbed oxygen species O^-_{ad}. The fast adsorption of NO_2 certainly promotes its electrochemical reduction in NO, and then produces adsorbed O^- species. Experimental observed decrease of the AuY overpotential is probably linked with the production of these intermediate species.

The sensitivity of polarized sensor equipped with a catalytic filter at 450°C is around 130 mV/decade in range 10-100 ppm NO_2. This is much higher than for potentiometric mixed-potential sensors with sensitivity around 35 mV/decade. The cross sensitivity to oxygen was also observed. The maximal variation of output signal with pO_2 in range of 5.7-13.7% is around -22 mV at 24 nA and -55 mV at 30 nA whereas the minimal response to 10 ppm NO_2 of the sensor is -148mV in 9.7 % O_2 in the applied current range 24-30 nA.

The used catalytic filter is active and reaches the thermodynamic equilibrium between NO, O_2 and NO_2 at 450°C.

The response time of the sensors is around 2 minutes for low concentrations of NO_2 (<30 ppm) and lower than 45 second for higher concentrations (30-100 ppm). The recovery time is longer, around few minutes and increases with NO_2 concentration.

References

1. Regulation No 715/2007 of the European Parliament and of the Council of 20 June 2007. Official Journal J L 171, 29.6.2007, 030, 284-299.
2. Docquier N., Candel S., 2002, Combustion control and sensors: a review, *Progress in energy and Combustion science*, 28, p.107-150.
3. Pârvulescu V.I., Grange P., Delmon B., 1998, Catalytic removal of NO, *Catalysis Today*, 46, p.233-316.
4. Guillet, R Lalauze, Viricelle J.-P., Pijolat C., Montanaro L., 2002, Development of a gas sensor by thick film technology for automotive applications: choice of materials—realization of a prototype, *Materials Science and Engineering: C,* 21 , p.97–103.
5. Gao J., Viricelle J.-P., Pijolat C., Breuil P., Vernoux P., Boreave A., Giroir-Fendler A., 2011, Improvement of the NOx selectivity for a planar YSZ sensor, *Sensors and Actuators B*, 154, p.106–110.
6. Somov S., Reinhardt G., Guth U., Göpel W., 1996, Gas analysis with arrays of solid state electrochemical sensors: implications to monitor HCs and NOx on exhaust, *Sensors and Actuators B*, 35-36, p.409-418.
7. Zhang W.-F., Schmidt-Zhang P., Guth U., 2004, Electrochemical studies on cell M/YSZ/Pt (M=Pt, Pt-Ga_2O_3) in NO, O_2, N_2 mixtures, *Solid state Ionics*, 169, p.121-128.
8. Yin C., Guan Y., Zhu Z., Liang X., Wang B., Diao Q., Zhang H., Ma J., Liu F., Sun Y., Zheng J., Lu G., 2013, Highly sensitive mixed-potential-type NO_2 sensor using porous double layer YSZ substrate, *Sensors and Actuators B*, 183, p.474-477.
9. Miura N., Zhuiykov S., Ono T., Hasei M., Yamazoe N., 2002, Mixed potential type sensor using stabilized zirconia and $ZnFeO_4$ sensing electrode for NOx detection at high temperature, *Sensors and. Actuators B*, 83, p.222–229.
10. Zosel J., Westphal D., Jakobs S., Müller R., Guth U., 2002, Au-oxide composites as HC-sensitive electrode material for mixed potential gas sensors, *Solid State Ionics*, 152-153, p.525-529.
11. Zosel J., Tuchtenhagen D., Ahlborn K., Guth U., 2008, Mixed potential gas sensor with short response time, *Sensors and Actuators B*, 130, p.326-329.
12. Striker T., Ramaswamy V., Armstrong E. N., Willson P. D., Wachsman E. D., Ruud J. A., 2013, Effect of nanocomposite Au–YSZ electrodes on potentiometric sensor response to NOx and CO, *Sensors and Actuators B*, 181, p.312-318.
13. Miura N., Lu G., Yamazoe N., 1998, High-temperature potentiometric/amperometric NOx sensors combining stabilized zirconia with mixed-metal oxide electrode, Sensors and Actuators B: Chemical, 52(1–2), p.169-178.
14. Miura N., Lu G., Ono M., Yamazoe N., 1999, Selective detection of NO by using an amperometric sensor based on stabilized zirconia and oxide electrode, *Solid State Ionics*, 117(3–4), p.283-290.

15. Sekhar P.K., Brosha E.L., Mukundan R., Li W., Nelson M. A., Palanisamy P., Garzon F.H., 2010, Application of commercial automotive sensor manufacturing methods for NOx/NH_3 mixed potential sensors for on-board emissions control, *Sensors and Actuators B: Chemical,* 144(1), p.112-119.
16. Fischer S., Pohle R., Farber B., Proch R., Kaniuk J., Fleischer M., Moos R., 2010, Method for detection of NOx in exhaust gases by pulsed discharge measurements using standard zirconia-based lambda sensors, *Sensors and Actuators B: Chemical*, 147(2-3), p.780-785.
17. Van Hassel B.A., Boukamp B.A., Burggraaf A.J., 1991, Electrode polarization at the Au, O_2(g)/yttria stabilized zirconia interface. Part I: Theoretical considerations of reaction model, Solid State Ionics, Volume 48(1–2), p.139-154.
18. Van Hassel B.A., Boukamp B.A., Burggraaf A.J., 1991, Electrode polarization at the Au O_2(g)/yttria stabilized zirconia interface. Part II: electrochemical measurements and analysis, Solid State Ionics, 48(1–2), p.155-171.
19. Raźniak A., Dudek M., Tomczyk P. 2011, Reduction of oxygen at the interface M|solid oxide electrolyte (M = Pt, Ag and Au, solid oxide electrolyte = YSZ and GDC). Autocatalysis or artifact?, *Catalysis Today,* 176(1), p.41-47.
20. Athanasiou C, Karagiannakis G, Zisekas S, Stoukides M, 2002, Electrode polarization at the O2(g), Pd/YSZ interface, Solid State Ionics, 136–137, p.873-877.
21. Sze Nga Sum O., Djurado E., Pagnier T., Rosman N., Roux C., Siebert E., 2005, Raman investigation of the O_2, Pt/YSZ electrode under polarization, *Solid State Ionics*, 176(35–36), p.2599-2607.
22. Sakai N., Yamaji K., Horita T., Kishimoto H., Brito M.E., Yokokawa H., Uchimoto Y., 2006, Application of SIMS analyses on oxygen transport in SOFC materials, *Applied Surface Science*, 252(19), p.7045-7047.
23. Kishimoto H., Sakai N., Yamaji K., Horita T., Brito M. E., Yokokawa H., Amezawa K., Uchimoto Y., 2008, Visualization of oxygen transport behavior at metal electrode/oxide electrolyte interface using secondary ion mass spectrometry, *Solid State Ionics,* 179(9–10), p.347-354.
24. Romanytsia I., Viricelle J.-P., Vernoux P., Pijolat C., Application of advanced morphology Au–X (X = YSZ, ZrO_2) composites as sensing electrode for solid state mixed-potential exhaust NOx sensor, Sensors and Actuators B, 2015, Pages 391-397.
25. Gerstl M., Navickas E., Friedbacher G., Kubel F., Ahrens M., Fleig J., 2011, The separation of grain and grain boundary impedance in thin yttria stabilized zirconia (YSZ) layers, *Solid State Ionics*, 185(1), p.32-41
26. Fischer S., Schönauer-Kamin D., Pohle R., Magori E., Farber B., Fleischer M., Moos R., 2012, NOx-Detection by Pulsed Polarization of Lambda Probes, 2012, Communication on 14th International meeting on Chemical sensors., doi 10.5162/IMCS2012/P1.6.4.

General Conclusions and Perspectives

Conclusions and Perspectives

The main objective of this work was to continue the development of a NOx sensor, started during previous J. Gao PhD and to improve its performances.

This demand was realized during long-term research program between Ecole Nationale Supérieure de Mines de Saint-Etienne (EMSE), Institut de Recherches sur la Catalyse et l'Environnement de Lyon (IRCELyon) and industrial partner Measurement Specialties (MEAS). As a result, solutions for selective detection of NO_2 are proposed, such as catalytic filter and continuous polarization of sensing electrode.

Modification of electrode selectivity can be realized by galvanostatic polarization. Potential of electrode fixed by polarization depends on NO_2 concentration. In presence of NO_2, potential of polarized sensing electrode decreases dramatically. This decrease is much higher than for mixed-potential sensors and is absolutely selective to NO_2. Despite advantages of selectivity, there are still problems to solve:

- Problem of "base line stability" – signal of sensor without NO_2/NO which is probably linked to electrochemical reaction of oxygen on working electrodes.
- Unknown mechanism of electrochemical detection of NO_2 and origin of "base line"
- Problem of oxygen concentration variation on the sensor response to NOx

So, the global scientific objectives of this PhD was to understand the sensor mechanism under polarization mode, to study the role of reference electrode, and to optimize the sensor design – electrodes material, geometry and area, and its working conditions.

Utilization of advanced electrode materials, like composites, allows to increase sensing characteristics of sensor, like response and recovery time, sensitivity, improvement of interface electrode/electrolyte stability, and increases number of triple phase boundaries.

The effect of YSZ and ZrO_2 additions to the gold electrode on the response toward NO_2 was investigated between 450°C and 550°C. The initial gold electrode was quite dense. SEM characterizations evidenced that the porosity and then the number of triple phase boundaries were increased when ZrO_2 or YSZ were incorporated into the Au electrode. However, with ZrO_2 addition, polarization resistance was not modified compared to reference Au/YSZ/Pt sensor. In this case, the presence of porosity in the electrode damages the sensor performances both in terms of NO_2 sensitivity and of signal stability.

On the contrary, as shown by electrochemical impedance measurements, the polarization resistance was significantly reduced in the case of Au-YSZ electrode. Such a result indicates that the electrochemical properties for the oxygen electrode reaction were only improved for the Au-YSZ composite electrode because the ionic conductivity of YSZ can delocalize the electrode reaction in the overall electrode volume. Furthermore, the addition of YSZ improved the

sensitivity toward NO_2 as well as the response time of Au-based electrodes. As a conclusion, porous Au-YSZ composite electrodes in a YSZ-based sensor have a beneficial effect compared to pure gold electrode.

In case of polarized thee-electrode sensor, Pt(CE)/Pt(RE)/Au(WE=SE), the different components of the sensor signals as overpotential, OCV and ohmic drop have been determined at 450°C. A large part (between 20 and 40%) of the measured signal of sensors is due to the ohmic drop linked with the high resistivity of the YSZ porous layer. This contribution is proportional to the intensity of the applied current and to the geometrical position of the reference electrode (resistance of electrolyte between RE and WE). EIS technique was used to measure the resistance between the reference electrode and the sensing electrode. Therefore, the ohmic drop voltage was subtracted to calculate the electrode overpotential of the sensing electrodes.

It was found that high drift with time of the overpotential of the Au sensing electrode perturbs the sensor signal and does not allow to achieve accurate measurements. Composite electrode material (AuY) made of Au and Yttria-Stabilized Zirconia (YSZ) improves the stability of the baseline and decreases the sensing electrode overpotential. However, the sensitivity to NO_2 also decreases from 290 mV/decade with the Au electrode to 35 mV/decade with the composite one, at 450°C. Nevertheless, this composite electrode could allow to work at higher polarization currents in order to reach higher overpotentials for which NO_2 could be higher.

Working in oxygen containing atmosphere, sensing parameters of sensor depend on oxygen concentration. The understandings and interpretation of relationship with sensitivity to NO_2 and O_2 were also a major axis of present work.

The investigation of electrode reaction shows that the reduction of oxygen on AuY composite with different oxygen concentrations and in presence of 10-100 ppm of NO_2 seems to follow a one electron charge transfer-step. The reduction may occur in two consecutive reactions with one electron transfer. The presence of NO_2, in range of 10-100 ppm, under 5.7-13.7 % O_2, increases the equilibrium exchange current. This indicates that the electrochemical reduction of NO_2 is faster than that of oxygen.

We have shown that the limitation step of oxygen reduction is the production of adsorbed O^-_{ad} species. The favorite adsorption of NO_2 and faster reduction with generation of reduced oxygen allows to decrease the overpotential corresponding to production of O^-_{ad}. Observed decrease of overpotential is proportional to concentration of NO_2

The sensitivity of polarized sensor equipped with a catalytic filter at 450°C is around 130 mV/decade in range 10-100 ppm injected NO_2. This is much higher than potentiometric mixed-potential sensors with sensitivity of around 35 mV/decade. The cross sensitivity to oxygen was also observed. The maximal variation of output signal with pO_2 in range of 5.7-13.7% is around -22 mV

at 24 nA and -55 mV at 30 nA with minimal response of sensor -148mV to 10 ppm of NO_2 in 9.7 % O_2 upon 24-30 nA.

The combination of two polarized sensors one with catalytic filter, the other without, can give the information not only on NO_2 concentration, but also on NO concentration in exhaust.

However, some drawbacks have to be solved before considering a real application and can be focused as perspectives of present work:

- Actual high ohmic drops (10 – 50 MΩ) due to the high porosity of the YSZ layer can be reduced by modification of actual composition of YSZ ink and parameters of layer deposition.

- The position of the reference electrode (RE) strongly influences the sensor response. The realization of real reference electrode placed out of the current lines and having constant potential in different atmospheres can be a second axis of perspective work.

- The demand of vehicle producers is also oriented on simultaneous selective detection of NH_3 in exhaust. The galvanostatic polarization method for modification of sensor selectivity may be adapted for selective detection of ammonia.

École Nationale Supérieure des Mines
de Saint-Étienne

NNT : 2014 EMSE 0760

Ivan ROMANYTSIA

STUDY OF ELECTRO-CATALITIC ACTIVITY OF ELECTRODES MATERIALS AND POLARIZATION PHENOMENA FOR DETECTION MECHANISM INVESTIGATION OF A NO_2 SENSOR AND ITS OPTIMIZATION.

Speciality : Chemical engineering

Keywords : Exhaust, NOx, Sensor, Polarization, Selectivity, Detection mechanism

Abstract :

Road transport is one of the main sources of NOx emitted into the atmosphere. The majority of this pollution is concentrated in urbanized areas. The permanent exposure to the exhaust gases has serious consequences for human health and for that, emission standards become more stringent.

The modern technologies present in automotive need the continuous control of the exhaust composition. The variations of temperature, composition of exhaust gas, vibrations and other factors require long life robust control systems.

In this work, we present the procedure of fabrication and characterization of an electrochemical sensor with three electrodes that can fulfill the demands of industrial applications in automotive industry. Manufacturing by screen-printing technology allows producing low-cost sensor with high reproducibility in industrial process.

The principle of our sensor is based on galvanostatic polarization of a gold sensing electrode allowing the selective detection of NO_2 without interference to other gases such as CO and NO. In order to increase stability, and to decrease the response and recovery time of the sensor, a new Au composite sensitive electrode was developed.

The electrochemical reduction of oxygen on gold and gold-based electrodes was then studied, to propose a detailed mechanism of NO_2 detection.

École Nationale Supérieure des Mines
de Saint-Étienne

NNT : 2014 EMSE 0760

Ivan ROMANYTSIA

ÉTUDE DES PROPRIETES ELECTRO-CATALYTIQUES DES MATERIAUX D'ELECTRODE ET DES PHENOMENES DE POLARISATION POUR LA COMPREHENSION DES MECANISMES DE DETECTION D'UN CAPTEUR D'OXYDES D'AZOTE ET L'OPTIMISATION DE SON FONCTIONNEMENT.

Spécialité: GÉNIE DES PROCÉDÉS

Mots clefs : Gaz d'échappement, NOx, Capteur, Polarisation, Sélectivité, Mécanisme de détection.

Résumé :

Le transport routier est responsable de la production de la majeure partie des oxydes d'azote (NOx) émis dans l'atmosphère. La majorité de cette pollution est donc concentrée dans des zones très urbanisées. L'exposition permanente aux gaz d'échappement a des conséquences graves pour la santé humaine et pour cela, des normes d'émission de plus en plus strictes sont mises en place.

Les technologies post-traitement embarquées dans les pots d'échappement sont de plus en plus complexes et nécessitent un control continu de la composition gazeuse. Les conditions sérères de ce milieu requièrent le développement de capteurs de gaz robustes et de longue durée de vie.

Dans ce travail, nous présentons la procédure de fabrication et la caractérisation d'un capteur électrochimique à trois électrodes pouvant satisfaire les exigences d'une application industrielle dans le domaine automobile. La technologie de sérigraphie utilisée a l'avantage d'être facilement transférable dans l'industrie pour une production de masse bas cout.

Le principe de fonctionnement du capteur est basé sur la polarisation galvanostatique de l'électrode sensible permettant une détection sélective de NO_2 sans interférence avec d'autres gaz comme CO et NO. De plus, afin d'augmenter la stabilité du capteur, de diminuer les temps de réponse et de recouvrement, un nouveau matériau d'électrode composite à base d'or a été développé.

Enfin, la réduction électrochimique de l'oxygène sur l'or et sur des électrodes composite a été étudiée, afin de proposer un mécanisme de détection de NO_2